

**Numerical Solution of a Transmission Problem  
with Prefractal Interface**

by

Rebecca Wasyk

A Thesis

Submitted to the Faculty

of

WORCESTER POLYTECHNIC INSTITUTE

In partial fulfillment of the requirements for the

Degree of Doctor of Philosophy

in

Mathematical Sciences

by

---

October 22, 2007

APPROVED:

---

Professor Umberto Mosco, Dissertation Advisor  
WPI Department of Mathematical Sciences

---

Professor Robert Gilbert  
University of Delaware Department of Mathematical Sciences

---

Professor Marcus Sarkis  
WPI Department of Mathematical Sciences

---

Professor Bogdan Vernescu  
WPI Department of Mathematical Sciences

---

Professor Homer Walker  
WPI Department of Mathematical Sciences



## Acknowledgements

Every page of acknowledgements in a dissertation must begin with one person, the advisor, so I won't break with that tradition. My advisor Umberto Mosco is responsible for introducing me to fractal analysis and for providing me with an interesting and challenging topic to work on. His bountiful knowledge in this and in many other areas has been indispensable during my research. But it is his unbridled enthusiasm and all of his colorful analogies that kept me moving forward throughout this difficult process, even when it seemed as if I just might get eaten by the wolves.

I am also grateful for every person on my committee who is about to embark on the lengthy task of reading my dissertation. Since most of you have been a big part of my graduate experience, it seems fitting that you are now part of the conclusion. I wish to thank you, and all of my other professors, for all of the help that you have given me along the way. Although she has never been my professor, I would also like to thank Maria Vivaldi for her very thorough, helpful comments and suggestions on early drafts of this dissertation. I would be negligent to not thank in particular Homer Walker for serving as my advisor when I initially arrived at WPI and for his continued assistance and guidance even to the present time. It has been greatly appreciated.

And now I must thank all of my wonderful friends and family who have suffered with me through more than 6 years of grad school, listening to my endless complaints and offering their much-needed support. I am fortunate that there are far too many of you to mention individually, but there is one person who I've leaned on more than any other. To my best friend, Jon, your sense of humor and well-timed "Keep on truckin" kept me going when I was ready to give up. And now that it's finally almost over, let's drop this giant ball of oil out the window and start looking for that Brougham.



# Contents

<b>Introduction</b>	<b>1</b>
<b>1 The Transmission Problem</b>	<b>3</b>
1.1 Introduction to the Transmission Problem . . . . .	3
1.2 The Family of Fractal von Koch Curves . . . . .	5
1.3 Fractal Transmission Problem . . . . .	9
1.3.1 Energy form and Laplacian on von Koch curves . . . . .	9
1.3.2 Solution to the Fractal Transmission Problem . . . . .	13
1.4 Prefractal Transmission Problem . . . . .	14
1.4.1 Sobolev and Trace Spaces on Polygonal Domains . . . . .	15
1.4.2 Introduction to the Prefractal Transmission Problem . . . . .	17
1.4.3 Regularity of the Prefractal Transmission Problem . . . . .	20
<b>2 Finite Element Theory</b>	<b>25</b>
2.1 Basic Error Estimates . . . . .	25
2.2 Error Estimates for Nonconvex Polygonal Domains . . . . .	39
<b>3 Numerical Treatment of the Prefractal Transmission Problem</b>	<b>49</b>
3.1 Generating the Mesh . . . . .	49
3.2 Properties of the Mesh . . . . .	61
3.3 Implementation and Results . . . . .	76
3.4 Future Work . . . . .	82
<b>General Notation</b>	<b>87</b>
<b>Finite Element Notation</b>	<b>89</b>

<b>Problem Notation</b>	<b>91</b>
<b>A Some Relevant Spaces and Definitions</b>	<b>93</b>
<b>B Miscellaneous Results</b>	<b>95</b>
B.1 Controlling the Aspect Ratio with a Minimum Angle . . . . .	95
B.2 Distance Between Vertices of Domain . . . . .	97
B.3 Finding the Aspect Ratio after Refinement . . . . .	99

# Introduction

Certain physical problems in electrostatics, magnetostatics, and heat transfer give rise to elliptic boundary value problems with transmission conditions on a layer. We focus on a particular problem with a second order transmission condition, representing an infinitely conductive layer. This problem is unusual because it couples a second order problem in a 2-dimensional space with a second order problem in a lower dimensional space. An introduction to this and other types of transmission problems can be found in [14]. In more recent years, there has been a growing interest in studying irregular interfaces that more realistically model certain physical structures, like those in many biological systems. So, we introduce a new level of complexity in the problem by considering fractal and prefractal geometries as model shapes for the interface. To our knowledge, this was first studied analytically in [18], [20], [21].

The main focus of this thesis will be on forming numerical approximations to solutions of this transmission problem on different domains. Once we begin searching for a numerical solution, we can no longer consider a fractal interface because it cannot be fully realized by the finite precision of a computer. However, the fractal curves we study can be viewed as the limit of a suitable sequence of prefractal curves. So, for all of the numerical work, we study the transmission problem with a prefractal interface. The numerical solution of a special class of these prefractal problems was studied in [27] and [4]. We will expand this work by allowing for a larger collection of prefractal curves. We develop a method for creating a finite element discretization of the domain having very different prefractal curves as interfaces. The main contribution of this thesis is showing that this discretization produces a finite element scheme with a known bound on the error between the true and computed solutions in a suitable norm. Results of computations done using the discretizations will be shown.

## Outline of Thesis

The thesis is organized into three chapters following the introduction. In the first of these chapters, we begin by describing the family of fractal von Koch curves and the prefractal curves that approximate them. After developing some notation and understanding some important properties of these curves, the reader is introduced to the transmission problem we plan to study having a fractal or prefractal interface. Since the primary focus of this thesis is the numerical solution of the transmission problem on domains with prefractal layers, the emphasis will be on the prefractal transmission problem. After defining this problem, we will give some known results about the regularity of the solution that will be essential in developing a finite element method that is appropriate for the problem.

The second chapter is devoted to recalling some results about the convergence of the finite element method in a general setting. The results are not new, and are repeated here in some detail for those who are unfamiliar with them and to serve as a reference for later sections. We begin by providing the proofs of the convergence of the finite element method using piecewise affine functions when the solution to the problem is  $H^2$ -regular. As will be shown in the first chapter, the solutions to the transmission problems we are interested in are not this regular. Reentrant corners occurring along the prefractal interfaces are one reason for the lack of regularity. So, the second section of this chapter explores convergence results for problems on nonconvex domains that are directly applicable to the transmission problem under consideration.

The third chapter is where the original work of the thesis resides. In this chapter, a scheme is developed to triangulate the domains of interest. Since the particular prefractal curve forming the layer can vary greatly, this alone is a delicate task. Once this triangulation method has been explained, we will use the theory that will be developed in the second chapter to prove error estimates for solving the transmission problem using the finite element method. We will conclude the chapter with some examples of computations done using the method developed in earlier sections of the chapter.

# Chapter 1

## The Transmission Problem

This chapter is organized into several sections. In the first section, we introduce a transmission problem with an unspecified interface and point out some of the interesting aspects of this problem. In the following section, the von Koch curves that will serve as an interface for the transmission problem are introduced. In the remaining sections of the chapter, results about the solutions to the transmission problem with both a fractal and prefractal layer are presented.

### 1.1 Introduction to the Transmission Problem

We begin by giving a description of the transmission problem we will consider. Let  $\Omega$  be the rectangle  $(0, 1) \times (-1, 1)$  and let  $S$  be a curve from  $A = (0, 0)$  to  $B = (1, 0)$  that divides  $\Omega$  into two regions as illustrated in Figure 1.1. We use  $\Omega^1$  and  $\Omega^2$  to refer to the

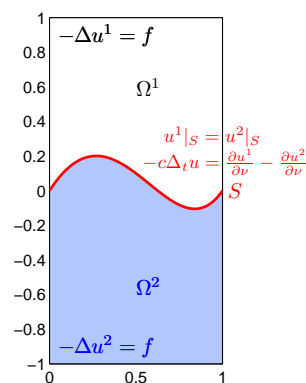


Figure 1.1: Example domain

portions of  $\Omega$  above and below  $S$ , respectively.

The problem is then described as follows. We seek functions  $u^1$ , defined on  $\Omega^1$ , and  $u^2$ , defined on  $\Omega^2$ , solving

$$\begin{aligned} -\Delta u^i &= f & \text{in } \Omega^i \\ u^i &= 0 & \text{on } \partial\Omega \cap \partial\Omega^i \end{aligned}$$

for  $i = 1, 2$  with  $f \in L^2(\Omega)$ . These functions are linked by the requirement that the trace of the functions on  $S$  is the same. With  $u^i|_S$  denoting the trace of  $u^i$  on  $S$ , we write this condition as  $u^1|_S = u^2|_S$ . Since the functions  $u^i$  must coincide on  $S$ , and  $\Omega = \Omega^1 \cup \Omega^2 \cup S$ , we may also think of a single function  $u$  defined on all of  $\Omega$  as

$$u = \begin{cases} u^1 & \text{in } \Omega^1 \\ u^2 & \text{in } \Omega^2 \\ u^S & \text{on } S, \end{cases} \quad (1.1)$$

where  $u^S$  is the common value of  $u^i|_S$ ,  $i = 1, 2$ . With this thought in mind, we will also represent the continuity condition as  $[u] = 0$  across  $S$ .

What makes this problem interesting is the second order transmission condition that further links  $u^1$  and  $u^2$ . The condition is stated as:

$$-c\Delta_t u^S = \frac{\partial u^1}{\partial \nu} - \frac{\partial u^2}{\partial \nu},$$

where  $\nu$  is the outward normal to  $\Omega^2$ ,  $\Delta_t$  is the Laplacian along  $S$ , and  $c$  is a positive constant. The notation  $\Delta_t$  is used because in many cases when the curve  $S$  is nice enough, this will be the tangential Laplacian. Once again using the definition of  $u$  in (1.1), we will also write this condition as  $-c\Delta_t u = [\frac{\partial u}{\partial \nu}]$  for brevity. We combine all of this information in the following formal description of the problem:

$$\begin{cases} -\Delta u = f & \text{in } \Omega^i, i = 1, 2 \\ -c\Delta_t u = [\frac{\partial u}{\partial \nu}] & \text{on } S \\ [u] = 0 & \text{across } S \\ u = 0 & \text{on } \partial\Omega \end{cases} \quad (\text{P})$$

It will also be useful at times to consider the weak formulation of this problem. For this, we define the space

$$V(\Omega, S) := \{v \in H_0^1(\Omega) : v|_S \in H_0^1(S)\}.$$

Depending on the curve  $S$ , some care must be given to properly defining the space  $H_0^1(S)$ , but for now, assume that a suitable definition can be made. Then, the weak formulation of the problem is:

$$\left\{ \begin{array}{l} \text{Find } u \in V(\Omega, S) \text{ such that:} \\ \iint_{\Omega} \nabla u \nabla v \, dx \, dy + c \int_S \nabla_t u \nabla_t v \, ds = \iint_{\Omega} f v \, dx \, dy \\ \text{for every } v \in V(\Omega, S) \end{array} \right.$$

As was mentioned previously, what makes this problem especially interesting is the transmission condition across the interface  $S$ . In the first place, it is not very common to see a second order boundary condition associated with a second order problem in the domain. Additionally, this term couples the 2-dimensional surface problem with a lower dimensional boundary value problem on the layer. This is significant because if we think of the problem in terms of electrostatics, for instance, where  $u$  is the electric potential, this problem models a case where the layer  $S$  is highly conductive and can itself support a charge. So the jump in the electrical field across the boundary between the two subdomains is equal to the current flowing along the layer. Thus, we think of  $S$  not just as a boundary between two regions, but as a separate body.

In many physical situations one might wish to model, the interface may not be smooth. We investigate a layer that is either a fractal or prefractal curve as a model case for these types of circumstances. Before remarking more about the transmission problem with such a layer, we introduce the fractal and prefractal curves we will be considering.

## 1.2 The Family of Fractal von Koch Curves

The family of von Koch curves belongs to the larger class of self-similar fractals explored by J. E. Hutchinson in [15]. There, it is shown that given any finite set  $\mathcal{S} = \{S_1, \dots, S_N\}$  of contraction maps on a complete metric space, there exists a unique closed, bounded

set  $K$  such that  $K = \cup_{i=1}^N S_i(K)$ . Using this result, each curve in the family of von Koch curves can be defined as the unique set fixed by four contraction maps.

**Definition 1.2.1.** Fix  $\alpha \in (2, 4)$ . Then the general von Koch curve with contraction factor  $\frac{1}{\alpha}$ , denoted by  $\Sigma^\alpha$ , is the unique closed set in  $\mathbb{C}$  ( $\mathbb{R}^2$ ) fixed by the maps:

$$\begin{aligned} \psi_1^\alpha(z) &= \frac{z}{\alpha} & \psi_2^\alpha(z) &= \frac{z}{\alpha}e^{i\theta} + \frac{1}{\alpha} \\ \psi_3^\alpha(z) &= \frac{z}{\alpha}e^{-i\theta} + \frac{1}{2} + i\sqrt{\frac{1}{\alpha} - \frac{1}{4}} & \psi_4^\alpha(z) &= \frac{z}{\alpha} + \frac{\alpha - 1}{\alpha} \end{aligned}$$

where  $\theta = \cos^{-1}\left(\frac{\alpha}{2} - 1\right)$ .

This is only one of several ways of defining the von Koch curves. For the present work, a constructive definition will be much more useful. We begin with a construction from segments after first establishing some notation. Fix  $\alpha \in (2, 4)$ . Then, for any set  $F \subset \mathbb{R}^2$ , let

$$\Psi_\alpha(F) := \bigcup_{i=1}^4 \psi_i^\alpha(F) \tag{1.2}$$

and for each integer  $n$ , let

$$\Psi_\alpha^n(F) = \underbrace{\Psi_\alpha \circ \dots \circ \Psi_\alpha}_{n \text{ times}}(F). \tag{1.3}$$

A general result for self-similar fractals in [15] implies that beginning with any compact set  $F \subset \mathbb{R}^2$ , the iterates  $\Psi_\alpha^n(F)$  converge to the set  $\Sigma^\alpha$  in the Hausdorff metric as  $n$  increases to infinity. For each  $\alpha \in (2, 4)$ , let  $\Sigma_0^\alpha$  be the unit interval from the point  $A = (0, 0)$  to the point  $B = (1, 0)$ , and for  $n \geq 1$ , let

$$\Sigma_n^\alpha = \Psi_\alpha(\Sigma_{n-1}^\alpha). \tag{1.4}$$

Since the limit of this sequence of sets is  $\Sigma^\alpha$ , we refer to  $\Sigma_n^\alpha$  as the  **$n^{\text{th}}$ -generation prefractal von Koch curve with contraction factor  $\alpha$** . The prefractal curves for  $n = 1, 2$ , and 3 and  $\alpha = 3$  and  $\alpha = 2.5$  can be seen in Figures 1.2 and 1.3. Some features of the maps  $\psi_i^\alpha$  that generate the curves become more apparent when viewing these pictures. We call a map  $S : \mathbb{R}^D \rightarrow \mathbb{R}^D$ ,  $D \geq 1$  a **similitude** if there exists a constant  $l > 0$  such that  $|S(x) - S(y)| = l|x - y|$  for every  $x, y \in \mathbb{R}^D$ , and if  $l \in (0, 1)$ ,  $S$  is called a **contractive similitude**. So, examining the maps  $\psi_i^\alpha$ , we see that they

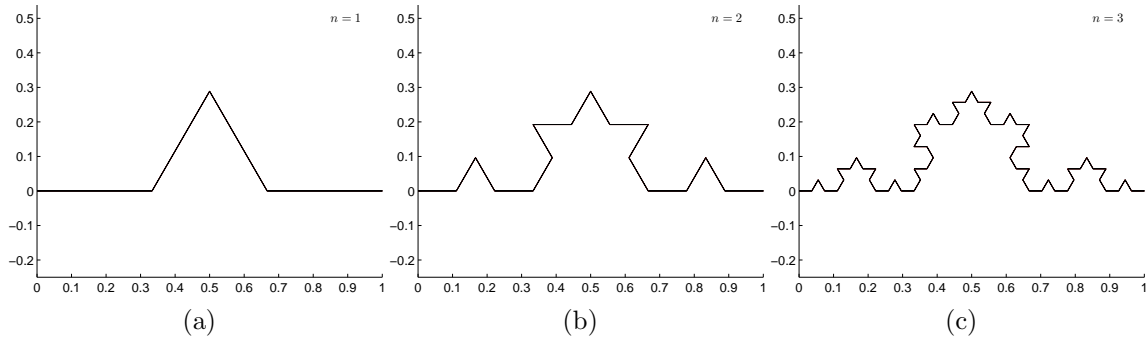


Figure 1.2: First 3 prefractal von Koch curves for  $\alpha = 3$

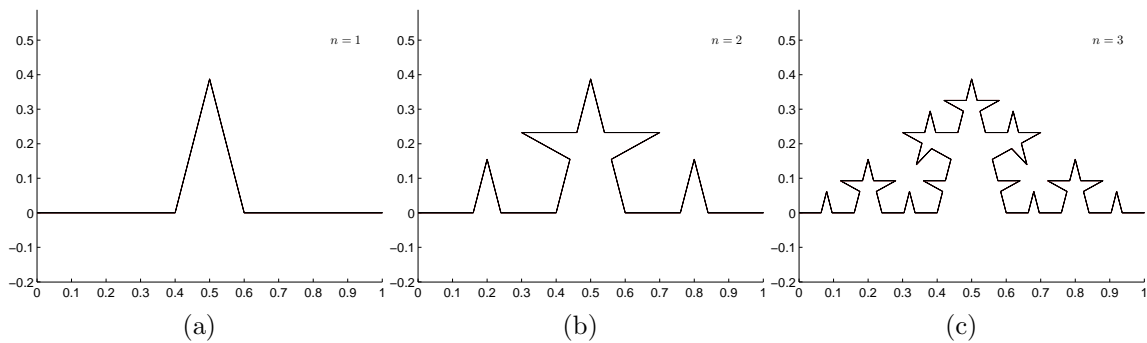


Figure 1.3: First 3 prefractal von Koch curves for  $\alpha = 2.5$

are contractive similitudes with a contraction factor of  $\alpha^{-1}$ . Thus, each segment of the  $n^{\text{th}}$ -generation prefractal curves has length  $\alpha^{-n}$ . Secondly,  $\theta$  can be seen as the angle the non-horizontal segments make with the  $x$ -axis when  $n = 1$ . Because the maps are similitudes, these angles are repeated at every generation of the prefractal curve wherever an inverted “V” ( $\wedge$ ) meets another segment. This angle will become very important in the future when we discuss the numerical treatment of the prefractal transmission problem.

A second constructive definition of the curves that we will make use of is due to Lindstrøm [22]. Once again, fix  $\alpha \in (2, 4)$  and let  $A = (0, 0)$  and  $B = (1, 0)$ . Then let  $V_\alpha^0 = \{A, B\}$ , and for  $n \geq 1$ , define

$$V_\alpha^n := \Psi_\alpha (V_\alpha^{n-1}). \quad (1.5)$$

We call the set of points  $V_\alpha^n$  the **vertices** of the  $n^{\text{th}}$ -generation prefractal von Koch

curve. As we will see later when we are designing a triangulation scheme for the domain of the problem, it is important to note that the von Koch curve belongs to the family of nested fractals, and as such, has the property that  $V_\alpha^n \subset V_\alpha^{n+1}$  for every  $n$ . If we define  $V_\alpha^\infty := \bigcup_{n \geq 0} V_\alpha^n$ , then  $\Sigma^\alpha$  is the closure of  $V_\alpha^\infty$  in the Hausdorff metric on  $\mathbb{R}^2$ .

With these equivalent definitions of  $\Sigma^\alpha$  in mind, we now describe some of the properties of these curves. First, it can be shown that each curve in this family has infinite length and Hausdorff dimension  $\frac{\log 4}{\log \alpha} > 1$  (see Appendix A for a reminder of the definition of Hausdorff dimension). This means the prefractal curve  $\Sigma_n^\alpha$  has length increasing to  $\infty$  as  $n \rightarrow \infty$ , which is especially interesting in our case because this curve serves as the boundary between two domains in the transmission problem.

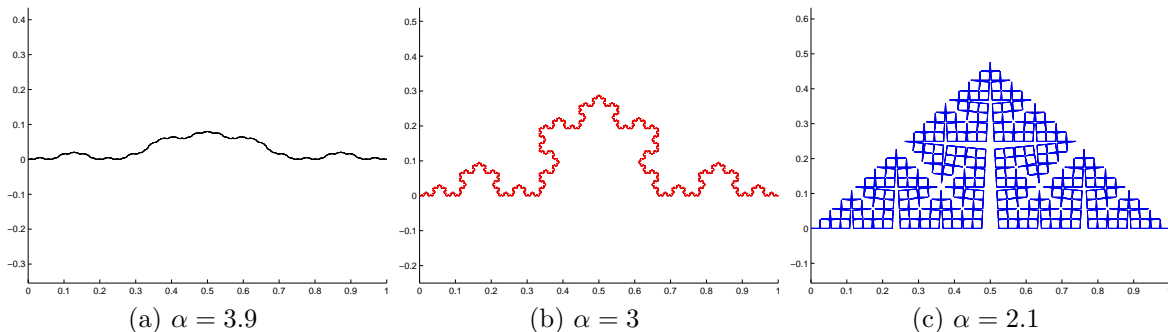


Figure 1.4: von Koch curve for different  $\alpha$

As  $\alpha \rightarrow 4$ , the dimension tends to one, with the curve becoming flat. In fact, if we were allow  $\alpha = 4$ ,  $\Sigma_n^4$  would reproduce the interval  $[0, 1]$  as the union of  $4^n$  segments of equal length, and  $\Sigma^4$  would not be a fractal curve at all. At the other extreme, as  $\alpha \rightarrow 2$ , the curve begins to fill the space and if we were to allow  $\alpha = 2$ , the limit would be the triangle with vertices  $(0, 0)$ ,  $(1, 0)$ ,  $(\frac{1}{2}, \frac{1}{2})$ . This contrast in the nature of the von Koch family of curves for different values of  $\alpha$  can be seen in Figure 1.4. The very irregular curves that result from  $\alpha$  near 2 will be the primary focus in this work since they present a more interesting case mathematically and a more difficult challenge for the numerical work, but the analytical results and numerical procedures we describe hold for  $\alpha$  near 4 as well.

### 1.3 Fractal Transmission Problem

Now that the family of fractal von Koch curves has been defined, for a fixed  $\alpha \in (2, 4)$ , we have the following formal statement of the transmission problem with a fractal interface:

$$\begin{cases} -\Delta u = f & \text{in } \Omega_\alpha^i, i = 1, 2 \\ -c_0 \Delta_\Sigma u = [\frac{\partial u}{\partial \nu}] & \text{on } \Sigma^\alpha \setminus \{A, B\} \\ [u] = 0 & \text{across } \Sigma^\alpha \\ u = 0 & \text{on } \partial\Omega \end{cases} \quad (P^\alpha)$$

In  $(P^\alpha)$ , we have essentially replaced the undetermined curve  $S$  of (P) in Section 1.1 with the fractal curve  $\Sigma^\alpha$ . We use  $\alpha$  in the notation here and elsewhere to draw attention to the problem's dependence on this parameter that singles out the particular curve in the family of von Koch curves we are considering. For instance,  $\Omega_\alpha^1$  and  $\Omega_\alpha^2$ , the portions of  $\Omega$  above and below the interface  $\Sigma^\alpha$ , vary greatly depending on the choice of  $\alpha$ .

Although  $(P^\alpha)$  describes the transmission problem with a fractal interface, at this point, this description is purely formal. To make the problem meaningful, we must attach a meaning to  $\Delta_\Sigma$ , the Laplacian along the fractal curve, and  $\frac{\partial u}{\partial \nu}$  across the curve. This is not a trivial task since  $\Sigma^\alpha$  is a non-differentiable curve. So, we now take an aside to explain how the Laplacian is defined on the von Koch curves.

#### 1.3.1 Energy form and Laplacian on von Koch curves

We begin by describing a measure  $\mu$  defined on  $\Sigma^\alpha$  that is invariant under the maps generating the curve, meaning  $\mu$  satisfies

$$\int_{\Sigma^\alpha} \phi d\mu = \frac{1}{4} \sum_{i=1}^4 \int_{\Sigma^\alpha} (\phi \circ \psi_i^\alpha) d\mu \quad (1.6)$$

for every  $\phi \in C_0(\Sigma^\alpha)$ , where  $\psi_i^\alpha$  for  $i = 1, \dots, 4$  are the contractive similitudes appearing in definition 1.2.1 (see [15]). Letting  $\mathcal{H}^D \llcorner K$  denote the restriction of the  $D$ -dimensional Hausdorff measure on  $\mathbb{R}^2$  to the set  $K$ , the measure  $\mu$  coincides with  $(\mathcal{H}^d(\Sigma^\alpha))^{-1} \mathcal{H}^d \llcorner \Sigma^\alpha$  where  $d = \frac{\log 4}{\log \alpha}$  is the Hausdorff dimension of  $\Sigma^\alpha$ . Additionally,  $\mu$  has the property [15, 9]

that there exist constants  $c_1, c_2 > 0$  such that

$$c_1 r^d \leq \mu(B(x, r) \cap \Sigma^\alpha) \leq c_2 r^d \quad (1.7)$$

for every  $x \in \Sigma^\alpha$  and  $0 < r < 1$ . Using the terminology of [16], this makes  $\Sigma^\alpha$  a  $d$ -set.

With this definition, we may now construct the energy form on the von Koch curve with contraction factor  $\alpha^{-1}$ . Since  $\Sigma^\alpha$  is a non-differentiable curve, it is not possible to classically define the energy  $\int_K |\nabla u|^2 dx$  for  $u : K \rightarrow \mathbb{R}$  when  $K = \Sigma^\alpha$ . So, we will replace this integral with an energy form that comes as the limit of finite difference schemes, following the construction given in [18].

The description will be facilitated by introducing some additional notation. Given a family of  $N$  maps,  $\phi = \{\phi_1, \dots, \phi_N\}$ , and an  $n$ -tuple of indices  $(i_1, i_2, \dots, i_n)$  with  $i_j \in \{1, 2, \dots, N\}$  for each  $j$ , we write

$$\phi_{i_1, \dots, i_n} = \phi_{i_1} \circ \dots \circ \phi_{i_n}.$$

Alternatively, we may write  $i|n$  for the  $n$ -tuple  $(i_1, i_2, \dots, i_n)$  as above, and correspondingly, write  $\phi_{i|n}$  for  $\phi_{i_1} \circ \dots \circ \phi_{i_n}$ . Finally, we use  $W^n$  to denote the set of all  $n$ -tuples taken from the set  $\{1, 2, \dots, N\}$ . With this notation fixed, we can now proceed to the construction of the energy form.

Begin by fixing  $\alpha \in (2, 4)$  and recall  $V_\alpha^\infty$  defined in Section 1.2 is the set of points  $\cup_{n>0} \Psi_\alpha^n(\{A, B\})$ , where  $A = (0, 0)$  and  $B = (1, 0)$ . Then for any function  $u : V_\alpha^\infty \rightarrow \mathbb{R}$ , define

$$E_\alpha^{(0)}(u, u) := [u(A) - u(B)]^2 \quad (1.8)$$

and for  $n > 0$ , let

$$E_\alpha^{(n)}(u, u) := 4^n \sum_{i|n \in W^n} [u(\psi_{i|n}^\alpha(A)) - u(\psi_{i|n}^\alpha(B))]^2. \quad (1.9)$$

The coefficient  $4^n$  in the expression for  $E_\alpha^{(n)}$  is a renormalization factor. A discussion of how this coefficient must be chosen can be found in [23]. It can be shown that  $E_\alpha^{(n)}(\cdot, \cdot)$

is an increasing sequence having a limit,

$$E_\alpha[u] = E_\alpha(u, u) := \lim_{n \rightarrow \infty} E_\alpha^{(n)}(u, u) \quad (1.10)$$

which we call the **energy form on  $\Sigma^\alpha$** . Additionally, it can be shown that the set  $\{u : V_\alpha^\infty \rightarrow \mathbb{R} \mid E_\alpha[u] < \infty\}$  is nonempty and any function in this set can be extended uniquely to a continuous function on  $\Sigma^\alpha$ . So, if for  $u : \Sigma^\alpha \rightarrow \mathbb{R}$ , we set

$$E_\alpha(u, u) := E_\alpha(u|_{V_\alpha^\infty}, u|_{V_\alpha^\infty})$$

and let

$$D(\Sigma^\alpha) = \{u \in C(\Sigma^\alpha) \mid E_\alpha[u] < \infty\},$$

we see that  $D(\Sigma^\alpha) \subset C(\Sigma^\alpha) \subset L^2(\Sigma^\alpha, \mu)$ , where  $\mu$  is the invariant measure on  $\Sigma^\alpha$  previously defined. Next, we extend  $D(\Sigma^\alpha)$  to form a complete space and then extend  $E_\alpha(u, u)$  to the whole space in the natural way.

**Definition 1.3.1.** Let  $\mathbf{D}_E(\Sigma^\alpha)$  be the completion of  $\{u \in C(\Sigma^\alpha) \mid E_\alpha[u] < \infty\}$  with respect to the norm:

$$\|u\|_{D_E(\Sigma^\alpha)} := \left\{ E_\alpha(u, u) + \|u\|_{L^2(\Sigma^\alpha, \mu)}^2 \right\}^{1/2} \quad (1.11)$$

which we call the **energy norm on  $\Sigma^\alpha$** .

Using the polarization identity, we create the bilinear form  $E_\alpha(\cdot, \cdot)$

$$E_\alpha(u, v) = \frac{1}{2} \{E_\alpha(u + v, u + v) - E_\alpha(u, u) - E_\alpha(v, v)\} \quad (1.12)$$

Then the space  $D_E(\Sigma^\alpha)$  is a Hilbert space with respect to the scalar product

$$E_\alpha(u, v) + \int_{\Sigma^\alpha} uv \, d\mu$$

and the form  $E_\alpha[u]$  is a closed Dirichlet form which is regular and strongly local in  $L^2(\Sigma^\alpha, \mu)$ . For completeness, we recall the definitions of these terms related to Dirichlet forms.

**Definition 1.3.2.** Let  $X$  be a locally compact metric space. Let  $\mathcal{E}$  be a symmetric form on  $L^2(X, \mu)$  and let  $D_\mathcal{E} = \text{Dom}(\mathcal{E})$ . Then  $\mathcal{E}$  is called a **Dirichlet form** if for every

$u \in D_{\mathcal{E}}$ ,  $\mathcal{E}(\bar{u}, \bar{u}) \leq \mathcal{E}(u, u)$  where

$$\bar{u}(p) = \begin{cases} 1 & \text{if } u(p) \geq 1 \\ u(p) & \text{if } 0 < u(p) < 1 \\ 0 & \text{if } u(p) \leq 0 \end{cases}$$

A Dirichlet form is:

1. **closed** if  $D_{\mathcal{E}}$  is complete with respect to the metric  $d(\cdot, \cdot)$  defined as  $d(u, v) = \mathcal{E}(u, v) + \int_X uv \, d\mu$ ,
2. **regular** if it possesses a core,  $C \subset D_{\mathcal{E}} \cap C_0(X)$ , that is dense in  $D_{\mathcal{E}}$  with respect to the norm induced by  $d(\cdot, \cdot)$  and dense in  $C_0(X)$  with respect to the supremum norm,
3. **local** if  $\mathcal{E}(u, v) = 0$  for every  $u, v \in D_{\mathcal{E}}$  with  $\text{supp}(u)$  and  $\text{supp}(v)$  compact, and  $\text{supp}(u) \cap \text{supp}(v) = \emptyset$ .

It can be shown (see [18] and the references therein) that the space  $D_E(\Sigma^\alpha)$  is continuously embedded in  $C^{0, \frac{d}{2}}(\Sigma^\alpha)$ , where  $C^{0, \beta}(K)$  is the set of Hölder continuous functions of order  $\beta$  on  $K$ , and  $d$  is the Hausdorff dimension of  $\Sigma^\alpha$ . This result allows us to unambiguously define the space

$$D_0(\Sigma^\alpha) := \{u \in D_E(\Sigma^\alpha) \mid u = 0 \text{ on } V_\alpha^0\} \quad (1.13)$$

which will arise in the description of the transmission problem with a fractal layer.

We are now prepared to define a Laplacian (with homogeneous boundary conditions) on each of the von Koch curves, which will also be necessary for properly defining the transmission problem with one of these curves as a layer. Since  $E_\alpha$ , considered with the domain  $D_0(\Sigma^\alpha)$  is also a closed form on  $L^2(\Sigma^\alpha, \mu)$ , there exists a self-adjoint operator  $\Delta_\Sigma$  in  $L^2(\Sigma^\alpha, \mu)$ , with dense domain  $D_{\Delta_\Sigma} \cap D_0(\Sigma^\alpha)$  in  $L^2(\Sigma^\alpha, \mu)$ , such that

$$E_\alpha(v, w) = - \int_{\Sigma^\alpha} (\Delta_\Sigma v) w \, d\mu \quad (1.14)$$

for  $v \in D_{\Delta_\Sigma} \cap D_0(\Sigma^\alpha)$  and for all  $w \in D_0(\Sigma^\alpha)$ .

We will also find it useful to have the Laplace operator on  $\Sigma^\alpha$  as a variational operator. So, letting  $(D_0(\Sigma^\alpha))'$  denote the dual of  $D_0(\Sigma^\alpha)$ , we define the variational operator from

$D_0(\Sigma^\alpha) \rightarrow (D_0(\Sigma^\alpha))'$  by

$$E_\alpha(v, w) = - \langle \Delta_\Sigma v, w \rangle_{(D_0(\Sigma^\alpha))', D_0(\Sigma^\alpha)} \quad (1.15)$$

for  $v \in D_0(\Sigma^\alpha)$  and for all  $w \in D_0(\Sigma^\alpha)$ , where  $\langle \cdot, \cdot \rangle_{(D_0(\Sigma^\alpha))', D_0(\Sigma^\alpha)}$  is the duality pairing between  $(D_0(\Sigma^\alpha))'$  and  $D_0(\Sigma^\alpha)$ .

Note that we will use the same notation for the Laplace operator in both cases, as a self-adjoint operator and as a variational operator. Also, we remark that these two Laplacians have analogs in the case of the classical Euclidean Laplacian. Specifically, one can define the Laplacian with homogeneous Dirichlet boundary conditions as either a self-adjoint operator with domain  $H^2(\cdot) \cap H_0^1(\cdot)$  or as a variational operator from  $H_0^1(\cdot)$  to  $H^{-1}(\cdot)$ .

### 1.3.2 Solution to the Fractal Transmission Problem

With the Laplacian on the fractal curve  $\Sigma^\alpha$  defined, we are now prepared to give a more rigorous description of the transmission problem with a fractal layer. Begin by defining

$$V(\Omega, \Sigma^\alpha) := \{u \in H_0^1(\Omega) \mid u|_{\Sigma^\alpha} \in D_0(\Sigma^\alpha)\}. \quad (1.16)$$

Following the proof given in [18], we have the following lemma.

**Lemma 1.3.3.**  *$V(\Omega, \Sigma^\alpha)$  is a Hilbert space equipped with the scalar product*

$$(u, v)_{V(\Omega, \Sigma^\alpha)} = \iint_{\Omega} \nabla u \nabla v \, dx \, dy + E_\alpha(u|_{\Sigma^\alpha}, v|_{\Sigma^\alpha}) \quad (1.17)$$

Using this result, it is easy to see that the bilinear form defined by

$$(u, v) \in V(\Omega, \Sigma^\alpha) \times V(\Omega, \Sigma^\alpha) \mapsto \iint_{\Omega} \nabla u \nabla v \, dx \, dy + E_\alpha(u|_{\Sigma^\alpha}, v|_{\Sigma^\alpha})$$

is continuous and coercive. Thus, by Lax-Milgram (Theorem 2.1.5), the following theorem holds.

**Theorem 1.3.4.** *Fix  $\alpha \in (2, 4)$ ,  $f \in L^2(\Omega)$ , and let  $c_0$  be a positive constant. Then, there exists a unique  $u \in V(\Omega, \Sigma^\alpha)$  such that for every  $v \in V(\Omega, \Sigma^\alpha)$ :*

$$\iint_{\Omega} \nabla u \nabla v \, dx \, dy + c_0 E_\alpha(u|_{\Sigma^\alpha}, v|_{\Sigma^\alpha}) = \iint_{\Omega} f v \, dx \, dy. \quad (\tilde{P}^\alpha)$$

$(\tilde{P}^\alpha)$  is the weak formulation of the transmission problem with a fractal interface  $\Sigma^\alpha$ . In [18], the regularity of the solution to  $(\tilde{P}^\alpha)$  is proved when  $\alpha = 3$ , and it is shown in what sense the solution to  $(\tilde{P}^\alpha)$  is also a solution of  $(P^\alpha)$ . One item of particular importance that is explained in [18] is that the normal derivative  $\frac{\partial u^i}{\partial \nu}$  appearing in  $(P^\alpha)$  exists in the dual of a particular Besov space. These regularity results can be extended to allow for the consideration of other values of  $\alpha \in (2, 4)$ , but introducing the spaces and other tools needed to extend the regularity result would require a substantial detour from the primary focus of this thesis, which is numerically solving the transmission problem with a prefractal interface.

At this point, the reader might wonder why we will only consider numerically solving the transmission problem with a prefractal interface, and not the transmission problem with a fractal interface. There are a couple of well-founded reasons for this. First, while the energy form developed in Section 1.3.1 allows for a precise mathematical statement of the transmission problem with a fractal interface, this energy form is found as the limit of a sequence of calculations of the energy on prefractal curves. As seen in Section 1.2, each member of the family of von Koch curves has detail at arbitrarily small scales and is also the result of a limiting process, so the curve itself can never be represented fully by the finite precision of a computer. Therefore an implementable numerical method for directly solving  $(\tilde{P}^\alpha)$  cannot be created.

However, noticing that the energy form that is used to define the Laplacian on  $\Sigma^\alpha$  results from calculations on prefractal curves and the fractal curve is itself the limit of prefractal curves, one sees the transmission problem with a prefractal interface as a reasonable approximation to the problem with a fractal interface. More importantly, it is shown in [21] that solutions of the prefractal transmission problem  $(\tilde{P}_n^\alpha)$  converge to the solution of the fractal transmission problem  $(\tilde{P}^\alpha)$  in the  $H^1$ -norm when  $\alpha = 3$ . Although some of the techniques used to prove this result are not easily extended to other values of  $\alpha$ , this still motivates our focus on numerically solving the transmission problem with a prefractal interface, which we will now define.

## 1.4 Prefractal Transmission Problem

To state and understand the transmission problem with a prefractal layer, we must make use of Sobolev spaces on polygonal boundaries. We use the definitions in [7] because they are best suited to our purposes. However, other definitions have been given for these

spaces that are not always in agreement with the definitions used here. To avoid any confusion, we take an aside now to introduce the definitions used in this thesis and to quote some results that we will make use of. For more details about alternate definitions for Sobolev spaces on polygonal boundaries, see Remark 4.1 in [21] and the references therein.

### 1.4.1 Sobolev and Trace Spaces on Polygonal Domains

We begin by introducing the polygonal domain and defining some notation. In this section, assume  $Q$  is an open polygon in  $\mathbb{R}^2$  with  $N$  vertices  $P_j$ ,  $j = 1, \dots, N$  numbered in counterclockwise order from  $P_1$ . Let  $l_j$  be the side from  $P_j$  to  $P_{j+1}$  for  $j = 1, \dots, N-1$ , and let  $l_N$  be the side from  $P_N$  to  $P_1$ . We let  $\Gamma$  denote the entire boundary of  $Q$ , having length  $L = \sum_{j=1}^N |l_j|$ , where  $|l_j|$  denotes the length of  $l_j$  in the Euclidean norm.  $\Gamma_0$  will denote any subset of the boundary going from a vertex  $P_i$  to another vertex  $P_j$  of  $Q$  with a counterclockwise orientation and having length  $L_0$ . For each vertex  $P_j$ , we have a smooth function  $\phi_j : [0, L] \rightarrow \Gamma$  that is the parameterization of  $\Gamma$  by arc length having the property that  $\phi_j(0) = P_j$ . We then have the following definitions for the Sobolev spaces on the boundary of  $Q$  (See Section 2.8 of [7]).

**Definition 1.4.1** (Sobolev Spaces on Polygonal Curves). Let  $H^s(\Gamma)$  be defined according to the value of  $s$  as follows.

1. For  $s \in [0, \frac{1}{2})$ :

$$H^s(\Gamma) = \{v \in L^2(\Gamma) \mid v \circ \phi_1 \in H^s(0, L)\} \quad (1.18)$$

with the norm  $\|v\|_{H^s(\Gamma)} = \|v \circ \phi_1\|_{H^s(0, L)}$ .

2. For  $s = \frac{1}{2}$ :

$$H^{\frac{1}{2}}(\Gamma) = \left\{ v \in L^2(\Gamma) \mid v \circ \phi_j \in H^{\frac{1}{2}}(0, |l_j|) \text{ and } \int_{-\delta}^{\delta} \frac{|v \circ \phi_j(|l_j| + t) - v \circ \phi_j(|l_j| - t)|}{|t|} dt < \infty, \text{ for } j = 1, \dots, N \right\} \quad (1.19)$$

with the norm

$$\|v\|_{H^{\frac{1}{2}}(\Gamma)}^2 = \sum_{j=1}^N \left( \|v \circ \phi_j\|_{H^{\frac{1}{2}}(0, |l_j|)}^2 + \int_{-\delta}^{\delta} \frac{|v \circ \phi_j(|l_j| + t) - v \circ \phi_j(|l_j| - t)|^2}{|t|} dt \right)$$

where  $\delta = \min_{j=1\dots N} |l_j|$ .

3. For  $s > \frac{1}{2}$ :

$$H^s(\Gamma) = \left\{ v \in L^2(\Gamma) \mid v \circ \phi_j \in H^s(0, |l_j|) \text{ and } v \circ \phi_j \text{ is continuous at } |l_j|, \text{ for } j = 1, \dots, N \right\} \quad (1.20)$$

with the norm

$$\|v\|_{H^s(\Gamma)} = \left( \sum_{j=1}^N \|v \circ \phi_j\|_{H^s(0, |l_j|)}^2 \right)^{\frac{1}{2}} \quad (1.21)$$

The next theorem gives some vital inclusions relating these Sobolev spaces. Before stating the result, we introduce some notation that we will adhere to in the remainder of the thesis. For normed spaces  $X$  and  $Y$ ,

$$\begin{array}{ll} X \hookrightarrow Y & X \subset Y \text{ with a continuous injection} \\ & \text{(i.e., there exists a constant } C \text{ s.t. } \|\cdot\|_Y \leq C \|\cdot\|_X) \\ X \hookrightarrow\hookrightarrow Y & X \subset Y \text{ with a compact injection} \\ & \text{(i.e., } v_n \xrightarrow{w} v \text{ in } X \Rightarrow \|v_n - v\|_Y \rightarrow 0) \end{array}$$

**Theorem 1.4.2.** *For the Sobolev spaces of definition 1.4.1, we have the inclusions*

$$H^s(\Gamma) \hookrightarrow C(\Gamma) \quad \text{for } s > \frac{1}{2} \quad (1.22)$$

and

$$H^{s_2}(\Gamma) \hookrightarrow H^{s_1}(\Gamma) \quad \text{for } s_1 < s_2. \quad (1.23)$$

**Remark:** In light of the preceding theorem, we can characterize the space  $H^s(\Gamma)$  for  $s > \frac{1}{2}$  as  $\{v \in C(\Gamma) \mid v|_{l_j} \in H^s(l_j) \text{ for } j = 1, \dots, N\}$ .

In what follows, we will also need to make use of the trace of an  $H^1$ -function on the boundary, so we supply the definition and a useful theorem here. The theorem corresponds to Theorem 2.24 of [7].

**Definition 1.4.3** (Trace operator). Let  $D$  be an open set in  $\mathbb{R}^2$ . Then for  $f \in H^s(D)$ , we put

$$\gamma_0 f = \lim_{r \rightarrow 0} \frac{1}{|B(x, r) \cap D|} \int_{B(x, r) \cap D} f(y) dy \quad (1.24)$$

at every point  $x \in \overline{D}$  where the limit exists. We call  $\gamma_0$  the **trace** (or **restriction**) operator on  $H^s(D)$ .

**Remark:** In the case where  $f \in C(\overline{D})$ ,  $\gamma_0 f$  on  $\partial D$  coincides with  $f|_{\partial D}$ , so we will preserve the notation  $f|_{\partial D}$  for  $\gamma_0 f$  on  $\partial D$ , even when  $f \in H^s(D)$ .

**Theorem 1.4.4.** Let  $Q$  be a polygon in  $\mathbb{R}^2$  with boundary  $\Gamma$  and let  $s > \frac{1}{2}$ . Then  $H^{s-\frac{1}{2}}(\Gamma)$ , is the trace space to  $\Gamma$  of  $H^s(Q)$  in the following sense:

1. the restriction operator,  $\gamma_0$  is a continuous linear operator from  $H^s(Q)$  to  $H^{s-\frac{1}{2}}(\Gamma)$ ,
2. there is a continuous linear operator  $Ext$  from  $H^{s-\frac{1}{2}}(\Gamma)$  to  $H^s(Q)$  such that  $\gamma_0 \circ Ext$  is the identity operator in  $H^{s-\frac{1}{2}}(\Gamma)$ .

**Remark:** The definitions for Sobolev spaces on polygonal boundaries given in definition 1.4.1 also hold with  $\Gamma$  replaced by  $\Gamma_0$  after making the appropriate modifications. So, in [7], Theorems 1.4.2 and 1.4.4 are also given with  $\Gamma$  replaced by  $\Gamma_0$ .

With these definitions completed, we may now proceed to the statement of the transmission problem with a prefractal interface.

## 1.4.2 Introduction to the Prefractal Transmission Problem

Fix  $n \in \mathbb{N}$  and  $\alpha \in (2, 4)$ . As before, let  $\Omega = (0, 1) \times (-1, 1)$  and denote by  $\Omega_{\alpha, n}^1$  and  $\Omega_{\alpha, n}^2$  the portions of  $\Omega$  above and below the prefractal curve  $\Sigma_n^\alpha$ , respectively (see Figure 1.5 for an example with  $\alpha = 2.5$  and  $n = 3$ ). Then the transmission problem we will consider on this domain is stated as follows:

$$\begin{cases} -\Delta u_n = f & \text{in } \Omega_{\alpha, n}^i, i = 1, 2 \\ -c_n \Delta_t u_n = \left[ \frac{\partial u_n}{\partial \nu} \right] & \text{on } \Sigma_n^\alpha \\ [u_n] = 0 & \text{across } \Sigma_n^\alpha \\ u_n = 0 & \text{on } \partial\Omega \end{cases} \quad (P_n^\alpha)$$

Unlike in the case of a fractal interface, it is not problematic to define derivatives on  $\Sigma_n^\alpha$ , because for any fixed  $n$ , this is a polygonal curve and  $\Delta_t$  is the tangential Laplacian,

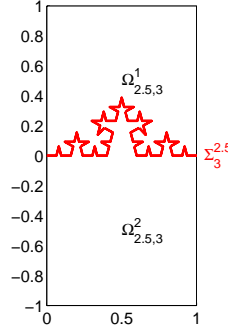


Figure 1.5: Domain with  $\alpha = 2.5$  and  $n = 3$

defined piecewise on each segment of  $\Sigma_n^\alpha$ . The constant  $c_n$  equals  $c_0\alpha^{(d-1)n}$ , where  $c_0$  is the constant appearing in  $(\tilde{P}^\alpha)$  and  $(P^\alpha)$ , and  $d = \frac{\log 4}{\log \alpha}$  is the Hausdorff dimension of  $\Sigma^\alpha$ . In the present context, it is enough to know that  $c_n$  is a positive constant. Only when the asymptotic convergence of solutions of  $(P_n^\alpha)$  to the solution of  $(P^\alpha)$  is considered, as mentioned in Section 1.3.2, is the exact value of this constant significant.

We will also make extensive use of the weak formulation of this problem, so we introduce that now. Although definitions for Sobolev spaces on polygonal curves were provided in Section 1.4.1, for concreteness, we supply a definition for the space  $H_0^1(\Sigma_n^\alpha)$  here.

**Definition 1.4.5.** The space  $H_0^1(\Sigma_n^\alpha)$  is defined as

$$\{v \in C_0(\Sigma_n^\alpha) : u|_M \in H^1(M), \text{ for every segment } M \in \Sigma_n^\alpha\}$$

with the norm

$$\|v\|_{H^1(\Sigma_n^\alpha)} = \left( \sum_{M \in \Sigma_n^\alpha} \|u|_M\|_{H^1(M)}^2 \right)^{\frac{1}{2}}.$$

We now define the space on which the problem will be posed as

$$V(\Omega, \Sigma_n^\alpha) := \{u \in H_0^1(\Omega) \mid u|_{\Sigma_n^\alpha} \in H_0^1(\Sigma_n^\alpha)\} \quad (1.25)$$

with the natural inner product

$$(u, v)_{V(\Omega, \Sigma_n^\alpha)} := \iint_{\Omega} \nabla u \nabla v \, dx \, dy + c_n \int_{\Sigma_n^\alpha} \nabla_t u \nabla_t v \, ds, \quad (1.26)$$

and corresponding norm

$$\|u\|_{V(\Omega, \Sigma_n^\alpha)} := \left( |u|_{H^1(\Omega)}^2 + c_n |u|_{H^1(\Sigma_n^\alpha)}^2 \right)^{\frac{1}{2}}. \quad (1.27)$$

Then, using this notation, the weak formulation of  $(P_n^\alpha)$  is:

$$\begin{cases} \text{Find } u_n \in V(\Omega, \Sigma_n^\alpha) \text{ such that} \\ \iint_{\Omega} \nabla u_n \nabla v \, dx \, dy + c_n \int_{\Sigma_n^\alpha} \nabla_t u_n \nabla_t v \, ds = \iint_{\Omega} f v \, dx \, dy \\ \text{for every } v \in V(\Omega, \Sigma_n^\alpha) \end{cases} \quad (\tilde{P}_n^\alpha)$$

We will begin the analysis of this transmission problem with a prefractal interface by showing that  $(\tilde{P}_n^\alpha)$  has a unique solution. This will follow easily from the Lax-Milgram Theorem (see Theorem 2.1.5 for reference) once we have shown that  $V(\Omega, \Sigma_n^\alpha)$  is a Hilbert Space.

**Lemma 1.4.6.**  *$V(\Omega, \Sigma_n^\alpha)$  is a Hilbert space with respect to the inner product (1.26).*

*Proof.* It is easy to see that (1.26) is an inner product, so it remains to show that  $V(\Omega, \Sigma_n^\alpha)$  is complete with respect to the induced norm. Let  $u_k$  be a Cauchy sequence in  $V(\Omega, \Sigma_n^\alpha)$ . Then by definition of the norm on  $V(\Omega, \Sigma_n^\alpha)$ ,  $u_k$  is a Cauchy sequence in  $H_0^1(\Omega)$  and  $u_k|_{\Sigma_n^\alpha}$  is a Cauchy sequence in  $H_0^1(\Sigma_n^\alpha)$ . Therefore, there exist functions  $u \in H_0^1(\Omega)$  with  $\lim_{k \rightarrow \infty} \|u_k - u\|_{H^1(\Omega)} = 0$ , and  $\hat{u} \in H_0^1(\Sigma_n^\alpha)$  with  $\lim_{k \rightarrow \infty} \|u_k|_{\Sigma_n^\alpha} - \hat{u}\|_{H^1(\Sigma_n^\alpha)} = 0$ . By Theorem 1.4.4, the restriction operator from  $H^1(\Omega) \rightarrow H^{\frac{1}{2}}(\Sigma_n^\alpha)$  is a continuous linear operator, so  $u_k|_{\Sigma_n^\alpha} \rightarrow u|_{\Sigma_n^\alpha}$  in  $H^{\frac{1}{2}}(\Sigma_n^\alpha)$ . By Theorem 1.4.2,  $H_0^1(\Sigma_n^\alpha) \hookrightarrow H^{\frac{1}{2}}(\Sigma_n^\alpha)$ , so  $\hat{u} = u|_{\Sigma_n^\alpha}$ , and hence,  $u \in V(\Omega, \Sigma_n^\alpha)$ .  $\square$

**Theorem 1.4.7.** *Fix  $n \in \mathbb{N}$  and  $\alpha \in (2, 4)$ . Then, for any  $f \in L^2(\Omega)$ , there exists a unique  $u_n \in V(\Omega, \Sigma_n^\alpha)$  satisfying  $(\tilde{P}_n^\alpha)$ . Additionally, there exists a constant  $C$ , independent of  $n$  and  $\alpha$ , such that*

$$\|u_n\|_{V(\Omega, \Sigma_n^\alpha)} \leq C \|f\|_{L^2(\Omega)} \quad (1.28)$$

*Proof.* Since  $(\cdot, \cdot)_{V(\Omega, \Sigma_n^\alpha)}$  is a symmetric, continuous, coercive bilinear form on the Hilbert Space  $V(\Omega, \Sigma_n^\alpha)$ , the existence of a unique solution to  $(\tilde{P}_n^\alpha)$  follows immediately from the Lax-Milgram Theorem.

For the inequality, let  $u_n$  be the solution to  $(\tilde{P}_n^\alpha)$ . Then, we have:

$$\|u_n\|_{V(\Omega, \Sigma_n^\alpha)}^2 = (u_n, u_n)_{V(\Omega, \Sigma_n^\alpha)} = \int_{\Omega} f u_n \, dx \, dy.$$

Using the Hölder and the Poincaré Inequalities gives:

$$\begin{aligned} \|u_n\|_{V(\Omega, \Sigma_n^\alpha)}^2 &\leq \left( \int_{\Omega} |f|^2 \, dx \, dy \right)^{\frac{1}{2}} \left( \int_{\Omega} |u_n|^2 \, dx \, dy \right)^{\frac{1}{2}} \\ &\leq C \|f\|_{L^2(\Omega)} \|u_n\|_{H^1(\Omega)} \\ &\leq C \|f\|_{L^2(\Omega)} \|u_n\|_{V(\Omega, \Sigma_n^\alpha)} \end{aligned}$$

where  $C$ , coming from Poincaré's Inequality, depends only on  $\Omega$ . Dividing both sides by  $\|u_n\|_{V(\Omega, \Sigma_n^\alpha)}$  yields (1.28).  $\square$

In the next section, we will explore the regularity of the prefractal transmission problem by stating more rigorously the sense in which the equalities in  $(P_n^\alpha)$  hold. We will conclude the section with a result showing that the solution is in a weighted Sobolev space. This last result will be essential for the numerical analysis in Chapter 3.

### 1.4.3 Regularity of the Prefractal Transmission Problem

In this section, we will present two main results. The first theorem describes in what sense the solution to  $(\tilde{P}_n^\alpha)$  is also a solution to  $(P_n^\alpha)$ . The second theorem will give the regularity of  $u_n$  in terms of fractional dimensional and weighted Sobolev spaces. Both results can be found in [20] for the special case when  $\alpha = 3$ , and the general result for other values of  $\alpha$  can be found in [19].

**Theorem 1.4.8.** *For any fixed  $\alpha \in (2, 4)$ ,  $n \in \mathbb{N}$ , and  $f \in L^2(\Omega)$ , let  $u_n \in V(\Omega, \Sigma_n^\alpha)$  be the solution to  $(\tilde{P}_n^\alpha)$  guaranteed by Theorem 1.4.7. Then,  $u_n$  is also a solution of  $(P_n^\alpha)$  in the following sense:*

$$\begin{cases} -\Delta u_n = f & \text{in } L^2(\Omega_{\alpha, n}^i), \, i = 1, 2 \\ -c_n \Delta_t u_n = \left[ \frac{\partial u_n}{\partial \nu} \right] & \text{in } L^2(\Sigma_n^\alpha) \\ [u_n] = 0 & \text{in } H^2(\Sigma_n^\alpha) \\ u_n = 0 & \text{in } H^{\frac{1}{2}}(\partial\Omega) \end{cases} \quad (1.29)$$

Due to the discontinuity in the normal derivative across  $\Sigma_n^\alpha$ ,  $u_n \notin H^2(\Omega)$ . The discontinuity in the derivative is not the only thing limiting the regularity of the solution though. Additionally, the corners in the domain have a strong effect on the regularity and will pose challenges in the numerical approximation.

The next theorem gives the regularity of  $u_n$  in terms of fractional dimensional Sobolev spaces and weighted Sobolev spaces. In both cases, the definition of the space relies on the angle  $\theta$  first appearing in the definition of the maps that generate the Von Koch curve in Section 1.2. This angle is important because the only reentrant corners in the domain are at vertices of the prefractal curve. Reentrant corners occur wherever the angle interior to the domain is greater than  $\pi$ . An example of these reentrant corners and their relation to the angle  $\theta$  can be seen in Figure 1.6. We see here that there are

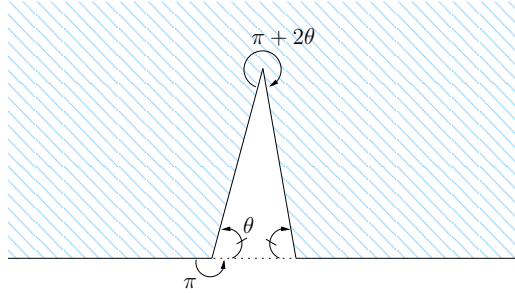


Figure 1.6: Typical reentrant corners

two type of reentrant corners in the domain. In the lower domain, angles at reentrant corners have measure  $\pi + \theta$ . In the upper portion of the domain, the reentrant corners have an angle of  $2\pi - (\pi - 2\theta) = \pi + 2\theta$ . Since the angles at reentrant corners are always greater in the upper domain, we expect, and will see, that the solution is less regular in this portion of the domain.

As mentioned before, the regularity results below are given in fractional Sobolev spaces as well as in weighted Sobolev spaces. This is done because defining the regularity of the solution using fractional Sobolev spaces is satisfactory for studying the problem from an analytical viewpoint, but, for the numerical work we will pursue, it is more convenient to consider the regularity in a weighted Sobolev space, which we now define.

**Definition 1.4.9.** Let  $Q$  be a polygonal domain in  $\mathbb{R}^2$  with vertices  $P_i$ ,  $i = 1, 2, \dots, N$  and  $\theta_i$  denote the angle formed at the vertex  $P_i$  in the interior of  $Q$ . With

$$R := \{1 \leq j \leq N \mid \theta_j > \pi\} \text{ and } \eta := \frac{1}{4} \min_{1 \leq i < j \leq N} |P_i - P_j|,$$

define  $r(x)$  for  $x \in Q$  as

$$r(x) = \begin{cases} |x - P_j| & \text{if } x \in B(P_j, \eta) \text{ for some } j \in R \\ \frac{1-\eta}{\eta}(|x - P_j| - \eta) + \eta & \text{if } x \in B(P_j, 2\eta) \setminus B(P_j, \eta) \text{ for some } j \in R \\ 1 & \text{if } x \notin \bigcup_{j \in R} B(P_j, 2\eta) \end{cases} \quad (1.30)$$

Then for  $0 < \mu < 1$ , let  $H^{2,\mu}(Q; r)$  be the space

$$\{u \in H^1(Q) \mid r^\mu \partial^\beta u \in L^2(Q) \forall |\beta| = 2\},$$

with the norm

$$\|v\|_{H^{2,\mu}(Q; r)} := \left( \|v\|_{H^1(Q)}^2 + \sum_{|\beta|=2} \|r^\mu \partial^\beta v\|_{L^2(Q)}^2 \right)^{\frac{1}{2}} \quad (1.31)$$

**Remarks:** First, notice that  $\{P_j\}_{j \in R}$  is the set of vertices of  $Q$  that are reentrant to the domain. Away from the reentrant corners, the weighting function  $r$  has a positive lower bound. Therefore, if  $u \in H^{2,\mu}(Q; r)$ , and  $D \subset Q \setminus \bigcup_{j \in R} B(P_j, \delta)$  for some  $\delta > 0$ , then  $u|_D \in H^2(D)$ . This information will be used in Section 2.2 to prove an error estimate for applying the finite element method to solve an elliptic problem on a domain with reentrant corners.

Next, we note that this is not the most general definition that can be given for the weighted Sobolev space  $H^{2,\mu}(Q; r)$ . While we have chosen to specify the function  $r$ , many results using these spaces require only that  $r : Q \rightarrow \mathbb{R}^+$  is a function in  $C(\overline{\Omega})$  with the property that  $r(x) = |x - P_j|$  if  $x$  belongs to a small neighborhood of  $P_j$  for some  $j \in R$ . Because of this flexibility, the function  $r$  appears in the notation for the space. Additionally, while we have used the same weight  $\mu$  at every reentrant corner of the domain, when the angle is not the same at each corner, it is appropriate to use a different weight depending on each angle. In the current work, we will seldom make use of a more general definition of  $r$ , and we will never need to use different weights at different corners. For more information about general weighted Sobolev spaces, see [17] and the references therein.

Finally, noticing that the function  $r$  depends on the reentrant corners in the domain, when we refer to a weighted Sobolev space on the domains  $\Omega_{\alpha,n}^1$  and  $\Omega_{\alpha,n}^2$ , we will

adopt a notation intended to capture the idea that the function  $r$  varies with  $n$ , even for a fixed  $\alpha$ . Hereafter, we will use the  $H^\mu(\Omega_{\alpha,n}^i; r_n^i)$  to refer to a weighted Sobolev space on  $\Omega_{\alpha,n}^i$ , using  $r_n^i$  to refer to the weighting function described in Definition 1.4.9, specialized to the case where  $Q$  is either  $\Omega_{\alpha,n}^i$  for  $i = 1$  or  $i = 2$ . In Chapter 3, when implementation of the algorithm for numerically solving the problem is discussed, we will give more consideration to properties of this weighting function. We now present the main regularity result for the problem  $(P_n^\alpha)$ , appearing in [19].

**Theorem 1.4.10.** *Fix  $\alpha \in (2, 4)$ ,  $n \in \mathbb{N}$ , and  $f \in L^2(\Omega)$ . Let  $u_n$  be as in Theorem 1.4.8. Then, letting  $u_n^i$  denote  $u_n|_{\Omega_{\alpha,n}^i}$ , we have:*

$$u_n^1 \in H^{s_1}(\Omega_{\alpha,n}^1) \quad \text{where } s_1 < \frac{2\pi+2\theta}{\pi+2\theta} \quad (1.32)$$

$$u_n^2 \in H^{s_2}(\Omega_{\alpha,n}^2) \quad \text{where } s_2 < \frac{2\pi+\theta}{\pi+\theta} \quad (1.33)$$

with the property that

$$\|u_n^i\|_{H^{s_i}(\Omega_{\alpha,n}^i)} \leq c(n) \|f\|_{L^2(\Omega)} \quad \text{for } i = 1, 2. \quad (1.34)$$

Additionally,

$$u_n^1 \in H^{2,\mu_1}(\Omega_{\alpha,n}^1; r_n^1) \quad \text{for } \mu_1 > \frac{2\theta}{\pi+2\theta} \quad (1.35)$$

$$u_n^2 \in H^{2,\mu_2}(\Omega_{\alpha,n}^2; r_n^2) \quad \text{for } \mu_2 > \frac{\theta}{\pi+\theta} \quad (1.36)$$

satisfying

$$\|r_n^{\mu_i} \partial^\beta u_n^i\|_{L^2(\Omega_{\alpha,n}^i)} \leq c(\mu_i, n) \|f\|_{L^2(\Omega_{\alpha,n}^i)} \quad \forall |\beta| = 2,$$

where  $\theta = \cos^{-1}(\frac{\alpha}{2} - 1)$  and  $r_n^i$  is the distance function described above.



# Chapter 2

## Finite Element Theory

This chapter will be divided into two sections. Both sections will provide important results that are used to study the finite element method for a large class of problems. In the first section, our goal will be to present some error estimates for the finite element method applied to  $H^2$ -regular problems. These results are well known and appear in numerous books, for instance [6], [8] and [26]. As we have seen in Theorem 1.4.10, the solution to  $(\tilde{P}_n^\alpha)$  is not in  $H^2(\Omega)$ , so the results of the first section will not be directly applicable. However, they are included here because we will still make some use of them and it will be useful to compare them to the results of the second section, in which problems with solutions in weighted Sobolev spaces, like the prefractal transmission problem, are considered. The results in the second section are not quite as widely known, but they also appear in some books. In particular, we will generally follow the presentation in [12]. Readers familiar with this theory may proceed directly to the next chapter and refer back to this chapter only as needed when theorems or notation are referenced. All results applying this pre-existing theory to our problem of interest,  $(\tilde{P}_n^\alpha)$ , will be postponed until the next chapter.

### 2.1 Basic Error Estimates

In this section, and in other portions of the thesis, we will use the Sobolev Embedding Theorem and the Rellich-Kondrashov Theorem. For ease of reference, the results are repeated here. Proofs can be found in [1].

**Theorem 2.1.1** (Sobolev Embedding Theorem). *Let  $\Omega \subset \mathbb{R}^2$  be an open set with*

*Lipschitz-continuous boundary. Let  $1 \leq p \leq q$ ,  $m \geq 1$ , and  $k \leq m$ . Then*

1. *if  $k < \frac{2}{p}$ ,  $W^{m,p}(\Omega) \hookrightarrow W^{m-k,q}(\Omega)$  for  $p \leq q \leq \frac{2p}{2-kp}$ .*
2. *if  $k = \frac{2}{p}$ ,  $W^{m,p}(\Omega) \hookrightarrow W^{m-k,q}(\Omega)$  for  $p \leq q < \infty$ .*
3. *if  $k > \frac{2}{p}$ ,  $W^{m,p}(\Omega) \hookrightarrow C^{m-k}(\overline{\Omega})$ .*

**Theorem 2.1.2** (Rellich-Kondrashov Theorem). *Let  $\Omega \subset \mathbb{R}^2$  be an open set with Lipschitz-continuous boundary. Let  $1 \leq p < \infty$  and  $m \geq 1$ . Fix  $1 \leq k \leq m$  and let  $\omega \subset \Omega$  be any open, bounded set. Then*

1. *if  $k < \frac{2}{p}$  and  $q < \frac{2p}{2-kp}$ ,  $W^{m,p}(\Omega) \hookrightarrow\hookrightarrow W^{m-k,q}(\omega)$ .*
2. *if  $k = \frac{2}{p}$ ,  $W^{m,p}(\Omega) \hookrightarrow\hookrightarrow W^{m-k,q}(\Omega)$  for all  $q < \infty$ .*
3. *if  $k > \frac{2}{p}$ ,  $W^{m,p}(\Omega) \hookrightarrow\hookrightarrow C^{m-k}(\overline{\Omega})$*

**Theorem 2.1.3.** *Let  $\Omega$  be a bounded open subset of  $\mathbb{R}^n$  with Lipschitz boundary. Then, for  $s_2 > s_1 \geq 0$ ,  $W^{s_2,p}(\Omega) \hookrightarrow\hookrightarrow W^{s_1,p}(\Omega)$ .*

The first theorem we will present gives the existence and uniqueness of the solution to an abstract variational problem. For concreteness, we introduce a model variational problem that satisfies the assumptions of the theorem. The model problem we will consider is:

$$\begin{cases} \text{Find } u \text{ in } H_0^1(\Omega) \text{ such that:} \\ \int_{\Omega} \nabla u \nabla v \, dx = \int_{\Omega} f v \, dx \\ \text{for every } v \in H_0^1(\Omega). \end{cases} \quad (\text{M})$$

Note that this is simply the variational formulation of the Poisson problem:

$$\begin{cases} -\Delta u = f & \text{in } \Omega \\ u = 0 & \text{on } \partial\Omega \end{cases}$$

To be consistent with the formulation of the following theorem, if we let  $a(u, v) = \int_{\Omega} \nabla u \nabla v \, dx$  and  $f(v) = \int_{\Omega} f v \, dx$ , we may rewrite the problem in the form:

$$\begin{cases} \text{Find } u \text{ in } H_0^1(\Omega) \text{ such that:} \\ a(u, v) = f(v) \\ \text{for every } v \in H_0^1(\Omega) \end{cases} \quad (2.1)$$

In order to prove that a solution to this problem exists, the bilinear form  $a$  must have certain properties. We recall some terms that express these properties here.

**Definition 2.1.4.** Let  $Y$  be a Hilbert space and let  $a : Y \times Y \rightarrow \mathbb{R}$  be a bilinear form. Then  $a(\cdot, \cdot)$  is

1. **continuous** provided there exists  $M > 0$  such that

$$|a(u, v)| \leq M \|u\|_Y \|v\|_Y, \quad \text{for all } u, v \in Y$$

2. **coercive** if there exists  $m > 0$  such that

$$a(v, v) \geq m \|v\|_Y^2 \quad \text{for all } v \in Y.$$

It can easily be shown that the bilinear form  $a(\cdot, \cdot) : H_0^1(\Omega) \times H_0^1(\Omega) \rightarrow \mathbb{R}$ , defined above for the model problem, satisfies both of these properties. Then, the Lax-Milgram theorem supplies us with the existence of a unique solution to the model problem. Because this result is so well-known, we have omitted the proof and have only provided a restatement of the theorem.

**Theorem 2.1.5** (Lax-Milgram). *Let  $Y$  be a Hilbert space, and let  $a(\cdot, \cdot) : Y \times Y \rightarrow \mathbb{R}$  be a symmetric, continuous, coercive bilinear form. Let  $f : Y \rightarrow \mathbb{R}$  be a continuous linear form. Then the abstract variational problem:*

$$\text{Find } u \in Y \text{ such that } a(u, v) = f(v) \quad \forall v \in Y \tag{2.2}$$

*has a unique solution  $u \in Y$ .*

Although this first theorem gives us existence and uniqueness of the solution to the model problem, it does not provide any means of actually calculating the solution  $u$ . The finite element method is one of a larger class of methods, called Galerkin methods, in which one seeks an approximate solution to the problem by solving the problem exactly in a subspace  $Y_h$  of  $Y$ , i.e. find  $u_h \in Y_h$  such that  $a(u_h, v_h) = f(v_h) \forall v_h \in Y_h$ . Since this subspace will itself be a Hilbert space, the above theorem implies that there exists a unique solution to the variational problem posed on  $Y_h$ . We hope to choose a subspace  $Y_h$  in which it is much easier to find a solution than in the original space  $Y$ , but contains enough functions that the actual solution can be adequately approximated by functions in the subspace.

Our goal in this section is to determine bounds for the error introduced by solving on a subspace instead of the entire space. What follows is the first approximation theorem

on our way to that goal. Like the existence theorem above, it is rather abstract. Before proceeding, we caution the reader that we will not always be concerned with the precise values of constants appearing in the proofs, so the notation for a constant may not change, even as the value of the constant changes over a sequence of steps.

**Theorem 2.1.6** (Cea's Lemma). *Let  $Y$  be a Hilbert space,  $Y_h$  a subspace of  $Y$ ,  $a(\cdot, \cdot) : Y \times Y \rightarrow \mathbb{R}$  a continuous, coercive bilinear form and  $f : Y \rightarrow \mathbb{R}$  a continuous linear form. Let  $u$  and  $u_h$  be the unique solutions, guaranteed by Lax-Milgram (Theorem 2.1.5), of the variational problems:*

$$\begin{aligned} a(u, v) &= f(v) \quad \forall v \in Y \quad \text{and} \\ a(u_h, v_h) &= f(v_h) \quad \forall v_h \in Y_h \end{aligned}$$

*respectively. Then there exists a constant  $C$ , independent of the subspace  $Y_h$ , such that*

$$\|u - u_h\|_Y \leq C \inf_{v_h \in Y_h} \|u - v_h\|_Y. \quad (2.3)$$

*Proof.* Since  $u$  is the solution of the variational problem in  $Y$  and  $Y_h \subset Y$ , we have

$$a(u, v_h) = f(v_h) \text{ for each } v_h \in Y_h.$$

Since  $u_h$  solves the variational problem in  $Y_h$ , we also have

$$a(u_h, v_h) = f(v_h) \text{ for any } v_h \in Y_h.$$

So, by subtraction, we have

$$a(u - u_h, v_h) = 0 \text{ for each } v_h \in Y_h.$$

Now, since  $a(\cdot, \cdot)$  is a continuous, coercive bilinear form, there exist constants  $m$  and  $M > 0$  such that  $m \|v\|_Y^2 \leq a(v, v)$  and  $|a(u, v)| \leq M \|u\|_Y \cdot \|v\|_Y$  for all  $u, v \in Y$ .

Putting these together, we have for any  $v_h \in Y_h$ :

$$\begin{aligned}
m \|u - u_h\|_Y^2 &\leq a(u - u_h, u - u_h) \\
&= a(u - u_h, u - u_h) + a(u - u_h, u_h - v_h) \\
&= a(u - u_h, u - v_h) \\
&\leq M \|u - u_h\|_Y \cdot \|u - v_h\|_Y
\end{aligned}$$

So, after dividing, we have  $\|u - u_h\|_Y \leq \frac{M}{m} \|u - v_h\|_Y$  for each  $v_h \in Y_h$ , implying the conclusion with  $C = \frac{M}{m}$ .  $\square$

Now that we have some understanding of the error incurred by solving on a subspace, we must define a subspace on which we wish to solve our problem. In the finite element method, the subspace is determined by a triangulation of the domain. Notice that up until this point, the domain  $\Omega$  on which the model problem (M) was posed did not explicitly enter into any of the theorems. However, since the triangulation is highly dependent on the particular domain  $\Omega$ , properties of the domain will affect the finite element error estimates.

In this section, we will make several assumptions about  $\Omega$  and its triangulation. We assume that  $\Omega \subset \mathbb{R}^2$  is a convex polygon and denote the boundary of  $\Omega$  by  $\Gamma$ . In order to state the assumptions about the triangulation, we will need a few definitions. The first definition will be used to assure that the triangulation of  $\Omega$  is actually composed of triangles.

**Definition 2.1.7.** Let  $\hat{K}$  and  $K$  be subsets of  $\mathbb{R}^n$ . Then  $\hat{K}$  and  $K$  are called **affine equivalent** if there exists an invertible affine mapping  $F : \mathbb{R}^n \rightarrow \mathbb{R}^n$  defined by  $F(\hat{x}) = B\hat{x} + b$  such that  $K = F(\hat{K})$ .

By varying angles and side lengths, very dissimilar triangles can be produced. To obtain error estimates, it is necessary to have some control over the variation among the triangles. The next definitions are used to quantify the variation between triangles in the mesh.

**Definition 2.1.8.** For any triangle,  $K$ , define

$$\mathbf{h}_K = \text{diam}(K) = \sup_{x,y \in K} |x - y|$$

$$\rho_K = 2 \sup\{r : B(x, r) \subset K\}$$

From the definitions, it is apparent that  $h_K$  is equal to the longest side of  $K$  and  $\rho_K$  is the diameter of the largest circle that can be inscribed in  $K$ . A triangle that is very skinny will have  $\rho_K \ll h_K$ . So, the ratio  $\frac{h_K}{\rho_K}$ , sometimes called the **aspect ratio**, is used to describe how thin a triangle is, with this ratio increasing to infinity as the triangle collapses to a segment. This is important because, as the error estimates will indicate, triangles that are very “skinny” can result in a poor finite element approximation. With this in mind, we formally define what we mean by a triangulation of the domain.

**Definition 2.1.9.** A **(conformal) triangulation**  $\mathcal{T}_h$  is a finite set of closed triangles, with the following properties:

$$\text{(T1)} \quad \bar{\Omega} = \bigcup_{K \in \mathcal{T}_h} K$$

$$\text{(T2)} \quad \text{For } K_1 \neq K_2 \in \mathcal{T}_h, \overset{\circ}{K}_1 \cap \overset{\circ}{K}_2 = \emptyset$$

**(T3)** Any edge of a triangle  $K_1 \in \mathcal{T}_h$  is either a subset of  $\Gamma$  or the edge of another triangle  $K_2 \in \mathcal{T}_h$ .

$$\text{(T4)} \quad h = \max_{K \in \mathcal{T}_h} h_K$$

**(T5)** For any  $K \in \mathcal{T}_h$ ,  $K$  is affine equivalent to the **reference triangle**  $\hat{K}$  formed by the vertices  $(0, 0)$ ,  $(0, 1)$ , and  $(1, 0)$ .

**Remark:** Although we have stated that the triangles  $K$  are closed and this is reinforced by **(T1)**, we will follow the convention in [8] and use the notation  $H^m(K)$  to refer to the space which would more properly be denoted by  $H^m(\overset{\circ}{K})$ . This is done for simplicity and to avoid confusing notation, especially when we consider the reference triangle  $\hat{K}$ .

Once the domain has been triangulated in this way, it is time to create a subspace  $Y_h$  corresponding to the triangulation  $\mathcal{T}_h$ . Throughout the thesis, we will consider the finite element space consisting of functions that are affine on each triangle  $K \in \mathcal{T}_h$  and continuous on  $\bar{\Omega}$ . We will denote this space by  $P_h^1(\Omega)$ . A basis for this space can easily be shown. Begin by labeling each vertex in the triangulation  $x_i$  for some integer  $i \in \{1, 2, \dots, N\}$ , where  $N$  is the number of triangle vertices in  $\mathcal{T}_h$ . Then define a set of functions  $\phi_i : \bar{\Omega} \rightarrow \mathbb{R}$  for  $1 \leq i \leq N$  by making  $\phi_i$  the unique function that is affine on each  $K \in \mathcal{T}_h$  and has the property that  $\phi_i(x_j) = \delta_{ij}$  for any vertex  $x_j \in \mathcal{T}_h$ . It is easily verified that these functions form a basis for the space, and hence the space

has dimension  $N$ . Now we define a linear interpolation operator taking functions from  $H^2(\Omega)$  to this space of piecewise affine functions contained in  $H^1(\Omega)$ .

**Definition 2.1.10.** Let  $K$  be a triangle with vertices  $z_1, z_2$  and  $z_3$  that is affine equivalent to the reference triangle  $\hat{K}$  and let  $P^1(K)$  denote the set of all polynomials of degree one defined on  $K$ . Then we define the map  $\Pi_K : C(K) \rightarrow P^1(K)$  by letting  $\Pi_K(v)$  be the unique affine function  $\bar{v} \in P^1(K)$  such that  $\bar{v}(z_i) = v(z_i)$  for  $i = 1, 2, 3$ . By the Sobolev Embedding Theorem (Theorem 2.1.1),  $H^2(K) \hookrightarrow C(K)$ . Thus every  $v \in H^2(K)$  has a continuous representative  $\tilde{v}$ , so we may define  $\Pi_K : H^2(K) \rightarrow P^1(K)$  by  $\Pi_K(v) = \Pi_K(\tilde{v})$ . If  $\mathcal{T}_h$  is a triangulation of  $\Omega$  as above, then we define  $\Pi_h : H^2(\Omega) \rightarrow P_h^1(\Omega) \subset H^1(\Omega)$  to be the map satisfying  $\Pi_h(v) = \Pi_K(v)$  for every  $v \in H^2(\Omega)$  and for every  $K \in \mathcal{T}_h$ .

With this linear interpolation operator defined, we are now prepared to give a bound on the error in approximating a function  $u \in H^2(\Omega)$  with an affine function when  $\Omega$  is a very simple domain. We will then expand this result to more complex domains.

**Lemma 2.1.11.** *Let  $\hat{K}$  be the reference triangle with vertices  $z_1 = (0, 0)$ ,  $z_2 = (0, 1)$  and  $z_3 = (1, 0)$ . Let  $\Pi_{\hat{K}} : H^2(\hat{K}) \rightarrow P^1(\hat{K})$  be the linear interpolation operator of Definition 2.1.10. Then there exists a constant  $C$  such that*

$$\|u - \Pi_{\hat{K}}u\|_{H^2(\hat{K})} \leq C |u|_{H^2(\hat{K})} \quad \forall u \in H^2(\hat{K}). \quad (2.4)$$

*Proof.* The idea of the proof is to first endow  $H^2(\hat{K})$  with the norm

$$\|v\|^* := |v|_{H^2(\hat{K})} + \sum_{i=1}^3 |v(z_i)|$$

and show that the norms  $\|\cdot\|^*$  and  $\|\cdot\|_{H^2(\hat{K})}$  are equivalent. Then the result follows from:

$$\begin{aligned} \|u - \Pi_{\hat{K}}u\|_{H^2(\hat{K})} &\leq C \|u - \Pi_{\hat{K}}u\|^* \\ &= C \left[ |u - \Pi_{\hat{K}}u|_{H^2(\hat{K})} + \sum_{i=1}^3 |(u - \Pi_{\hat{K}}u)(z_i)| \right] \\ &= C |u - \Pi_{\hat{K}}u|_{H^2(\hat{K})} \\ &= C |u|_{H^2(\hat{K})} \end{aligned}$$

where we have used the facts that  $(\Pi_{\hat{K}}u)(z_i) = u(z_i)$  for  $i = 1, 2, 3$  and  $|\Pi_{\hat{K}}u|_{H^2(\hat{K})} = 0$  since  $\Pi_{\hat{K}}u \in P^1(\hat{K})$ .

We begin by showing that  $\|\cdot\|^* \leq C \|\cdot\|_{H^2(\hat{K})}$ . By the Sobolev Embedding Theorem, we have  $H^2(\hat{K}) \hookrightarrow C^0(\hat{K})$ . Thus, there exists  $C > 0$  such that

$$\max_{i=1,2,3} |v(z_i)| \leq \|v\|_{C^0(\hat{K})} \leq C \|v\|_{H^2(\hat{K})}$$

for every  $v \in H^2(\hat{K})$ . So,  $\|v\|^* \leq (1 + 3C) \|v\|_{H^2(\hat{K})}$ .

Now, we will show that  $\|\cdot\|_{H^2(\hat{K})} \leq C \|\cdot\|^*$  by contradiction. Suppose such a  $C$  does not exist. Then there exists a sequence  $\{v_k\} \subset H^2(\hat{K})$  with  $\|v_k\|_{H^2(\hat{K})} = 1$  and  $\|v_k\|^* \leq \frac{1}{k}$  for each  $k$ . Since  $H^2(\hat{K}) \hookrightarrow H^1(\hat{K})$ , by the Rellich-Kondrashov Theorem, a subsequence of  $\{v_k\}$  converges in  $H^1(\hat{K})$ . Now, using the definition of  $\|\cdot\|_{H^2(\hat{K})}^2$  as  $\|\cdot\|_{H^1(\hat{K})}^2 + |\cdot|_{H^2(\hat{K})}^2$ , we note that for each  $k, l \in \mathbb{N}$ ,

$$\|v_k - v_l\|_{H^2(\hat{K})}^2 \leq \|v_k - v_l\|_{H^1(\hat{K})}^2 + (|v_k|_{H^2(\hat{K})} + |v_l|_{H^2(\hat{K})})^2. \quad (2.5)$$

Then, since  $\{v_k\}$  is a Cauchy sequence in  $H^1(\hat{K})$ , the first term on the right hand side goes to 0 as  $k, l \rightarrow \infty$ . By design,  $\|v_k\|^* \rightarrow 0$  as  $k \rightarrow \infty$ , and since  $|\cdot|_{H^2(\hat{K})} \leq \|\cdot\|^*$ , the second term on the right hand side of (2.5) also goes to 0 as  $k, l \rightarrow \infty$ . Thus  $\{v_k\}$  is also a Cauchy sequence in  $H^2(\hat{K})$ . Since  $H^2(\hat{K})$  is complete, there exists  $v^* \in H^2(\hat{K})$  such that  $\|v_k - v^*\|_{H^2(\hat{K})} \rightarrow 0$  as  $k \rightarrow \infty$ . By continuity of norms,  $\|v^*\|_{H^2(\hat{K})} = 1$  and  $\|v^*\|^* = 0$ . Since  $\|v^*\|^* = 0$ , we have that both  $|v^*|_{H^2(\hat{K})} = 0$  and  $v^*(z_i) = 0$  for  $i = 1, 2, 3$ . Since  $|v^*|_{H^2(\hat{K})} = 0$  implies  $v^* \in P_1(\hat{K})$  we must have  $v^* = 0$ , contradicting  $\|v^*\|_{H^2(\hat{K})} = 1$ .  $\square$

We wish to use the error estimate from the previous lemma to estimate the error in approximating a function  $u \in H^2(\Omega)$  with its linear interpolant  $\Pi_h u$  for a given triangulation,  $\mathcal{T}_h$  of  $\Omega$ . We will do so by making use of the assumption that for each  $K \in \mathcal{T}_h$ ,  $K$  is affine equivalent to  $\hat{K}$ . The next lemma makes use of differentiation and integration rules in  $\mathbb{R}^2$  to relate  $|v|_{H^m(K)}$  and  $|\hat{v}|_{H^m(\hat{K})}$  where  $v \in H^m(K)$  and  $\hat{v}$  is the corresponding function obtained by composing  $v$  with the affine map from  $\hat{K}$  to  $K$ . When combined with the previous lemma, this result will allow us to obtain an error estimate when the domain  $\Omega$  is formed as a union of triangles that are affine-equivalent to  $\hat{K}$ . The proof follows the one given in [8].

**Lemma 2.1.12.** *Let  $K$  and  $\hat{K}$  be affine equivalent and let  $F_K(\hat{x}) = B_K \hat{x} + b_K$  be the affine map from  $\hat{K} \rightarrow K$ . If  $v \in H^m(K)$  for some integer  $m$ , then  $\hat{v} := v \circ F_K \in H^m(\hat{K})$ ,*

and there exists a constant  $C$ , depending only on  $m$ , such that:

$$|\hat{v}|_{H^m(\hat{K})} \leq C \|B_K\|^m |\det B_K|^{-\frac{1}{2}} |v|_{H^m(K)} \quad (2.6)$$

where  $\|B_K\| = \max_{\substack{x \in \mathbb{R}^2 \\ x \neq 0}} \frac{|B_K x|}{|x|}$ .

*Proof.* We will first prove the statement when  $v \in C^m(K)$  and then extend our result to all functions  $v \in H^m(K)$ .

Suppose  $v \in C^m(K)$ . Then, since  $F_K$  is affine, we have that  $\hat{v} \in C^m(\hat{K})$ . Now, for any multi-index  $\beta$  with  $|\beta| = m$ , and  $e_{\beta_i}$  a basis vector in  $\mathbb{R}^2$  for each  $1 \leq i \leq m$ , one has:

$$\partial^\beta \hat{v}(\hat{x}) = D^m \hat{v}(\hat{x})(e_{\beta_1}, e_{\beta_2}, \dots, e_{\beta_m}).$$

Thus, letting  $\|D^m \hat{v}(\hat{x})\|$  represent the usual operator norm, it follows that

$$|\partial^\beta \hat{v}(\hat{x})| \leq \|D^m \hat{v}(\hat{x})\|.$$

Consequently,

$$\begin{aligned} |\hat{v}|_{H^m(\hat{K})}^2 &= \sum_{|\beta|=m} \int_{\hat{K}} |\partial^\beta \hat{v}(\hat{x})|^2 d\hat{x} \\ &\leq C_1 \int_{\hat{K}} \|D^m \hat{v}(\hat{x})\|^2 d\hat{x} \end{aligned} \quad (2.7)$$

where  $C_1$  is the cardinality of the set  $\{\beta \in \mathbb{N}^m : |\beta| = m\}$ . Now, using the differentiation rule for composition of functions, we note that for any vectors  $\xi_i \in \mathbb{R}^2$ ,  $1 \leq i \leq m$ ,

$$\begin{aligned} D^m \hat{v}(\hat{x})(\xi_1, \xi_2, \dots, \xi_m) &= D^m(v \circ F_K)(\hat{x})(\xi_1, \xi_2, \dots, \xi_m) \\ &= D^m v(x)(B_K \xi_1, B_K \xi_2, \dots, B_K \xi_m) \end{aligned}$$

where  $x = F_K(\hat{x})$ . Thus,  $\|D^m \hat{v}(\hat{x})\| \leq \|B_K\|^m \|D^m v(x)\|$ , so

$$\int_{\hat{K}} \|D^m \hat{v}(\hat{x})\|^2 d\hat{x} \leq \|B_K\|^{2m} \int_{\hat{K}} \|D^m v(x)\|^2 d\hat{x}. \quad (2.8)$$

Applying the change of variables on the right hand side yields:

$$\int_{\hat{K}} \|D^m \hat{v}(\hat{x})\|^2 d\hat{x} \leq \|B_K\|^{2m} |\det(B_K^{-1})| \int_K \|D^m v(x)\|^2 dx. \quad (2.9)$$

Since there exists a constant  $C_2$  such that  $\|D^m v(x)\| \leq C_2 \max_{|\beta|=m} |\partial^\beta v(x)|$ , by putting the previous inequalities together we have that

$$\begin{aligned} |\hat{v}|_{H^m(\hat{K})}^2 &\leq C_1 \int_{\hat{K}} \|D^m \hat{v}(\hat{x})\|^2 d\hat{x} \\ &\leq C_1 \|B_K\|^{2m} |\det B_K|^{-1} \int_K \|D^m v(x)\|^2 dx \\ &\leq C_1 \cdot C_2^2 \|B_K\|^{2m} |\det B_K|^{-1} |v|_{H^m(K)}^2 \end{aligned}$$

and our statement is proved for  $v \in C^m(K)$ .

Now, we will extend this statement to all  $v \in H^m(K)$ . From what we have just shown, the operator  $i : C^m(K) \rightarrow C^m(\hat{K})$  is in  $\mathcal{L}(H^m(K); H^m(\hat{K}))$ . Then, since  $C^m(K)$  is dense in  $H^m(K)$ , the map  $i$  can be extended (uniquely) to a continuous mapping  $i : H^m(K) \rightarrow H^m(\hat{K})$  which completes the proof.  $\square$

While the previous two results provided for estimates of error on a single triangle, in the following theorem, these results will be used to get an error estimate on the entire triangulated domain. This requires one further assumption about the triangulation which is defined below.

**Definition 2.1.13.** A triangulation  $\mathcal{T}_h$  is **shape-regular** if there exists a constant  $\sigma > 0$  such that  $\frac{h_K}{\rho_K} \leq \sigma$  for all  $K \in \mathcal{T}_h$ . A family of triangulations  $\{\mathcal{T}_h\}$ , indexed by  $h := \max_{K \in \mathcal{T}_h} h_K$ , is **regular** if  $\mathcal{T}_h$  is shape-regular with the same value of  $\sigma$  for each  $h$ , and  $h \rightarrow 0$ .

**Theorem 2.1.14.** *Let  $\Omega$  be an open set in  $\mathbb{R}^2$  with Lipschitz-continuous boundary and suppose  $\mathcal{T}_h$  is a shape-regular triangulation of  $\Omega$ . Then there exists a constant  $C$ , depending only on  $m$ , such that:*

$$\|u - \Pi_h u\|_{H^m(\Omega)} \leq C \sigma^m h^{2-m} |u|_{H^2(\Omega)} \quad \forall u \in H^2(\Omega) \text{ and } 0 \leq m \leq 2, \quad (2.10)$$

where  $\Pi_h$  is the linear interpolation operator of Definition 2.1.10, and  $\sigma$  is the regularity constant of Definition 2.1.13.

*Proof.* It suffices to establish the inequality for each  $K \in \mathcal{T}_h$  since

$$\|u - \Pi_h u\|_{H^m(\Omega)}^2 = \sum_{K \in \mathcal{T}_h} \|u - \Pi_h u\|_{H^m(K)}^2.$$

So, let  $K \in \mathcal{T}_h$  be given. Then by assumption,  $K$  is affine equivalent to  $\hat{K}$ , so there exists a bijective affine map  $F_K : \hat{K} \rightarrow K$  defined by  $F_K(\hat{x}) = B_K \hat{x} + b_K$ . Then by Lemmas 2.1.12 and 2.1.11, and using the fact that  $(\det B_K^{-1}) = (\det B_K)^{-1}$ , we have:

$$\begin{aligned} |u - \Pi_h u|_{H^m(K)} &\leq C \|B_K^{-1}\|^m |\det B_K^{-1}|^{-\frac{1}{2}} |\hat{u} - \Pi_h \hat{u}|_{H^m(\hat{K})} \\ &\leq C \|B_K^{-1}\|^m |\det B_K|^{\frac{1}{2}} \|\hat{u} - \Pi_h \hat{u}\|_{H^2(\hat{K})} \\ &\leq C \|B_K^{-1}\|^m |\det B_K|^{\frac{1}{2}} |\hat{u}|_{H^2(\hat{K})} \\ &\leq C \|B_K^{-1}\|^m |\det B_K|^{\frac{1}{2}} (\|B_K\|^2 |\det B_K|^{-\frac{1}{2}} |u|_{H^2(K)}) \\ &= C (\|B_K\| \|B_K^{-1}\|)^m \|B_K\|^{2-m} |u|_{H^2(K)}. \end{aligned}$$

Now, we look for bounds for  $\|B_K\|$  and  $\|B_K\| \|B_K^{-1}\|$  that are independent of the triangle  $K$ . By definitions of  $h_K$  and  $\rho_K$ , given  $x \in \mathbb{R}^2$  with  $|x| = \rho_{\hat{K}}$ , there exist points  $y, z \in \hat{K}$  with  $x = y - z$ . Then, since  $|B_K x| = |F_K(y) - F_K(z)|$ , and  $F_K(y), F_K(z) \in K$ , we have  $\|B_K\| \leq \frac{h_K}{\rho_{\hat{K}}}$ . By the same argument,  $\|B_K^{-1}\| \leq \frac{h_{\hat{K}}}{\rho_K}$ . So, using the assumption that  $\mathcal{T}_h$  is shape-regular, we have  $\|B_K\| \cdot \|B_K^{-1}\| \leq \frac{h_K h_{\hat{K}}}{\rho_K \rho_{\hat{K}}} \leq \sigma \frac{h_{\hat{K}}}{\rho_{\hat{K}}}$ . A simple calculation shows that  $h_{\hat{K}} = \sqrt{2}$  and  $\rho_{\hat{K}} = \frac{2}{2+\sqrt{2}}$ . Using these facts, we have

$$|u - \Pi_h u|_{H^m(K)} \leq \left[ C \left(1 + \frac{\sqrt{2}}{2}\right)^{2-m} (1 + \sqrt{2})^m \right] \sigma^m h^{2-m} |u|_{H^2(K)}$$

The result follows since the quantity in square brackets is a constant depending only on  $m$ .  $\square$

We are now ready to produce the first important estimate of the error between the solution to the variational problem in the whole space and the solution of the variational problem in the finite element space. In terms of the model problem, we plan to establish the error in approximating the solution of the model problem (M) by the solution of the

variational problem:

$$\left\{ \begin{array}{l} \text{Find } u_h \in P_h^1(\Omega) \cap H_0^1(\Omega) \text{ such that:} \\ \int_{\Omega} \nabla u_h \nabla v_h \, dx = \int_{\Omega} f v_h \, dx \\ \text{for every } v_h \in P_h^1(\Omega). \end{array} \right. \quad (M_h)$$

This result will show that the error, as measured in the  $H^1$ -norm, is on the order of  $h$  times the  $H^2$ -norm of  $u$  and will require an additional assumption which we explain now.

**Definition 2.1.15.** Let  $m \geq 1$ ,  $H_0^m(\Omega) \subset Y \subset H^m(\Omega)$  and suppose  $a(\cdot, \cdot)$  is a coercive bilinear form. Then the variational problem

$$a(u, v) = (f, v)_{L^2(\Omega)} \quad \forall v \in Y$$

is called  $H^s$ -regular if there exists a constant  $C$  such that for every  $f \in H^{s-2m}$  there is a solution  $u \in H^s(\Omega)$  with

$$\|u\|_{H^s(\Omega)} \leq C \|f\|_{H^{s-2m}(\Omega)}.$$

Remark: If  $a$  is an  $H_0^1(\Omega)$ -elliptic bilinear form with sufficiently smooth coefficient functions, and  $\Omega$  is a convex, polygonal domain then the Dirichlet problem is  $H^2$ -regular. So, the model problem is  $H^2$ -regular if  $\Omega$  is a convex polygon. We also remark that this is the first place where the convexity of  $\Omega$  has played a role. For more general results about the regularity of second order elliptic problems, see [10].

**Theorem 2.1.16.** *Suppose  $\Omega$  is a convex, polygonal domain and suppose  $\mathcal{T}_h$  is a family of regular triangulations of  $\Omega$  satisfying. Let  $u$  and  $u_h$  be the solutions of the abstract variational problems*

$$a(u, v) = \int_{\Omega} f v \, dx \, dy \quad \forall v \in H_0^1(\Omega) \quad (2.11)$$

$$\text{and} \quad (2.12)$$

$$a(u_h, v_h) = \int_{\Omega} f v_h \, dx \, dy \quad \forall v_h \in P_h^1(\Omega) \quad (2.13)$$

respectively, where  $a(\cdot, \cdot)$  is a continuous, coercive bilinear form on  $H_0^1(\Omega)$ ,  $f \in L^2(\Omega)$ ,

and  $P_h^1(\Omega)$  is the space of piecewise linear functions on  $\Omega$  defined previously (see Definition 2.1.10). Then if the variational problem (2.11) is  $H^2$ -regular, the finite element approximation  $u_h \in P_h^1(\Omega) \cap H_0^1(\Omega)$  satisfies:

$$\|u - u_h\|_{H^1(\Omega)} \leq Ch \|u\|_{H^2(\Omega)} \quad (2.14)$$

$$\leq Ch \|f\|_{L^2(\Omega)}. \quad (2.15)$$

*Proof.* A direct application of Cea's Lemma (Theorem 2.1.6) yields:

$$\|u - u_h\|_{H^1(\Omega)} \leq C \inf_{v \in H_0^1(\Omega)} \|u - v\|_{H^1(\Omega)}.$$

By Theorem 2.1.14, there exists  $v_h := \Pi_h u \in P_h^1(\Omega)$  such that:

$$\|u - v_h\|_{H^1(\Omega)} \leq Ch \|u\|_{H^2(\Omega)}.$$

Combining these two results gives (2.14). By definition of  $H^2$ -regular, there exists a constant  $C$  such that for every  $f \in L^2(\Omega)$ ,  $\|u\|_{H^2(\Omega)} \leq C \|f\|_{L^2(\Omega)}$ . Thus, (2.15) follows from (2.14).  $\square$

We now present another abstract result that will lead to a second estimate of the error between the solution to the variational problem in the whole space and the solution to the variational problem in the finite element space.

**Lemma 2.1.17** (Aubin-Nitsche Lemma). *Let  $a(\cdot, \cdot) : Y \times Y \rightarrow \mathbb{R}$  be a continuous, coercive form, and let  $f : Y \rightarrow \mathbb{R}$  be a continuous linear form. Let  $u$  and  $u_h$  be the solutions of the variational problems:*

$$a(u, v) = f(v) \quad \forall v \in Y$$

and

$$a(u_h, v_h) = f(v_h) \quad \forall v_h \in Y_h$$

respectively, where  $Y_h$  is a subspace of  $Y$ . Let  $H$  be a Hilbert space with norm  $|\cdot|_H$  and inner product  $(\cdot, \cdot)$  such that  $Y \hookrightarrow H$ . Denote the norm on  $Y$  (possibly different than

the norm on  $H$ ) by  $\|\cdot\|_Y$ . Then,

$$|u - u_h|_H \leq M \|u - u_h\|_Y \left( \sup_{g \in H} \left\{ \frac{1}{|g|_H} \inf_{\phi_h \in Y_h} \|\psi_g - \phi_h\|_Y \right\} \right), \quad (2.16)$$

where for any  $g \in H$ ,  $\psi_g \in Y$  is the unique solution of the variational problem:

$$a(v, \psi_g) = (g, v) \quad \forall v \in Y.$$

*Proof.* By Lax-Milgram, for each  $g \in H$ , there exists  $\psi_g \in Y$  such that  $\psi_g$  solves the variational problem  $a(v, \psi_g) = (g, v) \quad \forall v \in Y$ . Since  $u - u_h \in Y$ , in particular, we have:

$$a(u - u_h, \psi_g) = (g, u - u_h),$$

and since  $u, u_h$  solve the previously stated variational problems, we have

$$a(u - u_h, \phi_h) = 0 \quad \forall \phi_h \in Y_h.$$

Thus, by subtraction, we have:

$$a(u - u_h, \psi_g - \phi_h) = (g, u - u_h) \quad \forall \phi_h \in Y_h.$$

Therefore, by continuity of  $a(\cdot, \cdot)$ , for each  $\phi_h \in Y_h$ ,

$$\begin{aligned} |(g, u - u_h)| &= |a(u - u_h, \psi_g - \phi_h)| \\ &\leq M \|u - u_h\|_Y \cdot \|\psi_g - \phi_h\|_Y \end{aligned}$$

So,

$$|(g, u - u_h)| \leq M \|u - u_h\|_Y \inf_{\phi_h \in Y_h} \|\psi_g - \phi_h\|_Y.$$

Now, since  $H$  is a Hilbert space,  $F(g) = (g, u - u_h)$  is a linear operator and has operator norm  $|u - u_h|_H = \sup_{g \in H, g \neq 0} \frac{|(g, u - u_h)|}{|g|_H}$ . It follows that:

$$|u - u_h|_H \leq M \|u - u_h\|_Y \sup_{g \in H, g \neq 0} \left\{ \frac{1}{|g|_H} \inf_{\phi_h \in Y_h} \|\psi_g - \phi_h\|_Y \right\}.$$

□

**Corollary 2.1.18.** *Under the hypotheses of Theorem 2.1.16, if  $u \in H^1(\Omega)$  is the solution of (2.11) and  $u_h$  is the solution of (2.13), then*

$$\|u - u_h\|_{L^2(\Omega)} \leq Ch \|u - u_h\|_{H^1(\Omega)} \quad (2.17)$$

$$\leq Ch^2 \|f\|_{L^2(\Omega)} \quad (2.18)$$

*Proof.* Letting  $H = L^2(\Omega) = H^0(\Omega)$  and  $Y = H_0^1(\Omega)$ , we see that  $Y \subset H$  and since  $\|\cdot\|_{L^2(\Omega)} \leq \|\cdot\|_{H^1(\Omega)}$ , we have  $Y \hookrightarrow H$ . Letting  $Y_h = P_h^1(\Omega) \cap H_0^1(\Omega)$ , the Aubin-Nitsche Lemma (Lemma 2.1.17) implies that

$$\|u - u_h\|_{L^2(\Omega)} \leq C \|u - u_h\|_{H^1(\Omega)} \sup_{g \in L^2(\Omega)} \left\{ \frac{1}{\|g\|_{L^2(\Omega)}} \inf_{\phi_h \in P_h^1(\Omega) \cap H_0^1(\Omega)} \|\phi_g - \phi_h\|_{H^1(\Omega)} \right\}.$$

Now due to Theorem 2.1.16, the quantity in curly brackets is less than or equal to  $Ch$ , and the first result is immediate. Additionally, by (2.15) of Theorem 2.1.16,  $\|u - u_h\|_{H^1(\Omega)} \leq ch \|f\|_{L^2(\Omega)}$ , implying the second inequality. □

## 2.2 Error Estimates for Nonconvex Polygonal Domains

In Section 2.1, we confined our study to problems where the solution was very regular. In particular, the most important error estimates that we obtained, Theorem 2.1.16 and Corollary 2.1.18, relied on the fact that the problem was  $H^2$ -regular. In the case of the model problem, this conclusion can be made by assuming that the domain is convex. If we drop this assumption, we cannot guarantee that a solution to the model problem (M) is in  $H^2(\Omega)$ , and hence we will not achieve the same error estimate. Let us consider an example to demonstrate this point. This example can be found in Section 2.2 of [6].

Let  $D$  be the domain  $\{(x, y) \in \mathbb{R}^2 \mid x^2 + y^2 < 1\} \setminus \{(x, y) \in \mathbb{R}^2 \mid x > 0 \text{ and } y < 0\}$ , shown in figure 2.1. Identifying  $\mathbb{R}^2$  with  $\mathbb{C}$ ,  $D = \{re^{i\theta} \mid r < 1, 0 < \theta < \frac{3\pi}{2}\}$ . Consider

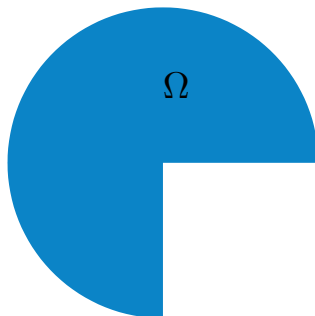


Figure 2.1: domain for (2.19)

solving the following problem on  $D$ :

$$\begin{cases} -\Delta u = 0 & \text{in } D \\ u(e^{i\phi}) = \sin\left(\frac{2\phi}{3}\right) & \text{for } 0 \leq \phi \leq \frac{3\pi}{2} \\ u = 0 & \text{elsewhere on } \partial D. \end{cases} \quad (2.19)$$

If we choose not to use the principal value for the argument of  $z$ , but instead take  $0 < \arg z \leq 2\pi$ , one sees that that  $w(z) := z^{\frac{2}{3}}$  is analytic in  $D$ , and thus its imaginary part, which we denote by  $u$  is harmonic in  $D$ . One may easily verify that  $u$  satisfies the boundary conditions, so  $u$  solves (2.19). Then,  $u \in H^1(D)$ , since

$$|u|_{H^1(D)}^2 = \frac{4}{9} \int_0^{\frac{3\pi}{2}} \int_0^1 r^{-\frac{2}{3}} r \, dr \, d\theta = \frac{\pi}{2},$$

but,  $u \notin H^2(D)$  since

$$|u|_{H^2(D)}^2 = \frac{20}{81} \int_0^{\frac{3\pi}{2}} \int_0^1 r^{-\frac{8}{3}} r \, dr \, d\theta = \infty.$$

Our goal in this section will be to obtain error estimates for the finite element approximation that apply to the model problem when  $\Omega$  is a nonconvex polygonal domain in the plane. Throughout most of this section, we will follow the line of proof given in Section 8.4 of [12], with some modifications made to allow more than one angle of  $\Omega$  to have measure greater than  $\pi$ . These results also appear in [3] under slightly different assumptions. As we proceed, we will try to point out the analogues to the presentation given in the previous section.

We begin by formally describing the domain  $\Omega$ . Throughout this section, we will assume  $\Omega \subset \mathbb{R}^2$  is a polygonal domain with boundary  $\Gamma$  composed of  $N$  sides. Starting at any one vertex, we label the vertices  $P_i$  in counter clockwise fashion, with the interior angle at vertex  $i$  having measure  $\theta_i$ . If the angle at the vertex has measure greater than  $\pi$ , we call this a **reentrant corner** of the domain. When we say that a point is at a reentrant corner of the domain, we mean that this point is the vertex of an angle created at the intersection of two edges of the boundary of the domain, and these edges form a reentrant corner. For example, in Figure 2.1, there is a reentrant corner at the origin since the measure of the angle interior to  $D$  at the origin has measure  $\frac{3\pi}{2}$ .

Recall that in section 1.4.3, we saw that the solution to the transmission problem with a prefractal layer that we are interested in applying our numerical methods to lies in a weighted Sobolev Space. So, our focus in this section will be to present convergence results for the finite element method for a problem with a solution in one of these weighted spaces. For a reminder of the definition of  $H^{2,\mu}(\Omega)$ , refer to definition 1.4.9.

Several proofs in the previous section relied on the inclusion of  $H^2(\Omega)$  in  $C(\overline{\Omega})$  and  $H^1(\Omega)$ . These results are given by the Sobolev Embedding Theorem (Theorem 2.1.1) and the Rellich-Kondrashev Theorem (Theorem 2.1.2). Similar results will be needed for the weighted space  $H^{2,\mu}(\Omega)$  and are provided by the next theorem.

**Theorem 2.2.1.** *For  $\mu < 1$ , the natural embedding of  $H^{2,\mu}(\Omega)$  into  $H^1(\Omega)$  is compact with respect to the norm  $\|\cdot\|_{H^{2,\mu}(\Omega)}$ , and additionally,  $H^{2,\mu}(\Omega)$  is continuously embedded in  $C(\overline{\Omega})$ .*

*Proof.* We begin by showing that  $H^{2,\mu}(\Omega) \hookrightarrow W^{2,p}(\Omega)$  for  $p$  such that  $1 < p < \frac{2}{\mu+1}$ . To this end, let  $u \in H^{2,\mu}(\Omega)$  and  $|\beta| = 2$ . Applying Hölder's Inequality to

$$\int_{\Omega} |\partial^{\beta} u|^p dx = \int_{\Omega} |r^{-\mu} (r^{\mu} \partial^{\beta} u)|^p dx$$

we have

$$\int_{\Omega} |r^{-\mu} (r^{\mu} \partial^{\beta} u)|^p dx \leq \left[ \int_{\Omega} (r^{-p\mu})^{\frac{2}{2-p}} dx \right]^{\frac{2-p}{2}} \left[ \int_{\Omega} |r^{\mu} \partial^{\beta} u|^2 dx \right]^{\frac{p}{2}}.$$

Since  $\Omega \subset \mathbb{R}^2$  is bounded, the first integral on the right hand side is bounded if  $\frac{-2p\mu}{2-p} > -2$ , which is true as long as  $1 < p < \frac{2}{\mu+1}$ . Furthermore, since this integral does not

depend on  $u$ , for a fixed  $p$ , the value is a constant depending only on  $\Omega$  so we have

$$\|u\|_{W^{2,p}(\Omega)}^p = \int_{\Omega} |\partial^\beta u|^p dx \leq C \left[ \int_{\Omega} |r^\mu \partial^\beta u|^2 dx \right]^{\frac{p}{2}}.$$

Since  $\Omega$  is bounded,  $H^1(\Omega) \hookrightarrow W^{1,p}(\Omega)$  for  $p < 2$ . Thus, for  $\mu < 1$ , we have  $\|\cdot\|_{W^{1,p}(\Omega)} \leq C \|\cdot\|_{H^1(\Omega)}$  for some constant  $C$ . Combined with the definition of  $\|\cdot\|_{W^{2,p}(\Omega)}^2$  as  $\|\cdot\|_{W^{1,p}(\Omega)}^2 + \|\cdot\|_{W^{2,p}(\Omega)}^2$ , it follows that

$$\|u\|_{W^{2,p}(\Omega)} \leq C \|u\|_{H^{2,\mu}(\Omega)}.$$

Thus,  $H^{2,\mu}(\Omega) \hookrightarrow W^{2,p}(\Omega)$  for  $p \in (1, \frac{2}{\mu+1})$ , where  $\mu < 1$ . By Theorem 2.1.3,  $W^{2,p}(\Omega) \hookrightarrow W^{1,p}(\Omega)$ , and as already stated,  $H^1(\Omega) \hookrightarrow W^{1,p}(\Omega)$ , so  $H^{2,\mu}(\Omega) \hookrightarrow H^1(\Omega)$ . Finally, the Sobolev Embedding Theorem (Theorem 2.1.1) gives us  $H^{2,\mu}(\Omega) \hookrightarrow W^{2,p}(\Omega) \hookrightarrow C(\bar{\Omega})$  if  $\mu < 1$ .  $\square$

**Remark:** Note that in the above proof, the actual expression for  $r$  was not very important. It was only necessary that  $\left[ \int_{\Omega} (r^{-p\mu})^{\frac{2-p}{2}} dx \right]^{\frac{2-p}{2}} < \infty$  for  $1 < p < \frac{2}{\mu+1}$ . So, it is clear that the inclusions hold for many choices of  $r$  besides the one made in Definition 1.4.9.

Now that we have shown that  $H^{2,\mu}(\Omega) \hookrightarrow C(\bar{\Omega})$ , we may define a linear interpolation operator on the space  $H^{2,\mu}(\Omega)$ , as was done before for the space  $H^2(\Omega)$  (see Definition 2.1.10). Although the definition is virtually identical in this case, the definition is repeated here for the sake of completeness and clarity.

**Definition 2.2.2.** Let  $K$  be a triangle with vertices  $z_1, z_2$  and  $z_3$  that is affine equivalent to the reference triangle  $\hat{K}$ . Then define the map  $\Pi_K : C(K) \rightarrow P^1(K)$  by letting  $\Pi_K(v)$  be the unique linear function  $\bar{v} \in P^1(K)$  such that  $\bar{v}(z_i) = v(z_i)$  for  $i = 1, 2, 3$ . By Lemma 2.2.1,  $H^{2,\mu}(\Omega) \hookrightarrow C(\bar{\Omega})$ . Thus every  $v \in H^{2,\mu}(\Omega)$  has a continuous representative  $\tilde{v}$ . If  $\mathcal{T}_h$  is a triangulation of  $\Omega$ , then define  $\Pi_h : H^{2,\mu}(\Omega) \rightarrow P_h^1(\Omega) \subset H^1(\Omega)$  to be the map satisfying  $\Pi_h(v) = \Pi_K(\tilde{v})$  for all  $v \in H^{2,\mu}(\Omega)$  and for all  $K \in \mathcal{T}_h$ . Recall that  $P_h^1(\Omega)$  is the space of functions that are continuous on all of  $\Omega$  and affine on each triangle  $K$  of the triangulation  $\mathcal{T}_h$ .

The next goal is to establish a result similar to Lemma 2.1.11 that gives the error in approximating a function  $u \in H^{2,\mu}(\hat{K})$  with a linear function on  $\hat{K}$ . The following lemma is so similar that an analogous proof can be used, so the proof is omitted here.

By the remark following Theorem 2.2.1, even though the lemma uses  $|x|$  instead of the function  $r$  specified in definition 1.4.9, the necessary inclusions still hold.

**Lemma 2.2.3.** *Let  $\hat{K}$  be the reference triangle with vertices  $z_1 = (0, 0)$ ,  $z_2 = (0, 1)$  and  $z_3 = (1, 0)$ . Let  $\mu < 1$  be given and let*

$$W := \left\{ v \in H^1(\hat{K}) : \sum_{|\beta|=2} \int_{\hat{K}} |\hat{x}|^{2\mu} |\partial^\beta v|^2 d\hat{x} < \infty \right\}.$$

*Then the linear interpolation operator  $\Pi_{\hat{K}} : W \rightarrow P^1(\hat{K})$  is well-defined and there exists a constant  $C$  such that*

$$\|u - \Pi_{\hat{K}} u\|_{H^1(\hat{K})}^2 + \sum_{\beta=2} \int_{\hat{K}} |\hat{x}|^{2\mu} |\partial^\beta u|^2 d\hat{x} \leq C \sum_{\beta=2} \int_{\hat{K}} |\hat{x}|^{2\mu} |\partial^\beta u|^2 d\hat{x} \quad (2.20)$$

for every  $u \in V$ .

The error estimate of Lemma 2.2.3 applies only to the reference triangle. As was the case in Section 2.1, in order to estimate the error in approximating a function  $u \in H^{2,\mu}(\Omega)$  with its piecewise affine interpolant  $\Pi_h u$  for a given triangulation of  $\Omega$ , the estimate must be extended to other triangles. So, as in Lemma 2.1.12, we use the relationship between a function  $v \in H^{2,\mu}(K)$  and the corresponding function  $\hat{v} = v \circ F$ , where  $F$  is the affine mapping from  $\hat{K} \rightarrow K$ . For this result, we require the following two additional assumptions about the family of triangulations  $\mathcal{T}_h$ .

Let  $\mathcal{T}_h$  be a regular triangulation of  $\Omega$ . For a fixed  $\mu$ , we have the properties:

**(T6)**  $h_K \leq \sigma h^{\frac{1}{1-\mu}}$  for every  $K \in \mathcal{T}_h$  having a vertex at a reentrant corner of the domain

**(T7)**  $h_K \leq C\sigma h \inf_{x \in K} r(x)^\mu$  for every  $K \in \mathcal{T}_h$  with no vertices at reentrant corners of the domain.

where  $\sigma$  is the regularity constant for the triangulation and  $C \geq 1$  is a positive constant, independent of  $h$ .

**Theorem 2.2.4.** *Let  $\mathcal{T}_h$  be a regular family of triangulations satisfying **(T6)** and **(T7)***

for some  $\mu < 1$ . Then there exists a constant  $C$ , independent of  $h$ , such that

$$\|u - \Pi_h u\|_{H^1(\Omega)} \leq Ch \left[ \sum_{|\beta|=2} \int_{\Omega} |r^\mu \partial^\beta u|^2 \right]^{1/2} \quad (2.21)$$

for every  $h > 0$  and every  $u \in H^{2,\mu}(\Omega)$ .

*Proof.* By definition of  $\Pi_h$ ,

$$\|u - \Pi_h u\|_{H^1(\Omega)}^2 = \sum_{K \in \mathcal{T}_h} \|u - \Pi_h u\|_{H^1(K)}^2,$$

so it suffices to establish the inequality

$$\|u - \Pi_h u\|_{H^1(K)}^2 \leq Ch^2 \sum_{|\beta|=2} \int_K |r(x)^\mu \partial^\beta u|^2 dx$$

for every  $K \in \mathcal{T}_h$  and some constant  $C$  independent of  $K$ . To that end, let  $K \in \mathcal{T}_h$  and consider two cases corresponding to the assumptions **(T6)** and **(T7)**.

**Case 1:** None of the vertices of  $K$  is at a reentrant corner of the domain.

Then for every  $x \in K$ ,  $r(x) > c_0 > 0$  and  $u|_K \in H^2(K)$ . So by Theorem 2.1.14 and using **(T6)**,

$$\begin{aligned} \|u - \Pi_K u\|_{H^1(K)}^2 &\leq C\sigma^2 h_K^2 |u|_{H^2(K)}^2 \\ &= C\sigma^2 h_K^2 \sum_{|\beta|=2} \int_K |r(x)^{-\mu} r(x)^\mu \partial^\beta u|^2 dx \\ &\leq C\sigma^2 h_K^2 \left( \inf_{x \in K} r(x)^{-2\mu} \right) \sum_{|\beta|=2} \int_K |r(x)^\mu \partial^\beta u|^2 dx \\ &\leq C\sigma^2 h_K^2 \left( \frac{\sigma h}{h_K} \right)^2 \sum_{|\beta|=2} \int_K |r(x)^\mu \partial^\beta u|^2 dx \\ &= C\sigma^4 h^2 \sum_{|\beta|=2} \int_K |r(x)^\mu \partial^\beta u|^2 dx, \end{aligned}$$

where  $C$  is independent of  $K$ .

**Case 2:**  $K$  has a vertex at a reentrant corner of the domain.

Let  $b_K$  denote the coordinates of the vertex of  $K$  at a reentrant corner of the

domain. Then by assumption (T5) on the triangulation  $\mathcal{T}_h$ , there exists a bijective map  $F_K : \hat{K} \rightarrow K$  defined by  $F_K(\hat{x}) = B_K \hat{x} + b_K$ , that maps  $b_K$  to the origin. Let  $\hat{u} = u \circ F_K$ . By Lemma 2.2.3,

$$\int_{\hat{K}} |\nabla(\hat{u} - \Pi_{\hat{K}} \hat{u})|^2 d\hat{x} \leq C \sum_{|\beta|=2} \int_{\hat{K}} |\hat{x}|^{2\mu} |\partial^\beta \hat{u}|^2 d\hat{x}. \quad (2.22)$$

Using the chain rule, this yields

$$\begin{aligned} \int_{\hat{K}} |B_K^T \nabla(u - \Pi_K u) \circ F_K|^2 d\hat{x} \\ \leq C \sum_{|\beta|=2} \int_{\hat{K}} |\hat{x}|^{2\mu} |(B_K^T)^2 \partial^\beta u \circ F_K|^2 d\hat{x}. \end{aligned} \quad (2.23)$$

Next, we perform a change of variables on each side of the inequality by setting  $x = F_K(\hat{x})$ . We obtain on the left hand side of (2.23),

$$\begin{aligned} \int_{\hat{K}} |B_K^T \nabla(u - \Pi_K u) \circ F_K|^2 d\hat{x} \\ = |\det B_K^{-1}| \int_K |B_K^T \nabla(u - \Pi_K u)|^2 dx \\ \geq |\det B_K^{-1}| \|B_K^{-1}\|^{-2} \int_K |\nabla(u - \Pi_K u)|^2 dx. \end{aligned} \quad (2.24)$$

Applying the change of variables to the integral on the right hand side of (2.23), we obtain for each  $|\beta| = 2$ ,

$$\begin{aligned} \int_{\hat{K}} |\hat{x}|^{2\mu} |(B_K^T)^2 \partial^\beta u \circ F_K|^2 d\hat{x} \\ \leq |\det B_K^{-1}| \|B_K\|^4 \int_K |B_K^{-1}(x - b_K)|^{2\mu} |\partial^\beta u|^2 dx \\ \leq |\det B_K^{-1}| \|B_K\|^4 \|B_K^{-1}\|^{2\mu} \int_K |x - b_K|^{2\mu} |\partial^\beta u|^2 dx. \end{aligned} \quad (2.25)$$

By definition,  $r(x) \geq |x - b_K|$ , so we have after combining (2.23), (2.24) and (2.25),

$$\int_K |\nabla(u - \Pi_K u)|^2 dx \leq \|B_K\|^4 \|B_K^{-1}\|^{2+2\mu} \sum_{|\beta|=2} \int_K |r(x)^\mu \partial^\beta u|^2 dx \quad (2.26)$$

Using the estimates derived in the proof of Theorem 2.1.14 and making use of assumption (T7), we have

$$\begin{aligned}
\|B_K\|^4 \|B_K^{-1}\|^{2+2\mu} &= (\|B_K\| \|B_K^{-1}\|)^{2+2\mu} \|B_K\|^{2-2\mu} \\
&\leq \left(\sigma \frac{h_{\hat{K}}}{\rho_{\hat{K}}}\right)^{2+2\mu} \left(\frac{h_K}{\rho_{\hat{K}}}\right)^{2-2\mu} \\
&\leq (\sigma h_{\hat{K}})^{2+2\mu} \rho_{\hat{K}}^{-4} \left(\sigma h^{\frac{1}{1-\mu}}\right)^{2-2\mu} \\
&= \sigma^4 h_{\hat{K}}^{2+2\mu} \rho_{\hat{K}}^{-4} h^2
\end{aligned}$$

Using this estimate in (2.26) gives:

$$\int_K |\nabla(u - \Pi_K u)|^2 dx \leq (\sigma^2 h_{\hat{K}}^{1+\mu} \rho_{\hat{K}}^{-2})^2 h^2 \sum_{|\beta|=2} \int_K |r(x)^\mu \partial^\beta u|^2 dx \quad (2.27)$$

which provides the desired result. □

**Corollary 2.2.5.** *Suppose  $\Omega$  is a nonconvex polygon in  $\mathbb{R}^2$ . Suppose  $\mathcal{T}_h$  is a regular family of triangulations for each  $h > 0$ , and  $\mathcal{T}_h$  satisfies (T6) and (T7) as  $h \rightarrow 0$ . Let  $u$  and  $u_h$  be solutions of the abstract variational problems*

$$a(u, v) = \int_{\Omega} f v \, dx \, dy \quad \forall v \in H_0^1(\Omega)$$

and

$$a(u_h, v_h) = \int_{\Omega} f v_h \, dx \, dy \quad \forall v_h \in P_h^1(\Omega)$$

respectively, where  $a(\cdot, \cdot)$  is a continuous, elliptic bilinear form on  $H_0^1(\Omega)$ ,  $f \in L^2(\Omega)$ , and  $u \in H^{2,\mu}(\Omega)$ . Then the finite element approximation  $u_h \in P_h^1(\Omega) \cap H_0^1(\Omega)$  satisfies:

$$\|u - u_h\|_{H^1(\Omega)} \leq Ch \|u\|_{H^{2,\mu}(\Omega)} \quad (2.28)$$

as  $h \rightarrow 0$ .

*Proof.* The assertion follows easily from (2.21) and Cea's Lemma (Theorem 2.1.6). □

**Remark:** This result is presented for comparison with Theorem 2.1.16. The above result shows that if the mesh is refined appropriately near the reentrant corners of the

domain, we can still achieve the same order of convergence in the  $H^1$ -norm for the less regular problem.



## Chapter 3

# Numerical Treatment of the Prefractal Transmission Problem

This chapter contains the original contributions of this thesis. In order to numerically solve the transmission problem  $(P_n^\alpha)$  using the finite element method, we must first have an algorithm to discretize the domain. The first section of this chapter will be devoted to introducing an algorithm for producing triangulations of the domains for each  $\alpha \in (2, 4)$  and each  $n \in \mathbb{N}$ . In the second section of the chapter, we will show that the triangulations produced by implementing this method satisfy the assumptions of Theorem 2.2.4, allowing us to give an estimate of the error made by numerically solving the problem. Finally, we will show some results of finite element solutions to  $(P_n^\alpha)$ .

Throughout this chapter, we will make use of a large amount of previously introduced notation. Because some readers familiar with the results of Chapter 2 may have chosen to bypass that chapter, we will recall all of the notation introduced there that will be used in the present chapter. For ease of reference for all readers, we will also recall some of the problem notation defined in Chapter 1 and preview some terminology related to the mesh generation that will be described in Section 3.1. The notation is shown in Table 3.1. Most of these terms, as well as some additional ones, can also be found in the lists of notation preceding Appendix A.

### 3.1 Generating the Mesh

Before giving the details of the algorithm, we will explain some of the considerations that shaped the algorithm. First of all, we must be able to reproduce the segments of

$\Omega$	the rectangular region $(0, 1) \times (-1, 1) \subset \mathbb{R}^2$
$\Sigma_n^\alpha$	the $n^{\text{th}}$ -generation prefractal von Koch curve with contraction factor $\alpha^{-1}$
$\Omega_{\alpha,n}^1$	the portion of $\Omega$ above $\Sigma_n^\alpha$
$\Omega_{\alpha,n}^2$	the portion of $\Omega$ below $\Sigma_n^\alpha$
$V_\alpha^n$	set of vertices of the $n^{\text{th}}$ -generation prefractal von Koch curve with contraction factor $\alpha^{-1}$
$R_{\alpha,n}$	set of points that are at reentrant corners of either $\Omega_{\alpha,n}^1$ or $\Omega_{\alpha,n}^2$ ; $R_{\alpha,n} = V_n^\alpha \setminus \{(0, 0), (1, 0)\}$
$h_K$	the length of the longest edge of a triangle $K$
$\rho_K$	the diameter of the largest circle contained in $K$
$\sigma$	the aspect ratio of a triangulation $\mathcal{T}_h$ , i.e. $\max_{K \in \mathcal{T}_h} \frac{h_K}{\rho_K}$
$r_n^i$	the weighting function given in definition 3.1.1
$\eta_n$	the minimum distance between vertices of the domain $\Omega_{\alpha,n}^i$ for $i = 1, 2$ ; $\eta_n = \alpha^{-n} \min(\alpha - 2, 1)$
$F$	the fractal region shown in Figure 3.3 and described in the surrounding text ( $F$ contains all points in $R_{\alpha,n}$ )
$\lambda$	$(\frac{1}{3})^{1/(1-\mu)}$

Table 3.1: Relevant Notation

$\Sigma_n^\alpha$  as the union of edges in the mesh. This is necessary, because in order to solve  $(P_n^\alpha)$ , we must be able solve the boundary value problem posed on  $\Sigma_n^\alpha$ . So, we must have a triangulation  $\mathcal{T}$  of  $\Omega$  such that  $\mathcal{T} = \mathcal{T}_1 \cup \mathcal{T}_2$ , where  $\mathcal{T}_1$  is a triangulation of  $\Omega_{\alpha,n}^1$  and  $\mathcal{T}_2$  is a triangulation of  $\Omega_{\alpha,n}^2$ .

Secondly, throughout this chapter, we will be considering the numerical solution of the problem  $(P_n^\alpha)$ , where both  $\alpha$  and  $n$  are fixed. However, since  $\alpha$  can be chosen arbitrarily from the interval  $(2, 4)$ , it is desirable to design an algorithm that can be used for any value of  $\alpha$ . In [27], a discretization and refinement scheme is developed for the problem  $(P_n^\alpha)$  with  $\alpha = 3$ . In this case, it is possible to create a mesh consisting entirely of equilateral triangles which have the best possible aspect ratio. However, as the value of  $\alpha$  approaches 2, very small angles are necessarily introduced into the mesh by the presence of the von Koch curve (see for example Figure 1.4). So, the discretization developed in [27] will not be applicable and we must develop a more general algorithm for creating a mesh for the problem.

Aside from letting  $\alpha$  vary in the interval  $(2,4)$ , any algorithm developed to create a mesh of  $\Omega_{\alpha,n}^1$  and  $\Omega_{\alpha,n}^2$  must be able to handle any integer value of  $n$ . Although  $n$  will also be fixed throughout this chapter when a particular problem is being considered, recall that the prefractal transmission problem  $(P_n^\alpha)$  was introduced in Section 1.4 as an approximation to the fractal transmission problem  $(P^\alpha)$ . One of our eventual goals is to study what happens to the solution to  $(P_n^\alpha)$  as  $n \rightarrow \infty$ . Since the vertices of the prefractal curve are always inherited from the previous iteration, we can take advantage of this structure to design a more efficient approach to the meshing procedure. Specifically, we will outline a procedure for triangulating the domains in such a way that a triangulation that includes  $\Sigma_n^\alpha$  as an interface also includes  $\Sigma_m^\alpha$  for  $m \leq n$ . Keeping in mind these considerations, we proceed to the explanation of the procedure for generating a mesh for the problem.

#### 1. DEFINE THE DOMAIN.

Having already chosen  $\alpha \in (2, 4)$  and  $n \in \mathbb{N}$ , apply the maps that generate the von Koch curve  $n$  times to produce the  $n^{\text{th}}$ -generation prefractal curve  $\Sigma_n^\alpha$ .

While the vertices of the prefractal curve are inherited from the previous generation, the segments linking the vertices are not maintained from one generation to the next. This can be seen by comparing Figures 3.1a and 3.1b. So, if the triangulation of the domain with interface  $\Sigma_n^\alpha$  is also to be a triangulation of the

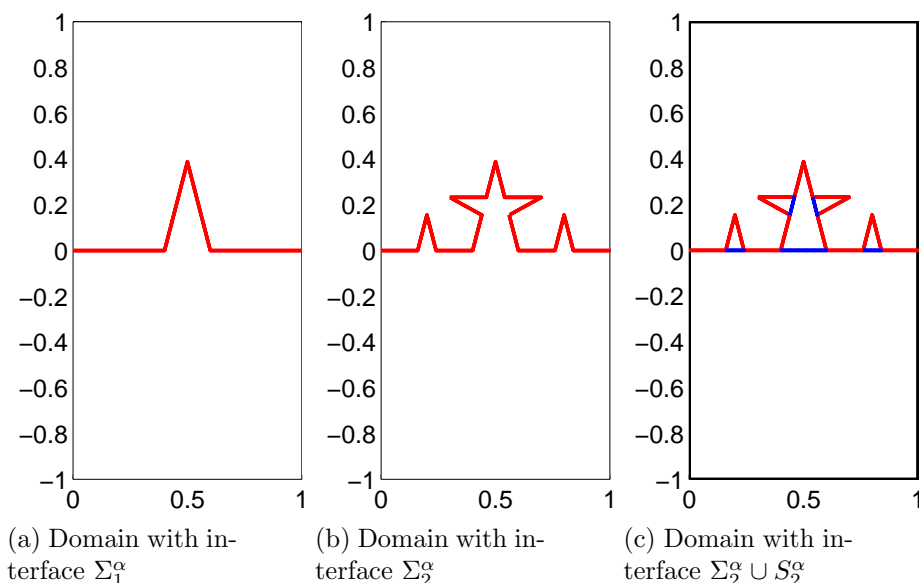


Figure 3.1: Illustration of  $S_n^\alpha$  with  $\alpha = 2.5$  and  $n = 2$

domain with interface  $\Sigma_m^\alpha$  for  $m \leq n$ , we must ensure that the segments joining vertices of the prefractal curve at previous generations are part of the mesh at this generation. To achieve this, let  $S_0^\alpha$  be the segment along the  $x$ -axis from  $\alpha^{-1}$  to  $1 - \alpha^{-1}$ . Then for  $m \geq 1$ , define

$$S_m^\alpha = \bigcup_{i=1}^4 \psi_i^\alpha(S_{m-1}^\alpha).$$

Then  $\Sigma_m^\alpha \subset \Sigma_n^\alpha \cup S_n^\alpha$  for  $m \leq n$ . Figures 3.1a and 3.1b show the domain with interface  $\Sigma_m^\alpha$  for  $m = 1$  and  $m = 2$ , respectively. In Figure 3.1c, the domain is shown with the interface  $\Sigma_2^\alpha$  in red and the segments comprising  $S_2$  shown in blue. Considering the group of Figures 3.1a, 3.1b, and 3.1c one verifies that  $\Sigma_1^\alpha \subset \Sigma_2^\alpha \cup S_2$ .

## 2. PRODUCE A COARSE MESH OF THE DOMAIN.

In this step, the goal is to produce a coarse mesh of the domain that includes  $\Sigma_n^\alpha \cup S_n$  as edges in the mesh. Since the curve  $\Sigma_n^\alpha$  varies significantly depending on the value of  $\alpha$ , a procedure that will triangulate the domain given any value of  $\alpha$  must be very general.

We use the Triangle program (a freely available 2-D mesh generator) to create a coarse mesh. For details of the algorithms used in the implementation, see [24] and

[25]. This program was chosen for a variety of reasons including its ease of use, its adept handling of very general polygonal domains, and its ability to control the quality of the mesh. The last feature, being able to control the quality of the mesh, is especially useful for error estimation.

The quality of the mesh is ensured by specifying a minimum acceptable angle for the triangulation. No triangles produced by the program will have a minimum angle smaller than the specified angle. In Appendix B, a proof is provided to show that enforcing a minimal angle constraint on the triangulation bounds the aspect ratio for the triangulation. Since the finite element approximation deteriorates as the regularity parameter of the triangulation increases, we wish to use as large an angle as possible. However the angles that appear at the vertices of the prefractal curve provide a bound on the minimum angle that we must be willing to accept in our triangulation. Recalling that  $\theta = \cos^{-1}(\frac{\alpha}{2} - 1)$  is the measure of the small angles appearing where the blue and red segments in Figure 3.1c meet, one sees that angles measuring  $\theta$  and  $\pi - 2\theta$  appear naturally. The algorithm in the Triangle program requires that the minimum angle be no greater than  $\frac{\pi}{3}$ , so we set the minimum angle for the triangulation to be  $\min\{\theta, \pi - 2\theta, \frac{\pi}{3}\}$ .

An example of a mesh created by the Triangle program with this minimum angle constraint can be seen in Figure 3.2. These figures demonstrate that the mesh serves as a triangulation of the domain with either  $\Sigma_1^\alpha$  or  $\Sigma_2^\alpha$  serving as the layer.

### 3. REFINE THE MESH.

In order to apply the error estimate in Theorem 2.2.4, the mesh must be a shape-regular triangulation of  $\Omega$  (see definitions 2.1.9 and 2.1.13) such that for  $i = 1, 2$ , the mesh restricted to  $\Omega_{\alpha,n}^i$  is a triangulation of  $\Omega_{\alpha,n}^i$  that satisfies

$$h_K \leq \sigma h^{\frac{1}{1-\mu_i}} \quad \text{if } K \text{ has a vertex at a reentrant corner of } \Omega_{\alpha,n}^i \quad (\text{T6}^*)$$

$$h_K \leq C\sigma h \inf_{x \in K} [r_n^i(x)]^{\mu_i} \quad \text{otherwise} \quad (\text{T7}^*)$$

where  $\mu_i$  is the weight given in Theorem 1.4.10 and  $C$  is a constant greater than 1. While the mesh generated in the previous step is guaranteed to be a shape-regular triangulation of  $\Omega$  and its restriction to  $\Omega_{\alpha,n}^i$  is a triangulation of  $\Omega_{\alpha,n}^i$ , we will perform at least one refinement of the mesh so that it also satisfies (T6\*) and (T7\*).

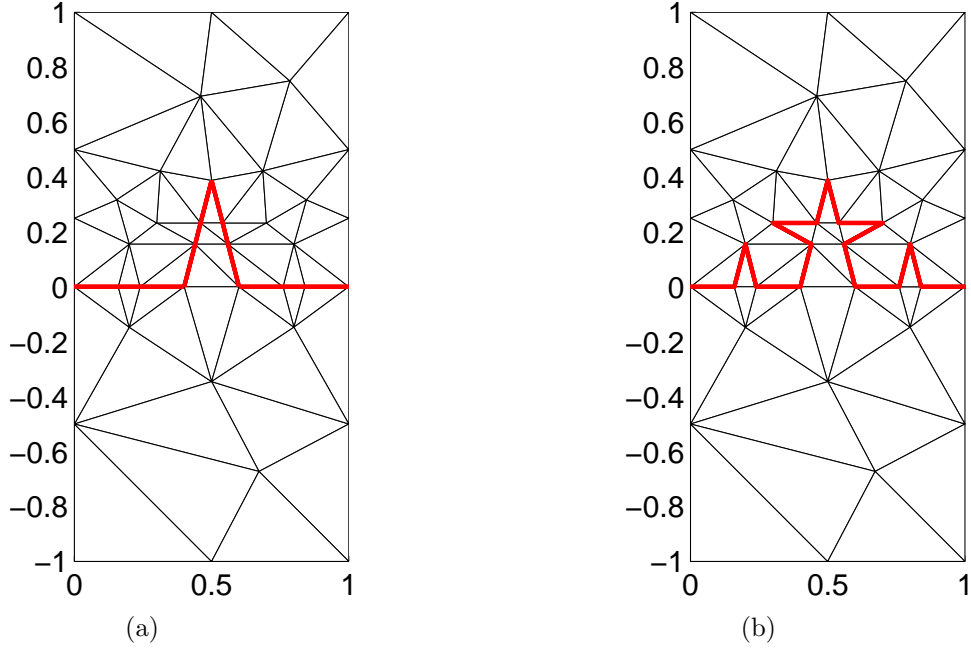


Figure 3.2: Coarse mesh of domain with interface (a)  $\Sigma_1^\alpha$  and (b)  $\Sigma_2^\alpha$ ,  $\alpha = 2.5$

To explain the refinement procedure, we first notice that the above conditions depend on the weighting function appearing in Definition 1.4.9 of weighted Sobolev spaces on polygonal domains. Since the definition given there was for a general polygon, to avoid any confusion, we will repeat the definition of the weighting function for the case in which the polygon is  $\Omega_{\alpha,n}^i$  for  $i = 1, 2$ . In this definition, we make use of the minimum distance between vertices of the domain calculated in Appendix B.2.

**Definition 3.1.1.** Let  $Q = \Omega_{\alpha,n}^i$  for  $i = 1$  or  $i = 2$ ,  $\alpha \in (2, 4)$  and  $n \in \mathbb{N}$ . Let  $R$  consist of the vertices of  $Q$  that are reentrant to  $Q$  and let

$$\eta_n = \frac{1}{4} \alpha^{-n} \min\{\alpha - 2, 1\}. \quad (3.1)$$

Then for  $x \in Q$ , define

$$r_n^i(x) = \begin{cases} |x - P| & \text{if } x \in B(P, \eta_n) \text{ for some } P \in R \\ 1 & \text{if } x \notin \bigcup_{P \in R} B(P, 2\eta_n) \\ \frac{1-\eta_n}{\eta_n} (|x - P| - \eta_n) + \eta_n & \text{otherwise} \end{cases} \quad (3.2)$$

Since reentrant corners of  $\Omega_{\alpha,n}^i$  for  $i = 1, 2$  only occur at vertices of the prefractal von Koch curve, the definition for  $r_n^i$  implies that if  $T$  is a triangle in the mesh with  $\inf_{x \in T} |x - V_\alpha^n| > 2\eta_n$ , then  $\inf_{x \in T} r_n^i(x) = 1$  for  $i = 1, 2$ . For such a triangle, (T7\*) only requires that

$$h_T \leq C\sigma h. \quad (3.3)$$

Since  $C\sigma > 1$  and  $h = \max_{K \in \mathcal{T}} h_K$ , (3.3) clearly holds for any triangle in the mesh, so we only need to focus our refinement efforts on triangles that are very near to reentrant corners of the domain.

It would be difficult and computationally expensive to exactly determine which triangles of the mesh are within  $2\eta_m$  of a reentrant corner of the domain. Because one of our driving goals in designing the mesh is to generate a mesh that can be used for solving the prefractal transmission problem with interface  $\Sigma_m^\alpha$  for any  $m \leq n$ , we would also need to find all triangles within  $2\eta_m$  of reentrant corners of  $\Omega_{\alpha,m}^i$  for  $i = 1, 2$ . So, we take a simpler approach in which we define a polygonal subset of  $\Omega$  that will include all such triangles, but it may contain some triangles for which  $r_m^i(x) = 1$  for every  $m \leq n$ .

We begin by defining a pentagon, which we will henceforth refer to as the fractal region and denote simply by  $F$ , with vertices  $F_1 = (0, 2\eta_1)$ ,  $F_2 = (0, -2\eta_1)$ ,  $F_3 = (1, -2\eta_1)$ ,  $F_4 = (1, 2\eta_1)$ , and  $F_5 = (1/2, y_*)$ . The value of  $y_*$  is chosen so that the line from  $F_1$  to  $F_5$  and the line from  $F_4$  to  $F_5$  are tangent to the circle with radius  $2\eta_1$  around the point  $C = \left(\frac{1}{2}, \sqrt{\frac{1}{\alpha} - \frac{1}{4}}\right)$  and so that the pentagon formed by these points contains this circle around  $C$ . Since  $C$  is the point in  $V_\alpha^n$  for  $n \geq 1$  with the largest  $y$ -value, choosing the pentagon in this way ensures that it contains circles of radius  $2\eta_m$  around each point in  $V_\alpha^m$  for  $m \geq 1$ . In Figure 3.3, one sees the coarse mesh of Figure 3.2 with the boundary of the fractal region marked by heavy blue lines. Around each vertex of the prefractal curve, we see circles of radius  $2\eta_m$  where  $m$  is the smallest integer for which the point is in  $V_\alpha^m$ . The shaded triangles are those with at least one vertex in the fractal region. Thus the shaded region contains all triangles separated by a distance of less than  $2\eta_m$  from a vertex in  $V_\alpha^m$  for some  $m \leq n$ . With these triangles identified, we are finally able to describe the refinement process.

The process begins by refining all of the triangles with at least one vertex in the fractal region. Recall that (T6\*) and (T7\*) specify that triangles closest to

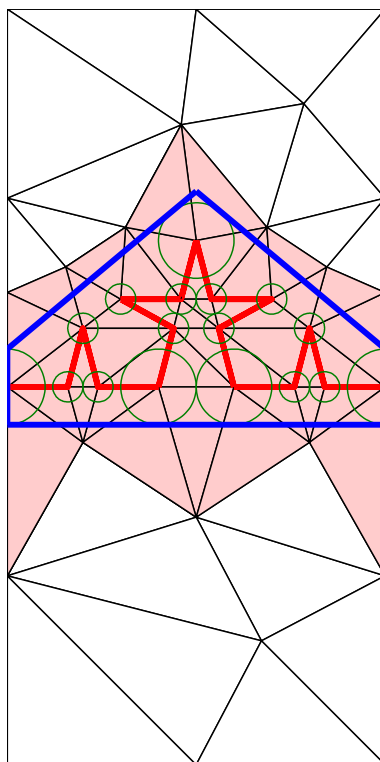


Figure 3.3: Fractal region,  $\alpha = 2.5$

any reentrant corner of the domain be smaller than those triangles that are some distance away. Also notice that each point in  $V_\alpha^n$ , with the exception of  $A = (0, 0)$  and  $B = (1, 0)$ , is the vertex of a reentrant corner of either  $\Omega_{\alpha,n}^1$  or  $\Omega_{\alpha,n}^2$ . Accordingly, the refinement will depend on the number of vertices each triangle has in  $V_\alpha^n \setminus \{A, B\}$ . Since this set will be used so frequently, we will use the notation  $R_{\alpha,n}$  to refer to it hereafter.

Figure 3.4 serves as a visual reference for the refinement of triangles with a vertex in the fractal region. Vertices at reentrant corners are marked with a red star. These subdivisions are easily explained in terms of barycentric coordinates. Let  $K$  be any triangle in the coarse mesh generated at the previous step with vertices  $V_1$ ,  $V_2$ , and  $V_3$  having barycentric coordinates  $(1, 0, 0)$ ,  $(0, 1, 0)$  and  $(0, 0, 1)$  respectively. Then a node with barycentric coordinates  $(c_1, c_2, c_3)$  is given by  $c_1V_1 + c_2V_2 + c_3V_3$ . For notational convenience in this explanation, let  $\lambda = (\frac{1}{3})^{\frac{1}{1-\mu}}$ , where  $\mu$  is chosen larger than  $\mu_1$  and  $\mu_2$ . Here,  $\mu_1$  and  $\mu_2$  are the weights used to describe the regularity of the problem  $(P_n^\alpha)$  in Theorem 1.4.7. Then if  $K$  has at least one vertex in the

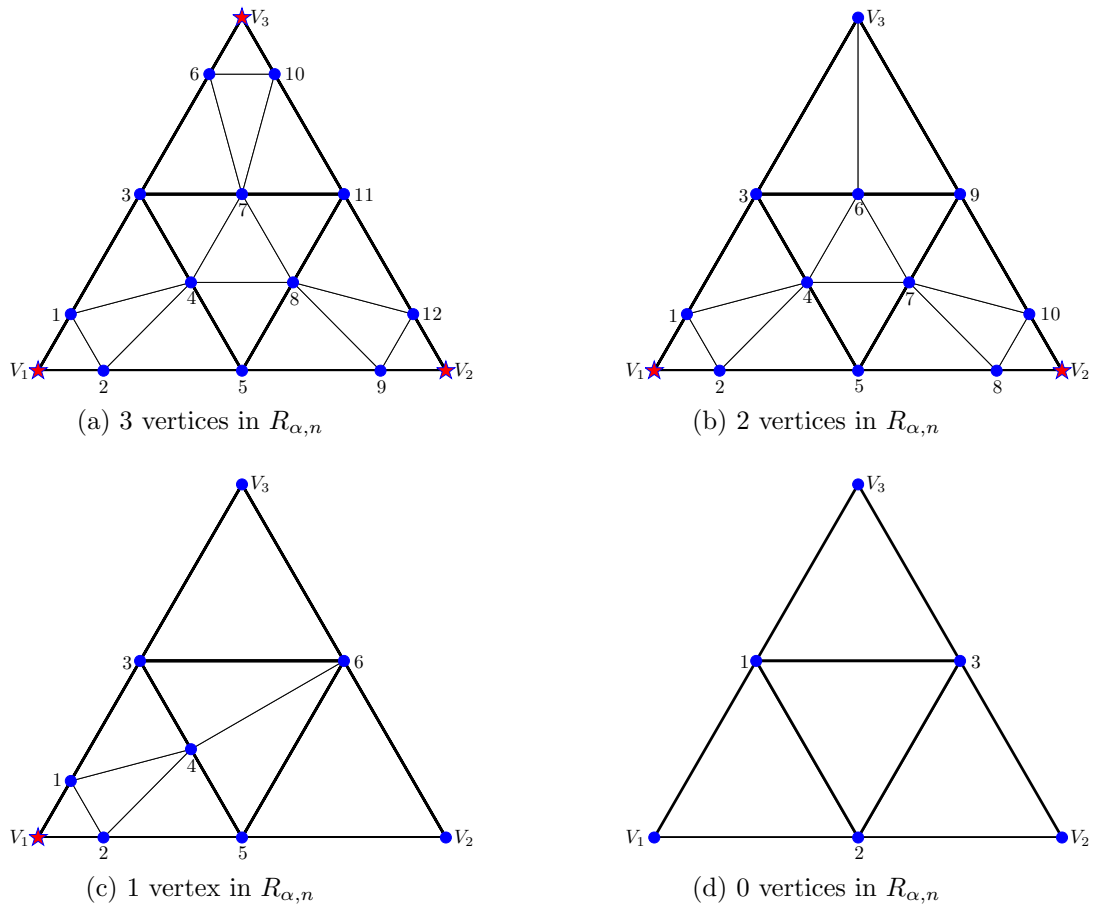


Figure 3.4: Refinement of coarse mesh according to number of vertices in  $R_{\alpha,n}$

fractal region,  $K$  is refined in one of the following four ways.

**3 vertices in  $R_{\alpha,n}$ :** The numbered nodes in Figure 3.4a are given by the following sets of barycentric coordinates.

$$\begin{array}{lll}
 N_1 = (1 - \lambda, 0, \lambda) & N_5 = \left(\frac{1}{2}, \frac{1}{2}, 0\right) & N_9 = (\lambda, 1 - \lambda, 0) \\
 N_2 = (1 - \lambda, \lambda, 0) & N_6 = (\lambda, 0, 1 - \lambda) & N_{10} = (0, \lambda, 1 - \lambda) \\
 N_3 = \left(\frac{1}{2}, 0, \frac{1}{2}\right) & N_7 = \left(\frac{1}{4}, \frac{1}{4}, \frac{1}{2}\right) & N_{11} = \left(0, \frac{1}{2}, \frac{1}{2}\right) \\
 N_4 = \left(\frac{1}{2}, \frac{1}{4}, \frac{1}{4}\right) & N_8 = \left(\frac{1}{4}, \frac{1}{2}, \frac{1}{4}\right) & N_{12} = (0, 1 - \lambda, \lambda)
 \end{array}$$

**2 vertices in  $R_{\alpha,n}$ :** Label the vertices of  $K$  so that  $V_1$  and  $V_2$  are the vertices of

$K$  that are also contained in  $R_{\alpha,n}$ . Then the numbered nodes in Figure 3.4b have the following barycentric coordinates.

$$\begin{aligned}
N_1 &= (1 - \lambda, 0, \lambda) & N_6 &= \left(\frac{1}{4}, \frac{1}{4}, \frac{1}{2}\right) \\
N_2 &= (1 - \lambda, \lambda, 0) & N_7 &= \left(\frac{1}{4}, \frac{1}{2}, \frac{1}{4}\right) \\
N_3 &= \left(\frac{1}{2}, 0, \frac{1}{2}\right) & N_8 &= (\lambda, 1 - \lambda, 0) \\
N_4 &= \left(\frac{1}{2}, \frac{1}{4}, \frac{1}{4}\right) & N_9 &= \left(0, \frac{1}{2}, \frac{1}{2}\right) \\
N_5 &= \left(\frac{1}{2}, \frac{1}{2}, 0\right) & N_{10} &= (0, 1 - \lambda, \lambda)
\end{aligned}$$

**1 vertex in  $R_{\alpha,n}$ :** Let  $V_1$  be the vertex of  $K$  in  $R_{\alpha,n}$ . Subdivide the triangle  $K$  so that the numbered nodes in Figure 3.4c have the specified barycentric coordinates.

$$\begin{aligned}
N_1 &= (1 - \lambda, 0, \lambda) & N_4 &= \left(\frac{1}{2}, \frac{1}{4}, \frac{1}{4}\right) \\
N_2 &= (1 - \lambda, \lambda, 0) & N_5 &= \left(\frac{1}{2}, \frac{1}{2}, 0\right) \\
N_3 &= \left(\frac{1}{2}, 0, \frac{1}{2}\right) & N_6 &= \left(0, \frac{1}{2}, \frac{1}{2}\right)
\end{aligned}$$

**0 vertices in  $R_{\alpha,n}$ :** The triangle  $K$  is subdivided into four congruent triangles by dividing each side of  $K$  in half as seen in Figure 3.4d.

With this part of the refinement complete, we now turn our attention to the triangles that do not intersect with the fractal region. As noted before, satisfying (T7\*) does not require any refinement of these triangles. However, the refinement of triangles with at least one vertex in the fractal region may result in hanging nodes, violating (T3), one of the requirements for a triangulation in definition 2.1.9. To maintain a conformal triangulation, it may be necessary to refine some of the triangles in the exterior of the fractal region, even though this is not necessitated by (T7\*).

The refinement procedure chosen for the remaining triangles is based on the obser-

vation that if a triangle  $K_1$  with no vertices in  $F$  shares an edge with a triangle  $K_2$  with at least one vertex in  $F$ , then  $K_1$  will have a hanging node at the midpoint of the shared edge. To see this, first note that any edge common to  $K_1$  and  $K_2$  cannot have an endpoint in  $R_{\alpha,n}$  since this would contradict the fact that  $K_1$  has no vertices in the fractal region. Thus  $K_2$  is refined as in Figure 3.4c or Figure 3.4d. Since  $K_1$  cannot share any edge of  $K_2$  with an endpoint in  $R_{\alpha,n}$ , the only new node on an edge shared by  $K_1$  and  $K_2$  occurs at the midpoint of the edge. If nothing was done to  $K_2$ , we would have a hanging node, violating assumption (T3) about the mesh. So, to maintain a conformal triangulation, we extend the refinement of the triangles in the fractal region to the entire domain by using an adaptive mesh refinement procedure introduced in [5] that suits our purposes well since hanging nodes are only created at the midpoints of edges. The procedure is explained below.

- (a) If  $K$  is a triangle in the mesh with two or more hanging nodes, subdivide  $K$  into four congruent subtriangles as in Figure 3.4d. Repeat as necessary until every triangle in the mesh has at most one hanging node.
- (b) If  $K$  has a single hanging node, create an edge from the hanging node to the vertex opposite it, bisecting  $K$  as shown in Figure 3.5. Edges created in this way are referred to as **green edges**.

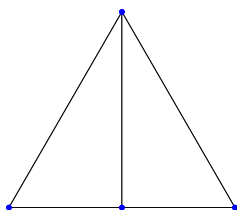


Figure 3.5: Subdivision by bisection

In Figure 3.6 one sees the result of applying the refinement procedure just outlined to the coarse mesh of Figure 3.2.

#### 4. REPEAT STEP 3 AS NECESSARY.

Knowing little about the coarse triangulation of the domain, it is not possible to know that one refinement of the mesh will suffice to satisfy (T6\*) and (T7\*). If the mesh produced by refining the coarse mesh once does not satisfy these assumptions,

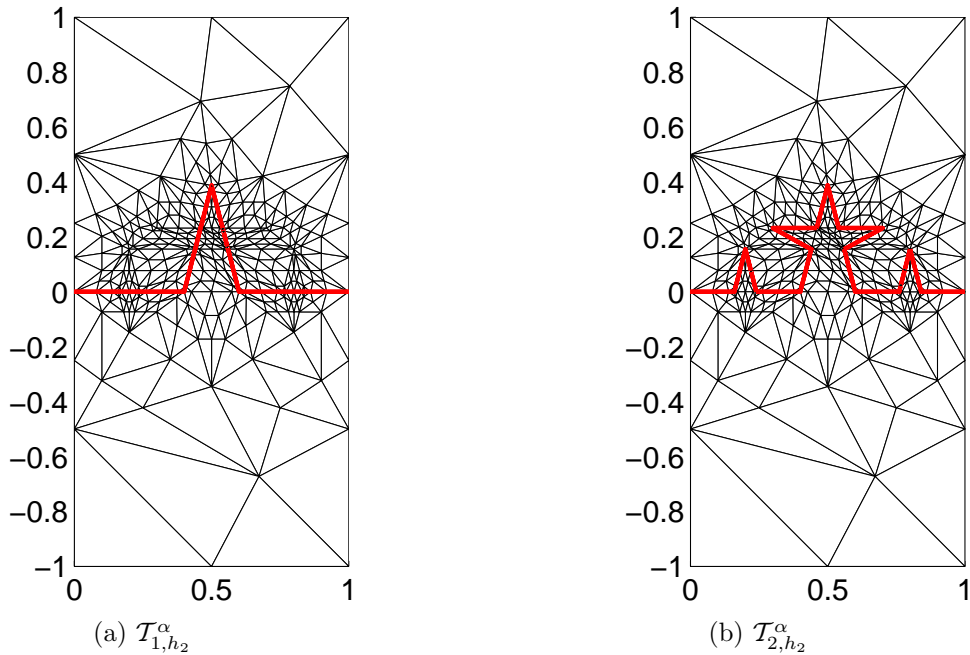


Figure 3.6: Refined mesh  $\mathcal{T}_{h_2}^\alpha$  with interface (a)  $\Sigma_1^\alpha$  and (b)  $\Sigma_2^\alpha$ ,  $\alpha = 2.5$

the refinement is repeated, with one small change. To avoid repeatedly bisecting the same angle of a triangle, which could result in a mesh that fails to be regular (see Definition 2.1.13), before refining any triangles in the exterior of the fractal region, all green edges are removed. As proved in [5], no triangle in the resulting mesh will have an angle that has been bisected more than once. In the next section it will be shown that after a finite number of such refinements of the coarse mesh, the resulting mesh satisfies (T6\*) and (T7\*). We refer to the mesh produced at the conclusion of this step as  $\mathcal{T}_{h_n}^\alpha$ .

**Remark:** In practice, it was never necessary to perform the refinement procedure more than once.

We wish to emphasize that  $\mathcal{T}_{h_n}^\alpha$  does not merely provide for a triangulation of  $\Omega_{\alpha,n}^1$  and  $\Omega_{\alpha,n}^2$ , but it also provides a triangulation of  $\Omega_{\alpha,m}^1$  and  $\Omega_{\alpha,m}^2$  for every  $m \leq n$ . We will now demonstrate a way in which we can exploit this fact. We remind the reader first that throughout this section  $\alpha$  and  $n$  are fixed. Now suppose that we have solved the problem  $(\tilde{P}_n^\alpha)$  numerically using the finite element method on the mesh  $\mathcal{T}_{h_n}^\alpha$ . When we are dealing with the finite element solution to any problem, the initial mesh considered may not be fine enough to give us a solution that is accurate enough for our specifications, so we may

wish to solve the same problem on a finer mesh to get a more accurate approximation to the solution. One way in which we could get a finer mesh would be to refine the mesh  $\mathcal{T}_{h_n}^\alpha$ . However, while at the moment we are focused on a fixed  $n$ , we must bear in mind that we wish to solve the problem  $(\tilde{P}_n^\alpha)$  for increasing values of  $n$ . So, if we instead use the above procedure to produce  $\mathcal{T}_{h_{n+1}}^\alpha$ , this new mesh will be a finer triangulation for the domain with interface  $\Sigma_n^\alpha$  and will also serve as a triangulation for the domain with interface  $\Sigma_{n+1}^\alpha$ . In this way, we can get more use out of each triangulation produced.

To emphasize this use of the same triangulation for domains with different generations of the prefractal curve, we use the more explicit notation  $\mathcal{T}_{m,h_n}^\alpha$  to refer to the mesh  $\mathcal{T}_{h_n}^\alpha$  being used as a triangulation of the domain  $\Omega$  with interface  $\Sigma_m^\alpha$ . Here  $m$  is the generation of the von Koch curve that is being considered as an interface in the transmission problem and  $n$  is the maximum generation of the prefractal curve for which this triangulation can be used to solve  $(\tilde{P}_n^\alpha)$ . Additionally,  $n$  can be thought of as the level of refinement of the mesh. This interpretation for  $n$  is justified since  $h_n$ , the length of the longest edge in  $\mathcal{T}_{h_n}^\alpha$ , is a decreasing sequence, so that  $\mathcal{T}_{m,h_k}^\alpha$  is a finer mesh of the domain with interface  $\Sigma_m^\alpha$  than  $\mathcal{T}_{m,h_j}^\alpha$  whenever  $m \leq j < k$ .

## 3.2 Properties of the Mesh

The primary goal of this section is to derive an estimate of the error made by using the finite element method to approximate the solution of  $(\tilde{P}_n^\alpha)$ . This result, stated in Theorem 3.2.6, will come fairly easily as a consequence of showing that the mesh created by the process detailed in Section 3.1 for each  $\alpha \in (2, 4)$  and each  $n \in \mathbb{N}$  satisfies the assumptions of Theorem 2.2.4.

Since most of the work will involve proving properties about the mesh, this section will rely heavily on understanding the refinement procedure introduced in the previous section. In particular, the refinements shown in Figures 3.4 and 3.5, and the accompanying explanations of these refinements in terms of barycentric coordinates will be referenced frequently. We will also often refer to the fractal region  $F$  pictured in Figure 3.3.

Before arriving at the eventual goal of this section, we will prove a number of preliminary results. The first result is a simple application of geometry that will be used in subsequent theorems to estimate the distance from a given triangle in the mesh to the nearest reentrant corner. For notational convenience in what follows, let the distance

between two sets  $A$  and  $B$  be written as  $d(A, B)$  and be defined as

$$d(A, B) := \inf_{\substack{x \in A \\ y \in B}} |x - y|.$$

**Lemma 3.2.1.** *Let  $K$  be a triangle with vertices  $V_1, V_2$  and  $V_3$  and aspect ratio  $\frac{h_K}{\rho_K} \leq \sigma$ . Use  $s_i$  to denote the side of  $K$  opposite  $V_i$  for each  $i \in \{1, 2, 3\}$  and let  $|K|$  denote the area of  $K$ . Then:*

$$d(\{V_i\}, s_i) > \rho_K \tag{3.4}$$

and

$$|K| > \frac{h_K^2}{2\sigma}. \tag{3.5}$$

*Proof.* By definition of  $\rho_K$  as the diameter of the largest circle that can be inscribed in  $K$ , it is clear that (3.4) holds. From basic geometry,  $\rho_K$  can be calculated as  $\frac{4|K|}{|\partial K|}$ , where  $|\partial K|$  is the perimeter of  $K$ . Since  $\frac{h_K}{\rho_K} \leq \sigma$  by assumption,

$$|K| \geq \frac{|\partial K| h_K}{4\sigma}. \tag{3.6}$$

Recalling that  $h_K$  is the length of the longest side of  $K$ , the sides of  $K$  have lengths  $l_1 \leq l_2 \leq l_3 = h_K$ . By the triangle inequality, we must have  $l_1 + l_2 > l_3$ , so  $|\partial K| > 2h_K$ , and (3.5) follows easily from (3.6).  $\square$

The next result quantifies the intuitive notion that refining a mesh by the algorithm in Section 3.1 results in a mesh that has smaller triangles near reentrant corners and larger triangles far away. This result will be critical to showing that the refinement procedure produces a triangulation that satisfies (T6\*) and (T7\*).

**Lemma 3.2.2.** *Let  $\alpha \in (2, 4)$  and  $n \in \mathbb{N}$  be given. Let  $\mathcal{T}$  be a triangulation of  $\Omega$  with the following properties:*

1. For each integer  $m \leq n$ ,  $\mathcal{T} \cap \Omega_{\alpha, m}^i$  is a triangulation of  $\Omega_{\alpha, m}^i$  for  $i = 1, 2$ ,
2.  $\mathcal{T}$  is shape-regular with aspect ratio  $\sigma$ , and
3.  $h_0 := \min_{K \in \mathcal{T}} h_k < \frac{1}{2} - \frac{1}{\alpha} \min(\alpha - 2, 1)$ .

Let  $\mathcal{T}^{(j)}$  denote the mesh produced by  $j$  refinements of  $\mathcal{T}$  by the procedure in Section 3.1 and let  $\mathcal{A}$  be the set

$$\{K \in \mathcal{T} \mid \text{if } K' \in \mathcal{T} \text{ and } K' \cap K \neq \emptyset \text{ then } K' \cap \overline{F} = \emptyset\}. \quad (3.7)$$

Then,  $\mathcal{A}$  is nonempty, and for each  $j \in \mathbb{N}$ :

$$\max_{\substack{K \in \mathcal{T}^{(j)} \\ K \cap \overline{F} \neq \emptyset}} h_K \leq 2^{-j} h_0 \quad (3.8)$$

and

$$h_j := \max_{K \in \mathcal{T}^{(j)}} h_K \geq 2^{-\lfloor j/2 \rfloor} \max_{K \in \mathcal{A}} h_K. \quad (3.9)$$

where  $F$  is the fractal region defined in Section 3.1 containing all reentrant corners of  $\Omega_{\alpha,n}^i$  for  $i = 1, 2$ .

*Proof.* To prove (3.8), suppose  $K \in \mathcal{T}$  is a triangle with  $K \cap \overline{F} \neq \emptyset$ . Then,  $K$  has at least one vertex in the fractal region, so  $K$  is refined according to one of the procedures shown in Figure 3.4. The heavy lines in each triangle of the figure highlight the subdivision of  $K$  into four congruent triangles by regular refinement. So, if  $K'$  is a triangle created in the refinement of  $K$ , then  $K'$  is contained in one of the four triangles with edges half the length of edges of  $K$ . It follows that  $h_{K'} \leq \frac{1}{2} h_K$ . Regardless of which one of these refinements is used to refine  $K$ , every vertex of  $K$  is the vertex of some triangle in  $\mathcal{T}^{(1)}$  created by refining  $K$ . Since  $K$  has at least one vertex in  $F$ , it follows that there exists  $K' \in \mathcal{T}^{(1)}$  such that  $K' \subset K$  and  $K'$  has a vertex in  $F$ . By the same argument made for  $K$ , any subtriangle created by refining  $K'$  has no edge longer than  $\frac{1}{2} h_{K'} \leq 2^{-2} h_K$ . Continuing this argument for an arbitrary number of refinements and making use of the definition of  $h_0$ , (3.8) follows.

The proof of (3.9) is considerably more involved. We begin by showing that  $\mathcal{A}$  is nonempty. Choose  $K \in \mathcal{T}$  to be a triangle with at least one vertex on the line  $y = -1$ . Such a triangle must exist since  $\mathcal{T}$  is a triangulation of  $(0, 1) \times (-1, 1)$ . Since  $h_0$  represents the length of the longest edge of any triangle in  $\mathcal{T}$ , the triangle  $K$  must be contained in  $\Omega$  below the line  $y = -1 + h_0$ . So, if  $K'$  is a triangle in  $\mathcal{T}$  sharing a vertex with  $K$ , then  $K'$  must be below the line  $y = -1 + 2h_0$ . From the assumption that  $h_0 < \frac{1}{2} - \frac{1}{\alpha} \min(\alpha - 2, 1)$ , we have  $K'$  below the line  $y = -\frac{2}{\alpha} \min(\alpha - 2, 1)$ . Noticing that  $\frac{1}{\alpha} \min(\alpha - 2, 1) = \eta_1$  and

by definition of  $F$ , the lower boundary of  $F$  is the line  $y = -2\eta_1$ , we see that  $K' \cap \overline{F} = \emptyset$ . Thus, we have shown that  $\mathcal{A} \neq \emptyset$ .

Now, to prove (3.9), choose  $K_1 \in \mathcal{A}$  and consider how  $K_1$  is refined. For this, it will be helpful to have a picture in mind. So, in Figure 3.7a one finds an example of such a triangle. Here,  $K_1$  is the triangle shaded gray and the triangles sharing a vertex with  $K_1$  are shown in yellow. For referencing purposes, let  $\mathcal{K}^1$  be the set  $\{K \in \mathcal{T} \mid K \cap K_1 \neq \emptyset\}$ .

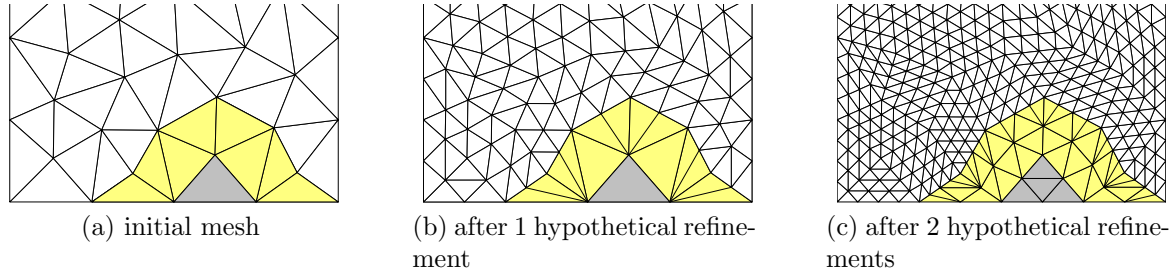


Figure 3.7: Illustration of refinement outside of  $F$

Then  $\mathcal{K}^1$  forms a polygon in  $\Omega$  with boundary  $\Gamma$ . For any  $T \in \mathcal{K}^1$ ,  $T$  can have at most one edge along  $\Gamma \setminus \partial\Omega$ . Now, suppose that  $\mathcal{T}$  is refined by the procedure of Section 3.1. From the refinement procedure, we see that the only hanging node  $T$  can have is at the midpoint an edge along  $\Gamma \setminus \partial\Omega$ . In the scenario that will produce the most refinement of  $\mathcal{K}^1$ , every triangle  $K \in \mathcal{K}^1$  with an edge on  $\Gamma \setminus \partial\Omega$  has a hanging node on this edge. So by the refinement process of Section 3.1, each of these triangles will be refined by adding an edge from the hanging node to the vertex opposite it, as in Figure 3.5. This refinement does not create any new hanging nodes, so it does not cause any additional triangles to be refined. In particular,  $K_1$  is not refined, so we have shown that  $h_1 \geq h_{K_1}$ . In Figure 3.7b, one sees the result of refining the mesh shown in Figure 3.7a under this hypothetical situation.

Suppose another refinement is necessary, and again, we envision the scenario which will result in the most refinement of triangles bordering  $K_1$ . After the previous refinement, every edge of a triangle  $T \in \mathcal{K}^1$  along  $\Gamma \setminus \partial\Omega$  was bisected forming two new edges. In the worst case, each of these newly created edges will also have a hanging node. So, from the refinement procedure of Section 3.1, the first step is to remove all of the so-called green edges. Recall that green edges are the edges created by joining the vertex of a triangle with the midpoint of the edge opposite it as in Figure 3.5. Once these green edges are removed, the triangles in  $\mathcal{T}$  with new hanging nodes will be divided into four congruent subtriangles in the normal way, and new green edges will be added to keep

the mesh conformal. Unlike the previous stage, this new refinement does create hanging nodes, so other triangles, including  $K_1$ , must be refined as in Figure 3.4d. This refinement divides  $K_1$  into 4 triangles, each similar to  $K_1$  but with lengths half the length of those in  $K_1$ . Thus,  $h_2 \geq \frac{1}{2}h_{K_1}$ . The result of this second hypothetical refinement is shown in Figure 3.7c.

To continue this argument for more refinements, let  $K_2$  be the triangle in the center of the refined  $K_1$  and let  $\mathcal{K}^2 = \{K \in \mathcal{T}^{(2)} \mid K \cap K_1 \neq \emptyset\}$ . Repeating the arguments made about refining  $K^1$ , we now see that  $h_3 \geq h_{K_2} = \frac{1}{2}h_{K_1}$  and  $h_4 \geq \frac{1}{2}h_{K_2} = 2^{-2}h_{K_1}$ . Thus  $K_1$  and its subtriangles are refined at most every other iteration. Since  $K_1 \in \mathcal{A}$  was arbitrary, (3.9) follows.  $\square$

The next theorem is where the bulk of the effort required to prove that the refinement procedure produces a mesh satisfying (T6\*) and (T7\*) is concentrated. As such, the proof is lengthy, detailed, and will require the two previous results of this section and a good understanding of the refinement procedure. In particular, Figure 3.4, and the description of the refinement in terms of barycentric coordinates that accompanies it, will be of great importance and will be referenced often.

**Theorem 3.2.3.** *Let  $\alpha \in (2, 4)$ ,  $n \in \mathbb{N}$ , and  $\mu \in (0, 1)$  be given. Let  $\mathcal{T}$  be a triangulation of  $\Omega$  with the following properties:*

1. *For each  $m \leq n$ ,  $\mathcal{T} \cap \Omega_{\alpha, m}^i$  is a triangulation of  $\Omega_{\alpha, m}^i$  for  $i = 1, 2$ ,*
2.  *$\mathcal{T}$  is shape-regular with aspect ratio  $\sigma$ ,*
3.  *$h_0 := \min_{K \in \mathcal{T}} h_K < \frac{1}{2} - \eta_1$ .*

*Let  $\mathcal{T}^{(j)}$  be the mesh produced by refining  $\mathcal{T}$  by the procedure in Section 3.1  $j$  times. Then, there exists  $j_* \in \mathbb{N}$  such that each  $K \in \mathcal{T}^{(j_*)}$  satisfies the following properties:*

$$h_K \leq \sigma h_*^{1/(1-\mu)} \quad \text{if } K \cap R_{\alpha, n} \neq \emptyset, \quad (3.10)$$

$$h_K \leq \sigma h_* d(K, R_{\alpha, n})^\mu \quad \text{if } K \cap R_{\alpha, n} = \emptyset \text{ and } K \cap \bar{F} \neq \emptyset, \quad (3.11)$$

*and for any integer  $m < n$ ,*

$$h_K \leq 3^{\mu/(1-\mu)} \sigma h_* d(K, R_{\alpha, m})^\mu \quad \text{if } K \cap R_{\alpha, m} = \emptyset \text{ and } K \cap \bar{F} \neq \emptyset \quad (3.12)$$

*where  $h_* = \min_{K \in \mathcal{T}^{(j_*)}} h_K$ .*

*Proof.* Begin by defining

$$\rho_0 := \min_{\substack{K \in \mathcal{T} \\ K \cap R_{\alpha,n} \neq \emptyset}} \rho_K \quad (3.13)$$

and let  $C_0 = h_0^{-1} \max_{K \in \mathcal{A}} h_K$ . Then choose  $j_* \in \mathbb{N}$  such that:

$$2^{\lfloor j_*/2 \rfloor} 3^{-j_*} \leq \sigma^{1-\mu} C_0 h_0^\mu \quad (3.14)$$

and

$$2^{\lfloor j_*/2 \rfloor} 2^{-j_*} \leq \sigma C_0 \rho_0^\mu. \quad (3.15)$$

Since conditions (3.10), (3.11), and (3.12) naturally separate the statement of the theorem into three cases, the proof will also follow this arrangement.

**Case 1:**  $K \in \mathcal{T}^{(j_*)}$  with  $K \cap R_{\alpha,n} \neq \emptyset$

Since  $\mathcal{T}^{(j_*)}$  is a refinement of  $\mathcal{T}$ , there exists a triangle  $K_0 \in \mathcal{T}$  such that  $K$  is created by refining  $K_0$ . The assumption that  $K \cap R_{\alpha,n} \neq \emptyset$  implies that  $K$  has a vertex in  $R_{\alpha,n}$ . Let us use  $P$  to denote this vertex. Using the fact that  $\mathcal{T} \cap \Omega_{\alpha,n}^i$  is a triangulation of  $\Omega_{\alpha,n}^i$  for  $i = 1, 2$ , every vertex of the prefractal curve  $\Sigma_n^\alpha$  is the vertex of a triangle in  $\mathcal{T}$ . Recalling that  $V_n^\alpha$  denotes the vertices of  $\Sigma_n^\alpha$  and that  $R_{\alpha,n} \subset V_n^\alpha$ ,  $P$  must also be a vertex of  $K_0$ .

Regardless of how many other vertices of  $K_0$  are in  $R_{\alpha,n}$ , when  $K_0$  is refined as specified in Section 3.1, exactly one subtriangle,  $K_1$ , will be created with a vertex at  $P$ .  $K_1$  will be similar to  $K_0$  and will have  $h_{K_1} = \lambda h_{K_0}$ . If  $j_* = 1$ , then  $K = K_1$ , but if  $j_* > 1$ , then  $K_1$  will be refined, creating a triangle  $K_2$  similar to  $K_1$ , with a vertex at  $P$ , and having  $h_{K_2} = \lambda h_{K_1} = \lambda^2 h_{K_0}$ . Continuing this argument,  $K$  will result from  $j_*$  refinements of  $K_0$  and  $h_K = \lambda^{j_*} h_{K_0}$ . From Lemma 3.2.2, we know that  $h_* \geq 2^{-\lfloor j_*/2 \rfloor} C_0 h_0$ . Thus, using (3.14) and recalling that  $\lambda = (\frac{1}{3})^{1/(1-\mu)}$ , we

have

$$\begin{aligned}
\sigma h_*^{1/(1-\mu)} &\geq \sigma (2^{-\lfloor j_*/2 \rfloor} C_0 h_0)^{1/(1-\mu)} \\
&\geq \sigma [(\sigma^{1-\mu} C_0 h_0^\mu 3^{j_*})^{-1} C_0 h_0]^{1/(1-\mu)} \\
&= \left[ \left( \frac{1}{3} \right)^{1/(1-\mu)} \right]^{j_*} h_0 \\
&= \lambda^{j_*} h_0 \geq h_K.
\end{aligned}$$

So, (3.10) is satisfied.

**Case 2:**  $K \in \mathcal{T}^{(j_*)}$  with  $K \cap R_{\alpha,n} = \emptyset$  and  $K \cap \overline{F} \neq \emptyset$

Since  $K \cap \overline{F} \neq \emptyset$ ,  $K$  has at least one vertex in the fractal region. Moreover, since  $K$  is an element of the refined mesh,  $K$  came from the refinement of a triangle  $K_0 \in \mathcal{T}$  with at least one vertex in  $\overline{F}$ . Although we know that  $K$  does not have a vertex in  $R_{\alpha,n}$ , from only this information, we cannot determine if  $K_0$  had a vertex in  $R_{\alpha,n}$ . This leads us to consider two separate subcases.

**Case 2a:**  $K \subset K_0 \in \mathcal{T}$  with  $K_0 \cap R_{\alpha,n} = \emptyset$ .

At the first stage of refinement,  $K_0$  is refined in the regular fashion by dividing  $K_0$  into four congruent subtriangles. One of these subtriangles, which we refer to as  $K_1$  must contain  $K$ , and  $h_{K_1} = \frac{1}{2}h_{K_0}$ . If  $j_* = 1$ , then  $K = K_1$ . Otherwise, since  $K \cap \overline{F} \neq \emptyset$  and  $K \subset K_1$ ,  $K_1 \cap \overline{F} \neq \emptyset$ . So, at the next refinement,  $K_1$  will be divided into four congruent subtriangles, one of which will contain  $K$ . Continuing this line of reasoning, there exists a sequence of triangles  $K_0 \supset K_1 \supset K_2 \supset \dots \supset K_{j_*-1} \supset K$  with  $h_{K_j} = 2^{-j}h_{K_0}$ . So,  $h_K = 2^{-j_*}h_{K_0}$ .

To see that (3.11) is satisfied, we must estimate  $\sigma h_* d(K, R_{\alpha,n})^\mu$ . From Lemma 3.2.1 and the definition of  $\rho_0$ , the distance from any vertex in  $R_{\alpha,n}$  to the edge opposite it is greater than  $\rho_0$ . Since  $K_0$  has no vertex at a reentrant corner, the distance from  $K_0$  to a reentrant corner must be greater than  $\rho_0$ . Then, since  $K \subset K_0$ , it follows that  $d(K, R_{\alpha,n}) > \rho_0$ . Thus, using (3.15) and

Lemma 3.2.2, we have

$$\begin{aligned}
\sigma h_* d(K, R_{\alpha, n})^\mu &> \sigma (2^{-\lfloor j^*/2 \rfloor} C_0 h_0) \rho_0^\mu \\
&\geq \sigma (\sigma C_0 \rho_0^\mu 2^{j^*})^{-1} C_0 h_0 \rho_0^\mu \\
&= 2^{-j^*} h_0.
\end{aligned}$$

Using this result along with the earlier conclusion that  $h_K = 2^{-j^*} h_{K_0}$ , and the fact, coming from the definition of  $h_0$ , that  $h_0 \geq h_{K_0}$ , (3.11) is satisfied.

**Case 2b:**  $K \subset K_0 \in \mathcal{T}$  with  $K_0 \cap R_{\alpha, n} \neq \emptyset$ .

Then, as in the previous case, there exists a sequence of triangles created by the refinement of  $K_0$  such that for each  $j < j_*$ ,  $K_j \in \mathcal{T}^{(j)}$  with  $K_j \cap \overline{F} \neq \emptyset$  and  $K_0 \supset K_1 \supset K_2 \supset \cdots \supset K_{j_*-1} \supset K$ . By the assumption that  $K_0 \cap R_{\alpha, n} \neq \emptyset$ , but  $K \cap R_{\alpha, n} = \emptyset$ , there exists some integer  $\tilde{j} \in [0, j_*)$  for which  $K_j$  has a vertex in  $R_{\alpha, n}$  if  $j \leq \tilde{j}$ , and  $K_j$  does not have a vertex in  $R_{\alpha, n}$  if  $j > \tilde{j}$ . From the argument made in Case 1 of the proof of this theorem, we deduce that

$$h_{K_{\tilde{j}}} = \lambda^{\tilde{j}} h_{K_0}. \quad (3.16)$$

Now, when  $K_{\tilde{j}}$  is refined according to the algorithm in Section 3.1, since  $K_{\tilde{j}} \cap R_{\alpha, n} \neq \emptyset$ ,  $K_{\tilde{j}}$  is refined as in Figure 3.4a, Figure 3.4b or Figure 3.4c. Using the same argument as in the proof of Lemma 3.2.2, the longest side of any subtriangle of  $K_{\tilde{j}}$ , has length no greater than  $\frac{1}{2} h_{K_{\tilde{j}}}$ . Thus, using (3.16),

$$h_{K_{\tilde{j}+1}} \leq \frac{1}{2} \lambda^{\tilde{j}} h_{K_0}. \quad (3.17)$$

For  $j \geq \tilde{j} + 1$ ,  $K_j$  has no vertices in  $R_{\alpha, n}$ , but since  $K_j \cap \overline{F} \neq \emptyset$ , if  $K_j$  is refined it will be refined as in Figure 3.4d, so that  $h_{K_{j+1}} = \frac{1}{2} h_{K_j}$ . Combining this with (3.17), we have

$$h_K \leq 2^{-(j_* - \tilde{j})} \lambda^{\tilde{j}} h_{K_0}. \quad (3.18)$$

To verify (3.11), it is necessary to approximate  $d(K, R_{\alpha, n})$ . Because of the nested nature of the sequence of triangles  $K_j$ , for any  $j \in [1, j_*)$ ,  $d(K_j, R_{\alpha, n}) \geq d(K_{j-1}, R_{\alpha, n})$ . By the definition of  $\tilde{j}$ , if  $j \leq \tilde{j}$ ,  $K_j$  has at least one vertex in

$R_{\alpha,n}$ , meaning that  $d(K_j, R_{\alpha,n}) = 0$ , while  $d(K_j, R_{\alpha,n}) > 0$  if  $j > \tilde{j}$ . Since the refinement process ensures that  $K_j$  is similar to  $K_0$  with a proportionality constant of  $\lambda^j$  if  $j \leq \tilde{j}$ , for  $j > \tilde{j}$ ,  $K_j$  is separated from any of the vertices in  $K_0$  that are also in  $R_{\alpha,n}$  by a triangle congruent to  $K_{\tilde{j}}$ . Thus, using Lemma 3.2.1,  $d(K, R_{\alpha,n} \cap K_0)$  is greater than  $\lambda^{\tilde{j}} \rho_{K_0} > \lambda^{\tilde{j}} \rho_0$ . To estimate  $d(K, R_{\alpha,n})$ , we must also consider  $d(K, R_{\alpha,n} \setminus K_0)$ . In this case, Lemma 3.2.1 and the definition of  $\rho_0$  imply that  $d(K_0, R_{\alpha,n} \setminus K_0) > \rho_0$ , and consequently,  $d(K, R_{\alpha,n} \setminus K_0) > \rho_0$ . Thus, we conclude that  $d(K, R_{\alpha,n}) > \lambda^{\tilde{j}} \rho_0$ . Using this result, (3.15), Lemma 3.2.2, and the definition of  $\lambda$ , we have:

$$\begin{aligned}
\sigma h_* d(K, R_{\alpha,n})^\mu &\geq \sigma (2^{-\lfloor j^*/2 \rfloor} C_0 h_0) (\lambda^{\tilde{j}} \rho_0)^\mu \\
&\geq \sigma (\sigma C_0 \rho_0^\mu 2^{j^*})^{-1} C_0 h_0 (\lambda^{\tilde{j}} \rho_0)^\mu \\
&= 2^{-j^*} (\lambda^\mu)^{\tilde{j}} h_0 \\
&= 2^{-(j^*-\tilde{j})} 2^{-\tilde{j}} \lambda^{\tilde{j}} (\lambda^{\mu-1})^{\tilde{j}} h_0 \\
&= \left(\frac{3}{2}\right)^{\tilde{j}} 2^{-(j^*-\tilde{j})} \lambda^{\tilde{j}} h_0.
\end{aligned}$$

From, (3.18), we see that (3.11) holds in this case as well.

**Case 3:**  $K \in \mathcal{T}^{(j^*)}$  with  $K \cap R_{\alpha,m} = \emptyset$ ,  $K \cap \bar{F} \neq \emptyset$  and  $m < n$ .

For the final case, we will make use of (3.10) and (3.11), which we have already shown. However, both of these results depend on whether  $K$  has a vertex in  $R_{\alpha,n}$  and although we know  $K \cap R_{\alpha,m} = \emptyset$ , since  $R_{\alpha,m}$  is a strict subset of  $R_{\alpha,n}$ , we cannot determine if  $K$  has any vertices in  $R_{\alpha,n}$ . So, we consider two subcases.

**Case 3a:**  $K \cap R_{\alpha,n} = \emptyset$ .

Using the fact that  $R_{\alpha,m} \subset R_{\alpha,n}$ , we have

$$d(\{x\}, R_{\alpha,n}) \leq d(\{x\}, R_{\alpha,m})$$

for every  $x \in \Omega$ . Thus, (3.11) shows that (3.12) holds.

**Case 3b:**  $K \cap R_{\alpha,n} \neq \emptyset$ .

Then  $K$  has a vertex, call it  $V$ , in  $R_{\alpha,n}$ . From the argument presented in Case 1 of this proof, there exists  $K_0 \in \mathcal{T}$  such that  $V$  is a vertex of  $K_0$ ,  $K$  is

created by  $j_*$  refinements of  $K_0$ , and  $h_K = \lambda^{j_*} h_{K_0}$ . To determine if  $K$  satisfies (3.12), we must also find a bound for  $d(K, R_{\alpha,m})$ .

Even though  $K$  does not have a vertex in  $R_{\alpha,m}$ , it is still possible that  $K_0$  does. If  $K_0$  does have a vertex  $P \in R_{\alpha,m}$ , then  $K_0$  has at least two vertices in  $R_{\alpha,n}$ , so  $K_0$  is refined as in Figure 3.4a or Figure 3.4b. Regardless of which of the two refinements is performed, there exist distinct triangles  $K_P$  and  $K_Q$  created by refining  $K_0$  such that  $K_P$  has a vertex at  $P$  and  $K_Q$  has a vertex at  $K_Q$ . From the description of the refinement in terms of barycentric coordinates, both  $K_P$  and  $K_Q$  are similar to  $K_0$  with a proportionality constant of  $\lambda$ . So, using Lemma 3.2.1, the distance from  $Q$  to a point in  $K \setminus K_Q$  is greater than  $\lambda\rho_{K_0} > \lambda\rho_0$ . It is evident that  $K \subseteq K_P \subset (K_0 \setminus K_Q)$ , so

$$d(K, R_{\alpha,m} \cap K_0) > \lambda\rho_0. \quad (3.19)$$

In order to evaluate  $d(K, R_{\alpha,m})$ , we must also consider  $d(K, R_{\alpha,m} \setminus K_0)$ . From previous arguments, any point in  $R_{\alpha,m} \setminus K_0$  is the vertex of a triangle  $K_1 \neq K_0 \in \mathcal{T}$  and by Lemma 3.2.1,

$$\rho_0 < d(K_0, R_{\alpha,m} \setminus K_0) < d(K, R_{\alpha,m} \setminus K_0). \quad (3.20)$$

So, combining (3.19) and (3.20), and noticing that  $\lambda < 1$  for any value of  $\mu \in (0, 1)$ ,

$$d(K, R_{\alpha,m}) \geq \lambda\rho_0. \quad (3.21)$$

Using (3.21), Lemma 3.2.2, (3.15), and the definition of  $\lambda$ ,

$$\begin{aligned} \sigma h_* d(K, R_{\alpha,m})^\mu &\geq \sigma h_*(\lambda\rho_0)^\mu \\ &\geq \sigma(2^{-\lfloor j_*/2 \rfloor} C_0 h_0)(\lambda\rho_0)^\mu \\ &\geq \sigma(\sigma C_0 \rho_0^\mu 2^{j_*})^{-1} C_0 h_0 (\lambda\rho_0)^\mu \\ &= \lambda^\mu 2^{-j_*} h_0. \end{aligned}$$

Recalling that  $\mu = (\frac{1}{3})^{1/(1-\mu)}$ ,  $2^{-j_*} \geq \lambda^{j_*}$  and  $\lambda^{-\mu} = 3^{\mu/(1-\mu)}$

$$\sigma h_* d(K, R_{\alpha,m})^\mu \geq 3^{-\mu/(1-\mu)} \lambda^{j_*} h_0.$$

From the earlier conclusion that  $h_K \leq \lambda^{j^*} h_{K_0}$ , and the fact that  $h_0 \geq h_{K_0}$ , (3.12) follows. □

With all of the previous results established, we are finally ready to show that the mesh created by refining a coarse mesh for the problem satisfies the assumptions of Theorem 2.2.4.

**Theorem 3.2.4.** *Let  $\alpha \in (2, 4)$  and  $n \in \mathbb{N}$  be given. Let  $\theta = \cos^{-1}(\frac{\alpha}{2} - 1)$ , and let  $\mu_1 > \frac{2\theta}{\pi+2\theta}$  and  $\mu_2 > \frac{\theta}{\pi+\theta}$  be given. Suppose  $\mathcal{T}$  is a triangulation of  $\Omega$  satisfying:*

1. *For each  $m \leq n$ ,  $\mathcal{T} \cap \Omega_{\alpha, m}^i$  is a triangulation of  $\Omega_{\alpha, m}^i$  for  $i = 1, 2$ ,*
2.  *$\mathcal{T}$  is shape-regular with aspect ratio  $\sigma$ ,*
3.  *$h_0 := \min_{K \in \mathcal{T}} h_K < \frac{1}{2} - \eta_1$ .*

*Then there exists  $j \in \mathbb{N}$  such that  $\mathcal{T}$  can be refined  $j$  times according to the procedure in Section 3.1 to create a mesh  $\mathcal{T}_{h_n}^\alpha$  of  $\Omega$  with the following properties:*

1.  *$\mathcal{T}_{h_n}^\alpha$  is shape-regular with aspect ratio  $\sigma' \leq \frac{3}{2}\sigma \max(6, 3^{1/(1-\mu)})$ ,*
2.  *$h_n := \min_{K \in \mathcal{T}_{h_n}^\alpha} h_K$ .*
3. *For each  $m \leq n \in \mathbb{N}$ , and  $i = 1, 2$ ,  $(\mathcal{T}_{m, h_n}^\alpha)^i := \mathcal{T}_{h_n}^\alpha \cap \Omega_{\alpha, m}^i$  is a triangulation of  $\Omega_{\alpha, m}^i$  satisfying:*

$$h_K \leq \sigma h_n^{1/(1-\mu_i)} \quad \text{if } K \text{ has a vertex at a reentrant} \quad (3.22)$$

*corner of  $\Omega_{\alpha, m}^i$*

$$h_K \leq 3^{\mu/(1-\mu)} \sigma h_n \left[ \inf_{x \in K} r_m^i(x) \right]^{\mu_i} \quad \text{otherwise} \quad (3.23)$$

*for every  $K \in \mathcal{T}_{m, h_n}^\alpha$ , where  $\mu = \max_{i=1,2} \mu_i$ .*

*Proof.* By Theorem 3.2.3, with  $\mu = \max\{\mu_1, \mu_2\}$ , there exists a  $j \in \mathbb{N}$  such that  $j$  refinements of  $\mathcal{T}$  according to the procedure in Section 3.1 produces a mesh satisfying (3.10)-(3.12). Call the resulting mesh  $\mathcal{T}_{h_n}^\alpha$ . Since the initial mesh,  $\mathcal{T}$ , provides a shape-regular triangulation of  $\Omega_{\alpha, m}^i$  for  $i = 1, 2$ , and each  $m \leq n$  and  $\mathcal{T}_{h_n}^\alpha$  is a conformal refinement of  $\mathcal{T}$ ,  $\mathcal{T}_{h_n}^\alpha$  also provides a triangulation of these domains.

To prove that  $\mathcal{T}_{h_n}^\alpha$  is shape-regular, we must show that there exists a constant  $\sigma'$  such that  $\max_{K \in \mathcal{T}_{h_n}^\alpha} \frac{h_K}{\rho_K} \leq \sigma'$ . In order to show this result, the refinement procedure must be considered. According to the algorithm in Section 3.1, triangles in  $\mathcal{T}$  are refined in only one of five ways, represented in Figures 3.4 and 3.5, or they are not refined at all. Clearly, if a triangle  $K$  is not refined, the ratio  $\frac{h_K}{\rho_K}$  cannot change, so this does not affect the aspect ratio of the triangulation. Next, it is clear that if  $K_1$  is similar to  $K_2$ ,  $\frac{h_{K_1}}{\rho_{K_1}} = \frac{h_{K_2}}{\rho_{K_2}}$ , so it is enough to show that only a limited number of similarity classes of triangles are created.

Let  $K$  have vertices  $V_1$ ,  $V_2$ , and  $V_3$  and suppose  $K$  is refined by one of the methods outlined in Section 3.1. The following figures reproduce the depiction of the refinements shown in Section 3.1, with the similarity class of each triangle denoted by a number in the center of the triangle. Shaded triangles with no label are similar to  $K$ . The similarity class of a triangle can easily be determined by the description of the refinement in terms of barycentric coordinates. From Figure 3.8, we see that only 13 similarity classes are

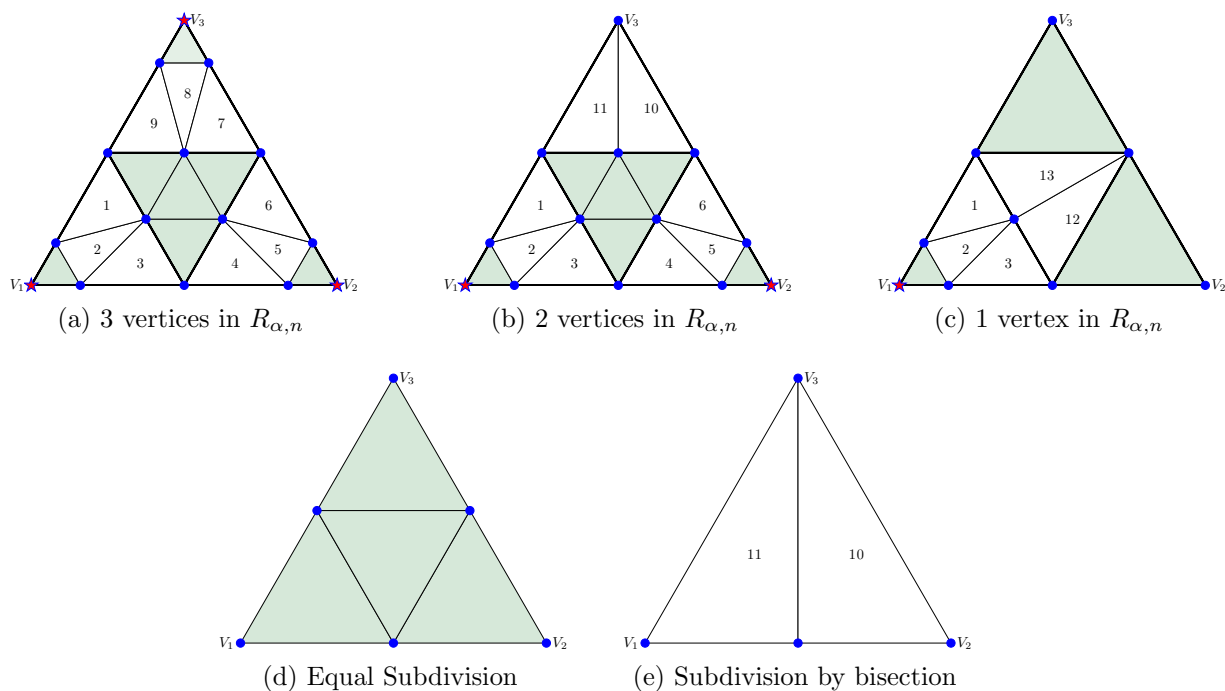


Figure 3.8: Refinement labeled according to similarity class

created. If only one refinement of  $\mathcal{T}$  was necessary this would be sufficient to show that the resulting mesh was shape regular.

Suppose instead that  $\mathcal{T}$  must be refined again. From Figure 3.8, it is clear that if  $K'$

is a triangle created by refining  $K \in \mathcal{T}$  and  $K'$  has a vertex in  $R_{\alpha,n}$ , then  $K'$  is similar to  $K$ . Thus, if  $K'$  is refined again by the algorithm in Section 3.1, since  $K'$  has exactly one vertex in  $R_{\alpha,n}$ ,  $K'$  will be refined as in Figure 3.4c, and no new similarity classes will be introduced. Now suppose  $K'$  is a triangle created by refining  $K$  and  $K'$  has no vertices in  $R_{\alpha,m}$ . Then, if  $K'$  is part of the fractal region,  $K'$  will be refined in the regular fashion, as in Figure 3.8e, and again no new similarity classes are introduced. If  $K'$  is not part of the fractal region, then  $K'$  will be refined according to the algorithm set forth in [5], where it is shown that even after repeated refinements, no angle will be bisected more than once thus limiting the aspect ratio. This argument shows that regardless of the number of iterations required, the aspect ratio satisfies  $\max_{K \in \mathcal{T}_{h_n}^\alpha} \frac{h_K}{\rho_K} \leq \sigma'$ . To see that  $\sigma' \leq \frac{3}{2}\sigma \max(6, 3^{1/(1-\mu)})$ , we refer the reader to Appendix B.3.

It remains to show that (3.22) and (3.23) hold. First, recall that  $R_{\alpha,m}$  is the set of all points that are at reentrant corners of  $\Omega_{\alpha,n}^1 \cup \Omega_{\alpha,n}^2$ , and  $R_{\alpha,m} := V_\alpha^m \setminus \{(0,0), (1,0)\}$  for each  $m \in \mathbb{N}$ . The nested nature of the vertices of the von Koch curve described in Section 1.2 implies that  $R_{\alpha,m} \subset R_{\alpha,n}$  for any  $m < n$ . Since the set of points that are at reentrant corners of  $\Omega_{\alpha,m}^i$  is a strict subset of  $R_{\alpha,m}$  for  $i = 1$  or  $i = 2$ , let us denote the points at reentrant corners of  $\Omega_{\alpha,m}^i$  by  $R_{\alpha,m}^i$ .

Now, fix  $i \in \{1, 2\}$  and  $m \leq n \in \mathbb{N}$ . Suppose first that  $K \in (\mathcal{T}_{m,h_n}^\alpha)^i$  has a vertex in  $R_{\alpha,m}^i$ . Then, since  $\mu > \max\{\mu_1, \mu_2\}$ , (3.10) holds with  $\mu$  replaced by either  $\mu_1$  or  $\mu_2$  and (3.22) follows.

For (3.23), suppose  $K \in (\mathcal{T}_{m,h_n}^\alpha)^i$  does not have a vertex in  $R_{\alpha,m}^i$ . Then, since  $R_{\alpha,m}^i$  is a strict subset of  $R_{\alpha,m}$ ,  $K$  may or may not have a vertex in  $R_{\alpha,m}$ . If  $K$  does have a vertex in  $R_{\alpha,m}$ , then the argument that  $h_K \leq 3^{\mu/(1-\mu)}\sigma h_n d(K, R_{\alpha,m}^i)^\mu$  is essentially the same as the one presented in Case 3b of Theorem 3.2.3, so it will not be repeated here. From the definition of  $r_m^i(x)$ ,  $r_m^i(x) \geq d(\{x\}, R_{\alpha,m})$  for any  $x \in \Omega$ , so using the fact that  $\mu \geq \mu_i$ , (3.23) holds. If  $K$  does not have a vertex in  $R_{\alpha,m}$ , then  $K$  may or may not have a vertex in the fractal region  $F$ . If  $K$  does have a vertex in  $F$ , then either (3.11) or (3.12) holds, depending on whether  $m = n$ . Using again that  $r_m^i(x) \geq d(\{x\}, R_{\alpha,m})$  and  $\mu \geq \mu_i$ , (3.23) follows. The final case remaining to consider is the one in which  $K \in (\mathcal{T}_{m,h_n}^\alpha)^i$  and  $K$  does not have a vertex in the fractal region  $F$ . Recall that  $F$  was defined in such a way that if  $K \cap \bar{F} = \emptyset$ , then  $\inf_{x \in K} r_m^i(x) = 1$ . So, in this case (3.23) requires only that  $h_K \leq 3^{\mu/(1-\mu)}\sigma h_n$ . This is easily verified since  $h_n \geq h_K$  by definition,  $3^{\mu/(1-\mu)} \geq 1$  whenever  $\mu \in (0, 1)$ , and  $\sigma \geq \sqrt{3}$ .  $\square$

The following short lemma essentially shows that given any  $\alpha \in (2, 4)$  and  $n \in \mathbb{N}$ ,

there exists a triangulation of  $\Omega$  satisfying the assumptions of the previous theorem. This result is a consequence of the fact that the algorithm implemented in the Triangle program produces a triangulation of  $\Omega$  with an aspect ratio that depends only on the minimum angle allowed in the triangulation.

**Lemma 3.2.5.** *Let  $\alpha \in (2, 4)$  and  $n \in \mathbb{N}$  be given. Suppose  $\mu_1 > \frac{2\theta}{\pi+2\theta}$  and  $\mu_2 > \frac{\theta}{\pi+\theta}$  are given, with  $\theta = \cos^{-1}(\frac{\alpha}{2} - 1)$ . Letting  $\theta_{\min} = \min\{\theta, \pi - 2\theta, \frac{\pi}{3}\}$ , there exists a sequence  $\{\mathcal{T}_{h_j}^\alpha\}_{j \geq n}$  of triangulations of  $\Omega$  with  $\{h_j\}_{j \geq n}$  decreasing to 0, each of which satisfies the conclusion of Theorem 3.2.4 with  $\sigma \leq \frac{1+\cos\theta_{\min}}{\sin\theta_{\min}}$ .*

*Proof.* Let  $\bar{h}_j$  be a positive sequence of real numbers decreasing to zero with  $\bar{h}_n < \frac{1}{2} - \frac{1}{\alpha} \min(\alpha - 2, 1)$ . For each  $j \geq n$ , the algorithm implemented by the Triangle program (see [25] and [24]) can produce a triangulation  $\mathcal{T}_{\bar{h}_j}$  of  $\Omega$  such that  $\max_{K \in \mathcal{T}_{\bar{h}_j}} \leq \bar{h}_j$ , the smallest angle of any triangle in  $\mathcal{T}_{\bar{h}_j}$  is no less than  $\theta_{\min}$ , and for  $i = 1, 2$ ,  $\mathcal{T}_{\bar{h}_j} \cap \Omega_{\alpha,n}^i$  is a triangulation of  $\Omega_{\alpha,n}^i$ . By Lemma B.1.1, the aspect ratio of  $\mathcal{T}_{\bar{h}_j}$  is less than or equal to  $\sigma = \frac{1+\cos\theta_{\min}}{\sin\theta_{\min}}$ . Thus, by Theorem 3.2.4, for each  $j$ , there exists an integer  $N(j)$  such that the mesh created by  $N(j)$  refinements of  $\mathcal{T}_{\bar{h}_j}$  according to the algorithm in Section 3.1 satisfies the conclusion of Theorem 3.2.4. We call such a mesh  $\mathcal{T}_{h_j}^\alpha$ . Since  $\mathcal{T}_{h_j}^\alpha$  results from refining a mesh with no edge longer than  $\bar{h}_j$ , it is clear that  $\mathcal{T}_{h_j}^\alpha$  also has no edge longer than  $\bar{h}_j$  and the result is proven.  $\square$

All of the results in this section have led up to the following result, in which we give an estimate of the error between the true solution to  $(\tilde{P}_n^\alpha)$  and the solution to  $(\tilde{P}_n^\alpha)$  in the finite element space. The statement will require the definition of Sobolev spaces on the boundaries of a polygonal domains, so we recall from Section 1.4.1 that we can characterize the space  $H^s(\Sigma_n^\alpha)$  for  $s > \frac{1}{2}$  as

$$\{v \in C(\Sigma_n^\alpha) \mid v|_M \in H^s(M) \text{ for every segment } M \in \Sigma_n^\alpha\}$$

with norm

$$\|v\|_{H^s(\Sigma_n^\alpha)} = \left( \sum_{M \in \Sigma_n^\alpha} \|v|_M\|_{H^s(M)}^2 \right)^{1/2}.$$

Also, recall from Section 1.4.2 the definition of  $V(\Omega, \Sigma_n^\alpha)$  as

$$V(\Omega, \Sigma_n^\alpha) := \{u \in H_0^1(\Omega) \mid u|_{\Sigma_n^\alpha} \in H_0^1(\Sigma_n^\alpha)\}.$$

**Theorem 3.2.6.** Let  $\alpha \in (2, 4)$  and  $n \in \mathbb{N}$  be given. Suppose  $\mu_1 > \frac{2\theta}{\pi+2\theta}$  and  $\mu_2 > \frac{\theta}{\pi+\theta}$  are given, with  $\theta = \cos^{-1}(\frac{\alpha}{2} - 1)$ . Let  $\{\mathcal{T}_{h_j}^\alpha\}_{j \geq n}$  be a sequence of triangulations of  $\Omega$  guaranteed by Lemma 3.2.5. For each integer  $j \geq n$ , let  $P_{h_j}^1(\Omega)$  denote the space of functions in  $C(\overline{\Omega}) \cap H_0^1(\Omega)$  that are affine on each triangle of  $\mathcal{T}_{h_j}^\alpha$ . Let  $u_n \in V(\Omega, \Sigma_n^\alpha)$  be the solution of  $(\tilde{P}_n^\alpha)$  and use  $u_n^i$  to denote the restriction of  $u_n$  to  $\Omega_{\alpha,n}^i$  for  $i = 1, 2$ . Let  $u_{n,j} \in P_{h_j}^1(\Omega)$  be the solution to the finite element approximation of the problem, satisfying

$$\iint_{\Omega} \nabla u_{n,j} \nabla v_j \, dx \, dy + c_n \int_{\Sigma_n^\alpha} \nabla_t u_{n,j} \nabla_t v_j \, ds = \iint_{\Omega} f v_j \, dx \, dy \quad (3.24)$$

for every  $v_j \in P_{h_j}^1(\Omega)$ . Then the following error estimate holds for every  $j \geq n \in \mathbb{N}$ :

$$\|u_n - u_{n,j}\|_{V(\Omega, \Sigma_n^\alpha)} \leq C h_j \left\{ \sum_{i=1,2} \sum_{|\beta|=2} \|(r_n^i)^{\mu_i} \partial^\beta u_n^i\|_{L^2(\Omega_{\alpha,n}^i)}^2 + c_n |u_n|_{H^2(\Sigma_n^\alpha)}^2 \right\}^{1/2} \quad (3.25)$$

where  $C$  is a constant independent of  $j$ .

*Proof.* From Cea's Lemma (Theorem 2.1.6) with  $Y = V(\Omega, \Sigma_n^\alpha)$  and  $a(u, v) = \iint_{\Omega} \nabla u \nabla v \, dx \, dy + c_n \int_{\Sigma_n^\alpha} \nabla_t u \nabla_t v \, ds$ , along with definition of the norm on  $V(\Omega, \Sigma_n^\alpha)$ ,

$$\begin{aligned} \|u_n - u_{n,j}\|_{V(\Omega, \Sigma_n^\alpha)} & \leq C \inf_{v_j \in P_{h_j}^1} \left[ \|u_n - v_j\|_{H^1(\Omega)}^2 + c_n \|(u_n - v_j)|_{\Sigma_n^\alpha}\|_{H^1(\Sigma_n^\alpha)}^2 \right]^{1/2} \end{aligned}$$

where  $C$  is a constant independent of  $j$ .

To estimate the right hand side of the above inequality, we first notice that Theorem 1.4.10 states that  $u_n^i \in H^{2,\mu_i}(\Omega_{\alpha,n}^i)$  for  $i = 1, 2$ . So, by Theorem 2.2.1,  $u_n^i$  for  $i = 1, 2$  has a continuous representative  $\bar{u}_n^i \in C(\overline{\Omega_{\alpha,n}^i})$ . Since  $u_n^1|_{\Sigma_n^\alpha} = u_n^2|_{\Sigma_n^\alpha}$ ,  $u_n$  actually has a continuous representative as well. Thus, we may define  $\Pi_{h_j} u_n$  to be the unique element of  $P_{h_j}^1(\Omega)$  that coincides with  $u_n$  at each node of the mesh  $\mathcal{T}_{h_j}^\alpha$ , as was done in definition 2.1.10. Thus,

$$\begin{aligned} \|u_n - u_{n,j}\|_{V(\Omega, \Sigma_n^\alpha)} & \leq C \left[ \|u_n - \Pi_{h_j} u_n\|_{H^1(\Omega)}^2 + c_n \|(u_n - \Pi_{h_j} u_n)|_{\Sigma_n^\alpha}\|_{H^1(\Sigma_n^\alpha)}^2 \right]^{1/2} \end{aligned} \quad (3.26)$$

Using the fact that  $\|v\|_{H^1(\Omega)}^2 = \sum_{i=1,2} \|v|_{\Omega_{\alpha,n}^i}\|_{H^1(\Omega)}^2$  for any  $v \in H^1(\Omega)$ , along with the result of Theorem 2.2.4, we have

$$\|u_n - \Pi_{h_j} u_n\|_{H^1(\Omega)}^2 \leq C_1 h_j^2 \sum_{i=1,2} \sum_{|\beta|=2} \iint_{\Omega_{\alpha,n}^i} |[r_n^i(x, y)]^{\mu_i} \partial^\beta u_n^i(x, y)|^2 dx dy$$

where  $C_1$  is independent of  $j$ .

For the second term on the right hand side of (3.26), we will use the information provided by Theorem 1.4.8 that  $u_n|_{\Sigma_n^\alpha} \in H^2(\Sigma_n^\alpha)$ . Although all of the results in Chapter 2 referred to a 2-dimensional domain, the results hold in the case of a 1-dimensional domain as well, so applying Theorem 2.1.14 gives

$$\|(u_n - \Pi_{h_j} u_n)|_{\Sigma_n^\alpha}\|_{H^1(\Sigma_n^\alpha)}^2 \leq C_2 h_j^2 |u_n|_{\Sigma_n^\alpha}|_{H^2(\Sigma_n^\alpha)}^2$$

where  $C_2$  is independent of  $j$ . Combining these three inequalities yields (3.25).  $\square$

**Remark:** It is important to note that without refining the coarse mesh so that it satisfies (T6\*) and (T7\*), we would not be able to obtain this linear convergence rate. Using, for instance, Theorem 8.4.14 in [13] along with Theorem 1.4.10 giving the regularity of the solution to  $(\tilde{P}_n^\alpha)$ , we would obtain the following error estimate

$$\|u_n - u_{n,h_j}\|_{V(\Omega, \Sigma_n^\alpha)} \leq C h_j^{s_1-1} \left\{ \|u_n\|_{H^{s_1}(\Omega_{\alpha,n}^1)} + \|u_n\|_{H^{s_2}(\Omega_{\alpha,n}^1)} + \|u_n\|_{H^2(\Sigma_n^\alpha)} \right\},$$

with  $s_1 < \frac{2\pi+2\theta}{\pi+2\theta}$  and  $s_2 < \frac{2\pi+\theta}{\pi+\theta}$  for  $\theta = \cos^{-1}(\frac{\alpha}{2} - 1)$ . Since  $s_1 \in (1, 2)$  for every  $\alpha \in (2, 4)$ , it is clear that this convergence rate is slower than the one found in (3.25).

### 3.3 Implementation and Results

In this section, we will provide some details to make a practical implementation of the finite element method applied to the prefractal transmission problem feasible. We will conclude with some results of computations.

We begin by considering the algebraic formulation of the finite element approximation to the problem  $(\tilde{P}_n^\alpha)$ . So, fix  $\alpha \in (2, 4)$  and  $n \in \mathbb{N}$ . Then, for a fixed  $j \geq n$ , let  $\mathcal{T}_{h_j}^\alpha$  be a triangulation as in Theorem 3.2.6. Then, given this triangulation, the finite element

approximation to the solution  $u_n$  of  $(\tilde{P}_n^\alpha)$  is the element  $u_{n,j} \in P_{h_j}^1(\Omega)$  satisfying

$$\iint_{\Omega} \nabla u_{n,j} \nabla v_j \, dx \, dy + c_n \int_{\Sigma_n^\alpha} \nabla_t u_{n,j} \nabla_t v_j \, ds = \iint_{\Omega} f v_j \, dx \, dy \quad (3.27)$$

for every  $v_j \in P_{h_j}^1(\Omega)$ .

Recall that  $P_{h_j}^1(\Omega)$  is the space of functions in  $C(\bar{\Omega})$  that are affine on each triangle in  $\mathcal{T}_{h_j}^\alpha$ . As was mentioned in Section 2.1, there is a simple basis for this space. For each node  $x_i$  in the triangulation, let  $\phi_i$  be the unique function in  $P^1(\Omega)$  that is one at  $x_i$  and zero at every other node in the mesh. We refer to this basis as the nodal basis for  $\mathcal{T}_{h_j}^\alpha$ .

We will now use this basis to transform the variational problem into an algebraic one. Suppose  $\mathcal{T}_{h_j}^\alpha$  has  $N$  nodes. Then, since  $\{\phi_i\}_{i=1}^N$  is a basis for  $P_{h_j}^1(\Omega)$ ,  $u_{n,j} \in P_{h_j}^1(\Omega)$  satisfies (3.27) if and only if  $u_{n,j}$  satisfies

$$\iint_{\Omega} \nabla u_{n,j} \nabla \phi_i \, dx \, dy + c_n \int_{\Sigma_n^\alpha} \nabla_t u_{n,j} \nabla_t \phi_i \, ds = \iint_{\Omega} f \phi_i \, dx \, dy \quad (3.28)$$

for every  $i \in \mathbb{N}$  with  $1 \leq i \leq N$ . Because  $u_{n,j} \in P_{h_j}^1(\Omega)$ , there exist constants  $\{\beta_k\}_{k=1}^N$  such that

$$u_{n,j} = \sum_{k=1}^N \beta_k \phi_k$$

Using this decomposition of  $u_{n,j}$ , (3.28) becomes

$$\sum_{k=1}^N \beta_k \left[ \iint_{\Omega} \nabla \phi_k \nabla \phi_i \, dx \, dy + c_n \int_{\Sigma_n^\alpha} \nabla_t \phi_k \nabla_t \phi_i \, ds \right] = \iint_{\Omega} f \phi_i \, dx \, dy,$$

and we can determine the solution  $u_{n,j}$  by finding the coefficients  $\beta_k$  that satisfy this equation. So, we have converted the variational problem of finding  $u_{n,j} \in P_{h_j}^1(\Omega)$  satisfying (3.27) into a purely algebraic problem. To make it even more clear that this problem is algebraic, for  $1 \leq i, k \leq N$ , set

$$A(i, k) = \iint_{\Omega} \nabla \phi_k \nabla \phi_i \, dx \, dy + c_n \int_{\Sigma_n^\alpha} \nabla_t \phi_k \nabla_t \phi_i \, ds \quad (3.29)$$

and

$$b(i) = \iint_{\Omega} f \phi_i dx dy. \quad (3.30)$$

We will refer to  $A$  as the **stiffness matrix** and call  $b$  the **load vector**. Then with  $\beta = [\beta_1, \beta_2, \dots, \beta_N]^T$ ,  $\beta$  is the solution to the linear system

$$A\beta = b.$$

Given the nature of the basis functions,  $\phi_i$  is nonzero on a triangle  $T \in \mathcal{T}_{h_j}^\alpha$  only if  $x_i$  is a vertex of  $T$  and  $\nabla \phi_k \nabla \phi_i$  is nonzero only if  $x_i$  and  $x_k$  are both vertices of the same triangle  $T \in \mathcal{T}_{h_j}^\alpha$ . Thus, it is practical to calculate the integrals in the previous equations as sums over the triangles in the mesh. Then, we have

$$A(i, k) = \sum_{T \in \mathcal{T}_{h_j}^\alpha} \iint_T \nabla \phi_k \nabla \phi_i dx dy + c_n \sum_{M \in \Sigma_n^\alpha} \int_M \nabla_t \phi_k \nabla_t \phi_i ds \quad (3.31)$$

and

$$b(i) = \sum_{T \in \mathcal{T}_{h_j}^\alpha} \iint_T f \phi_i dx dy \quad (3.32)$$

where  $M \in \Sigma_n^\alpha$  is one of the segments forming the prefractal curve. To actually calculate the values of the entries in the stiffness matrix and the load vector, we essentially follow [2]. There, a very detailed description of a simple MATLAB program implementing the finite element method is given. We will not attempt to replicate the exceptional instructional nature of this paper. Instead, we will only mention some of the aspects most important to our application.

Let  $T$  be a triangle with vertices  $(x_1, y_1)$ ,  $(x_2, y_2)$ , and  $(x_3, y_3)$ . In [2], it is shown that for  $(x, y) \in T$ , the gradient of the nodal basis function at the  $i^{\text{th}}$  vertex of  $T$  for  $i = 1, 2, 3$ , is given by

$$\nabla \phi_i(x, y) = \frac{1}{2|T|} \begin{pmatrix} y_{i+1} - y_{i+2} \\ x_{i+2} - x_{i+1} \end{pmatrix} \quad (3.33)$$

where

$$2|T| = \det \begin{pmatrix} x_2 - x_1 & x_3 - x_1 \\ y_2 - y_1 & y_3 - y_1 \end{pmatrix} \quad (3.34)$$

and the indices in (3.33) are given modulo 3. Using this information,

$$\iint_T \nabla \phi_i \nabla \phi_k dx dy = \frac{|T|}{(2|T|)^2} \begin{pmatrix} y_{i+1} - y_{i+2} & x_{i+2} - x_{i+1} \end{pmatrix} \begin{pmatrix} y_{k+1} - y_{k+2} \\ x_{k+2} - x_{k+1} \end{pmatrix}. \quad (3.35)$$

To calculate  $A(i, k)$ , we also need  $\nabla_t \phi_i$  on a segment  $M$  of  $\Sigma_n^\alpha$ . So, suppose in the triangle  $T$ , the edge from  $(x_1, y_1)$  to  $(x_2, y_2)$  is a segment of  $\Sigma_n^\alpha$ . Then,  $\nabla_t \phi_i = \nabla \phi_i \cdot \bar{v}$ , where  $\bar{v}$  is the unit vector in the direction of

$$v = \begin{pmatrix} x_2 - x_1 & y_2 - y_1 \end{pmatrix}.$$

With  $M$  denoting the segment from  $(x_1, y_1)$  to  $(x_2, y_2)$ ,

$$\begin{aligned} \int_M \nabla_t \phi_i \nabla_t \phi_k ds \\ = \frac{\|v\|}{(\|v\|)^2 (2|T|)^2} \begin{bmatrix} y_{i+1} - y_{i+2} \\ x_{i+2} - x_{i+1} \end{bmatrix} \cdot v \begin{bmatrix} y_{k+1} - y_{k+2} \\ x_{k+2} - x_{k+1} \end{bmatrix} \cdot v, \end{aligned} \quad (3.36)$$

and  $A(i, k)$  is easily calculated from (3.35) and (3.36).

Next, we must calculate the entries in the load vector  $b$ . This is not quite as simple as calculating the entries in the stiffness matrix. Looking back to (3.27), the integrals on the left hand side only involve functions in  $P_{h_j}^1(\Omega)$ , but on the right hand side, we have only required that  $f \in L^2(\Omega)$ . Even assuming that  $f \in C(\bar{\Omega})$ , in most cases, this integral would have to be approximated numerically. In [26], it is shown that if the numerical approximation of the integral is such that the first derivatives of every function in  $P_{h_j}^1(\Omega)$  can be integrated exactly, we will be able to maintain the  $H^1$ -convergence of Section 3.2. So, letting  $(x_C, y_C)$  denote the barycenter of  $T$ , we have the following simple approximation for the  $i^{\text{th}}$  entry in the load vector,

$$b(i) = \iint_T f \phi_i dx dy \approx \frac{1}{6} \det \begin{pmatrix} x_2 - x_1 & x_3 - x_1 \\ y_2 - y_1 & y_3 - y_1 \end{pmatrix} f(x_C, y_C). \quad (3.37)$$

This approximation is used in [2] and satisfies the properties in [26] that allow the linear

convergence in the last section to be realized.

From the above formulas for the stiffness matrix and load vector, it is relatively easy to write code to set up and solve the linear system. We have chosen to use MATLAB for the implementation and have built our code from that in [2].

With these formulas, we are also able to see another benefit of our use of the mesh  $\mathcal{T}_{h_j}^\alpha$  to solve the problem  $(\tilde{P}_n^\alpha)$  for any  $n \leq j$ . If we write the  $(i, k)$  entry in the stiffness matrix as  $B(i, k) + C(i, k)$  where

$$B(i, k) = \sum_{T \in \mathcal{T}_{h_j}^\alpha} \iint_T \nabla \phi_k \nabla \phi_i \, dx \, dy \quad (3.38)$$

and

$$C(i, k) = c_n \sum_{M \in \Sigma_n^\alpha} \int_M \nabla_t \phi_k \nabla_t \phi_i \, ds \quad (3.39)$$

only  $C(i, k)$  is affected by a change in  $n$ .  $B(i, k)$  and the load vector  $b$  are completely independent of  $n$ , so if we save this part of the stiffness matrix and the load vector, they need not be calculated again for each new value of  $n$ , hopefully saving computation time.

For the storage and management of the mesh data structure, we have followed the model in [11], again with some necessary modifications for our specific problem. The most important modification that must be made is providing a means for identifying nodes that are at reentrant corners of the domain and edges that form the prefractal curve. The bulk of the original code written to numerically solve  $(\tilde{P}_n^\alpha)$  involves creating the prefractal curves and implementing the refinement procedure. The prefractal curves are created easily from the maps in Section 1.2 and implementing the refinement procedure is a straightforward task using the barycentric coordinates provided in Section 3.1 to define new nodes and triangles.

Having provided these implementation notes, we are now prepared to show some results of the computations. In all of the computations, we have chosen  $f \equiv 1$ . With this choice of  $f$ , we have the following physical interpretation of the problem. We can consider the domain  $\Omega$  as a single elastic membrane being pushed upward with a constant force throughout the domain. In this light, the transmission condition  $-c_n \Delta_t u_n = \left[ \frac{\partial u_n}{\partial \nu} \right]$  gives  $\Sigma_n^\alpha$  the role of being a reinforcement of the material. One can think of this as a

heavy thread woven through the more loosely woven fabric in the rest of the domain.

We begin by showing a sequence of solutions to (3.27) with both  $\alpha$  and  $n$  fixed, and the mesh size  $h_j$  decreasing. For this example, we have chosen  $\alpha = 3$  and  $n = 1$ . In Figures 3.9-3.12, one sees the mesh  $\mathcal{T}_{1,h_i}^3$  for  $i = 1 \dots 4$  and the corresponding solution to the transmission problem using each discretization of the domain. It is evident from

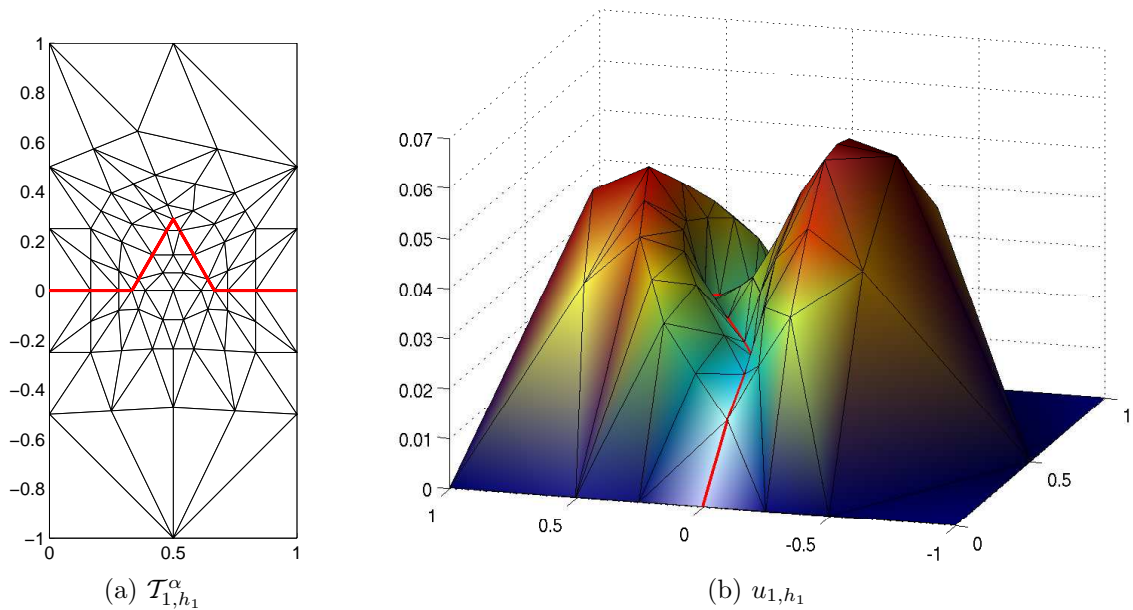


Figure 3.9: Mesh and Solution with  $\alpha = 3$ ,  $n = 1$ , and  $h_1$

the figures that as  $h_j$  decreases, the solution  $u_{n,j}$  to (3.27) becomes much more smooth, better approximating the true solution  $u_n$  to  $(\hat{P}_n^\alpha)$ .

In the next set of figures, we show how one mesh can be used to solve a series of problems. In Figure 3.13, one finds the mesh  $\mathcal{T}_{h_4}^\alpha$  for  $\alpha = 2.5$ . This discretization of the domain will be used to solve (3.27) with  $\alpha = 2.5$  and  $n = 1 \dots 4$ . The solutions to these problems can be seen in Figure 3.14. These figures are important because they emphasize how a single discretization of the domain  $\Omega$  can be used to solve a number of problems with different interfaces. From the figures, we can also visually inspect how the increasing value of  $n$  affects the shape of the solution. It appears that as  $n$  increases, causing the length of  $\Sigma_n^\alpha$  to increase and intrude further into the upper portion of the domain, the peak of the solution in this part of the domain decreases. This is consistent with the interpretation of  $\Sigma_n^\alpha$  serving as a reinforcement of the elastic material that forms the rest of the domain.

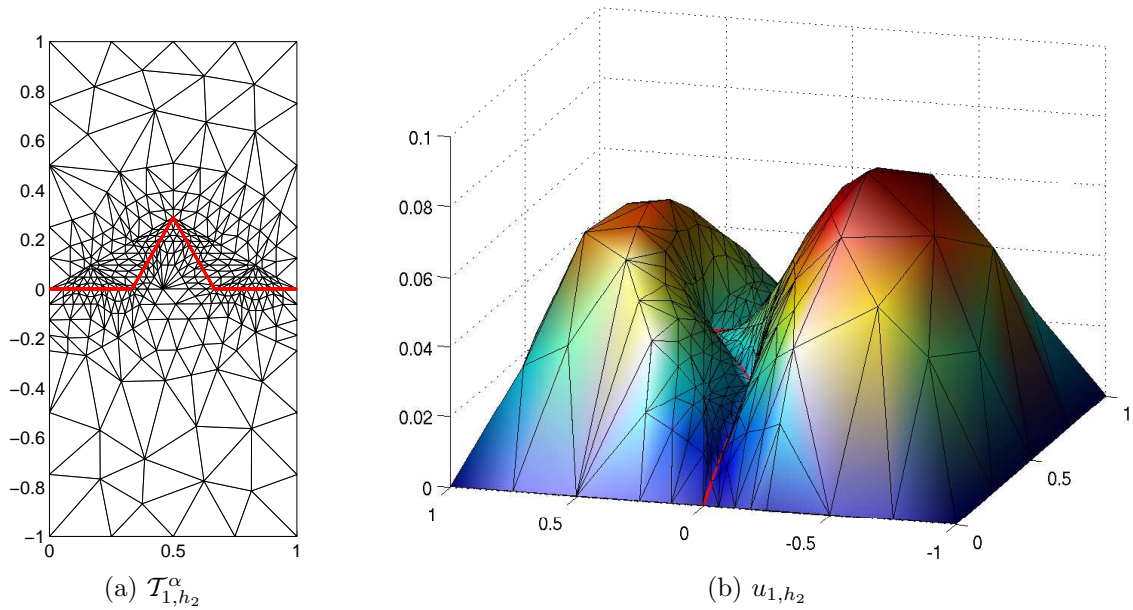


Figure 3.10: Mesh and Solution with  $\alpha = 3$ ,  $n = 1$ , and  $h_2$

In the final set of figures, we see the solutions to  $(\tilde{P}_n^\alpha)$  with  $n$  fixed and  $\alpha$  varying in  $(2, 4)$ . Notice that the value of  $\alpha$  also has an affect on the maximum height of the solution in  $\Omega_{\alpha,n}^1$ . For values of  $\alpha$  near 2, the prefractal curve intrudes much further into the upper domain, limiting the extent to which the elastic material nearby is stretched upward by the constant force being applied.

### 3.4 Future Work

With the conclusion of this thesis, we remark on some of the work that remains to be done. In Section 3.3, we mentioned some ways in which the solution to the prefractal transmission problem was affected by changing  $\alpha$  and  $n$ . However, these observations were based only on visualizing the solution. Additional work be done to make a more systematic study of how this and other properties of the solution are affected by changing these parameters.

A very important part of this problem that remains incomplete is understanding how the solution to the prefractal transmission problem relates to the solution of the fractal transmission problem. In Section 1.3, it was mentioned that in 1.3 it is shown that for  $\alpha = 3$ , the solutions  $u_n$  to the sequence of problems  $(\tilde{P}_n^\alpha)$  converge in the  $H^1$ -norm to

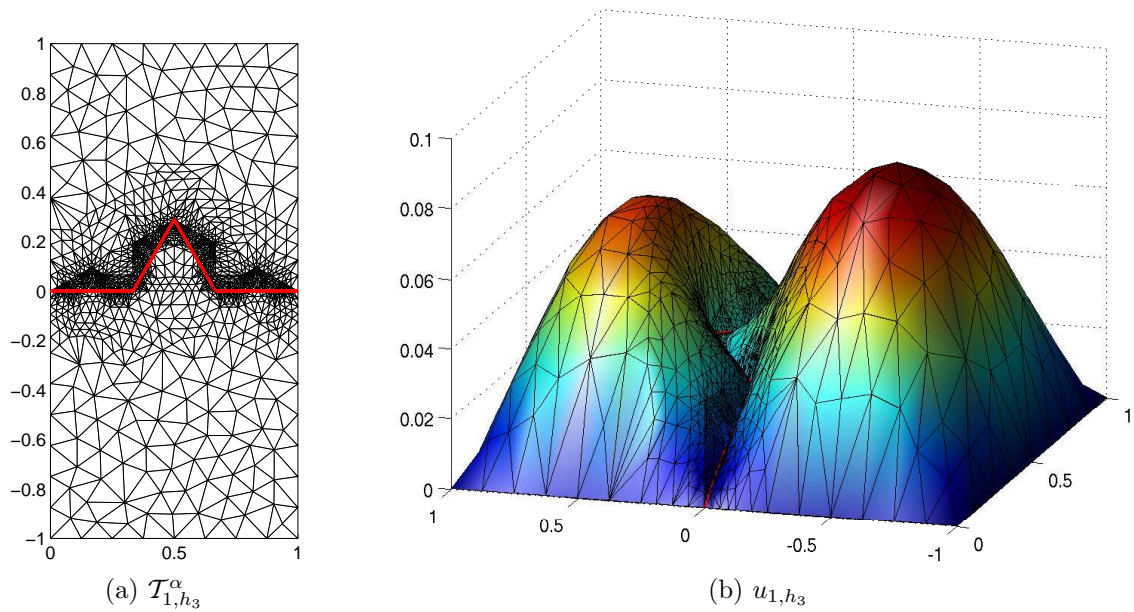


Figure 3.11: Mesh and Solution with  $\alpha = 3$ ,  $n = 1$ , and  $h_3$

the solution of  $(\tilde{P}^\alpha)$  as  $n \rightarrow \infty$ . While we expect that this is true for other values of  $\alpha \in (2, 4)$ , it is important that this analytical result be extended.

Finally, while the technique developed here for discretizing the domain takes some advantage of the nested nature of the prefractal curve, a more specialized technique using the self-similarity of the curve may allow for more computational time savings generating the mesh and solving the problem numerically. Work is currently underway by Emily Evans to devise such an algorithm.

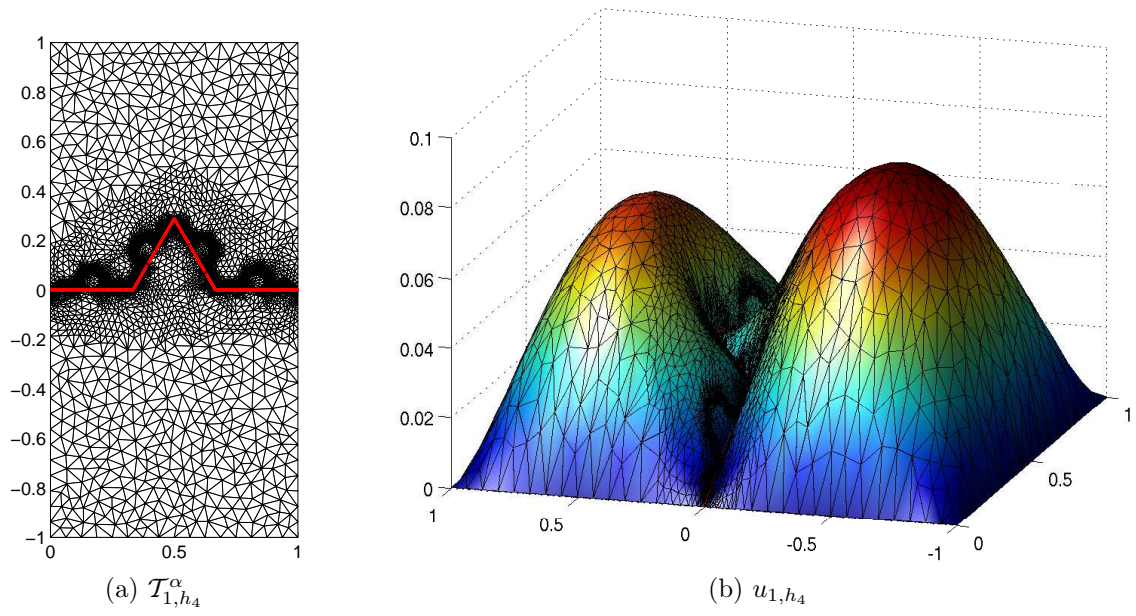


Figure 3.12: Mesh and Solution with  $\alpha = 3$ ,  $n = 1$ , and  $h_4$

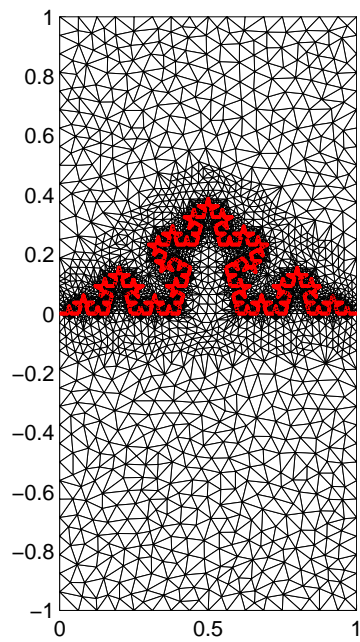
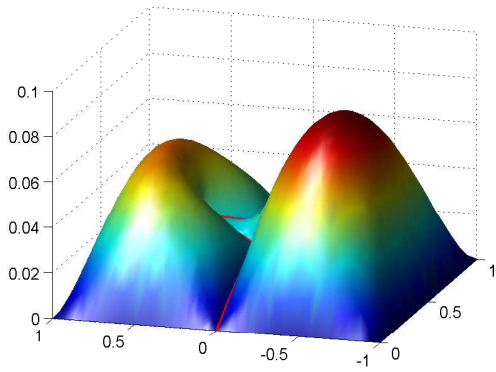
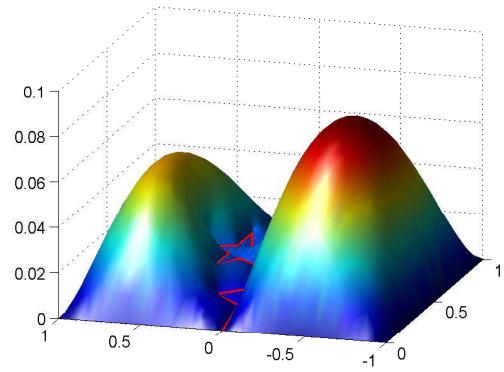


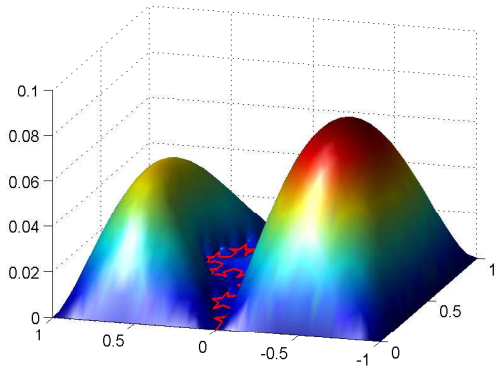
Figure 3.13: Mesh  $\mathcal{T}_{h_4}^\alpha$  for  $\alpha = 2.5$



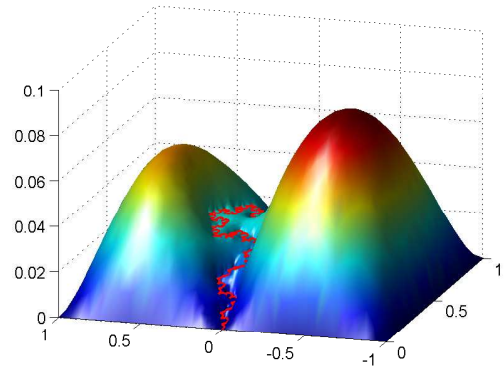
(a)  $u_{1,4}$



(b)  $u_{2,4}$

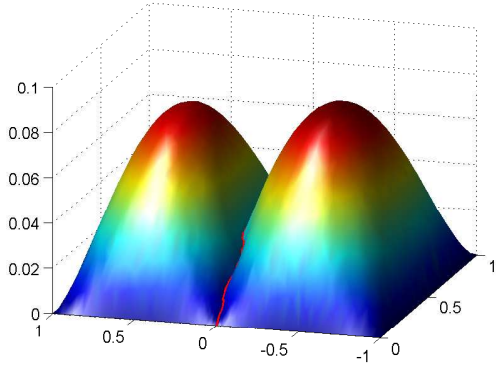


(c)  $u_{3,4}$

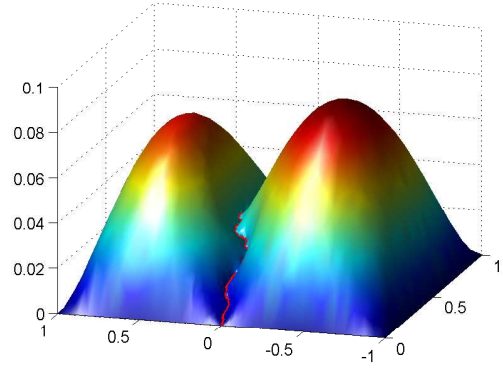


(d)  $u_{4,4}$

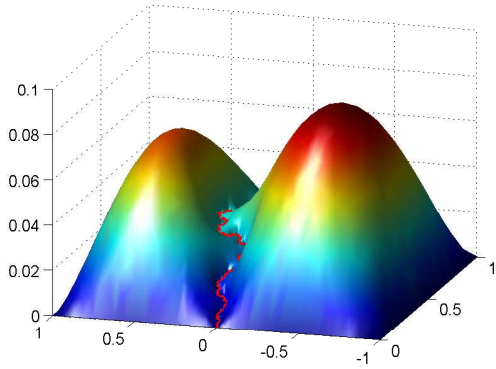
Figure 3.14: Solutions to (3.27) with  $\alpha = 2.5$  and  $n = 1 \dots 4$  using the mesh in Figure 3.13



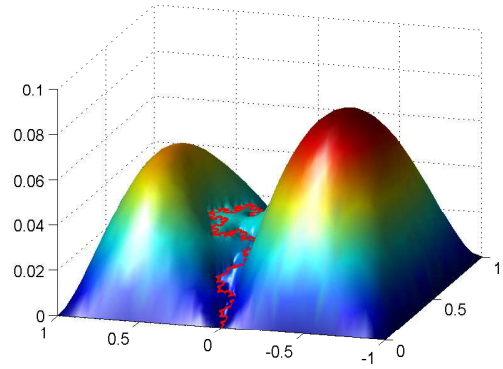
(a)  $u_{3,4}$  with  $\alpha = 3.9$



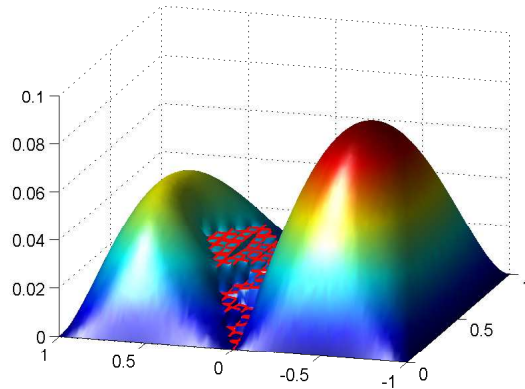
(b)  $u_{3,4}$  with  $\alpha = 3.5$



(c)  $u_{3,4}$  with  $\alpha = 3$



(d)  $u_{3,4}$  with  $\alpha = 2.5$



(e)  $u_{3,4}$  with  $\alpha = 2.1$

Figure 3.15: Solutions to (3.27) for fixed mesh size  $h_4$  with  $n = 3$  and a selection of values of  $\alpha \in (2, 4)$

# General Notation

Notation	Description	
$\overline{A}$	closure of the set $A$	26, 30
$\overset{\circ}{A}$	interior of the set $A$	30
$B(x, r)$	$\{y :  x - y  < r\}$	17
$C^{0,\beta}(K)$	space of Hölder continuous functions of order $\beta$	12
$d(A, B)$	Euclidean distance between the sets $A$ and $B$	61
$\mathbf{diam}(A)$	diameter of the set $A$ , $\sup_{x,y \in A}  x - y $	29
$H^{2,\mu}(\Omega; r)$	weighted Sobolev space	22
$\mathcal{L}(X; Y)$	space of bounded linear functions from $X$ to $Y$	34
$\mu _A$	measure $\mu$ restricted to the set $A$	9
$v_n \xrightarrow{w} v$	$v_n$ converges weakly to $v$	16
$X \hookrightarrow Y$	$X$ is continuously embedded in $Y$	16
$X \hookrightarrow\hookrightarrow Y$	$X$ is compactly embedded in $Y$	16



# Finite Element Notation

Notation	Description	
$h$	$\max_{K \in \mathcal{T}_h} h_K$	34
$h_K$	length of the longest side of a triangle $K$	29
$\hat{K}$	the reference triangle with vertices $(0, 0)$ , $(0, 1)$ , and $(1, 0)$	30
$P_h^1(\Omega)$	subset of $C(\Omega)$ that is linear on each triangle $K$ of $\mathcal{T}_h$	30
$\Pi_h$	the linear interpolating operator from $H^2(\Omega) \rightarrow P_h^1(\Omega)$ or $H^{2,\mu}(\Omega) \rightarrow P_h^1(\Omega)$	31, 42
$\Pi_K$	the linear interpolating operator from $H^2(K) \rightarrow P_1(K)$	31, 42
$\rho_K$	diameter of the largest circle that can be inscribed in a triangle $K$	29
$\mathcal{T}_h$	triangulation of domain	30



# Problem Notation

Notation	Description	
$D_E$	domain of energy form on fractal von Koch curve $\Sigma^\alpha$	11
$D_0(\Sigma^\alpha)$	$\{u \in D_E \mid u = 0 \text{ on } V_\alpha^0\}$	12
$E_\alpha$	energy form on fractal von Koch curve $\Sigma^\alpha$	10
$\Omega$	$(0, 1) \times (-1, 1) \subset \mathbb{R}^2$	17
$\Omega_{\alpha,n}^1$	the portion of $\Omega$ above $\Sigma_n^\alpha$	17
$\Omega_{\alpha,n}^2$	the portion of $\Omega$ below $\Sigma_n^\alpha$	17
$\psi_i^\alpha$	contraction maps that generate von Koch curve with contraction factor $\frac{1}{\alpha}$	6
$\Psi_\alpha(F)$	$\bigcup_{i=1}^4 \psi_i^\alpha(F)$	6
$\Psi_\alpha^n(F)$	$\underbrace{\Psi_\alpha \circ \dots \circ \Psi_\alpha}_{n \text{ times}}(F)$	6
$R_{\alpha,n}$	reentrant corners of $\Omega_{\alpha,n}^1 \cup \Omega_{\alpha,n}^2$	55
$r_n^i$	weighting function for $H^{2,\mu_i}(\Omega_{\alpha,n}^i; r_n^i)$	54
$\Sigma^\alpha$	von Koch curve with contraction factor $\frac{1}{\alpha}$	6
$\Sigma_n^\alpha$	$n^{\text{th}}$ -generation prefractal von Koch curve with contraction factor $\frac{1}{\alpha}$	6
$V_\alpha^n$	vertices of $n^{\text{th}}$ -generation prefractal von Koch curve with contraction factor $\frac{1}{\alpha}$	7

<b>Notation</b>	<b>Description</b>	
$V_\alpha^\infty$	$\bigcup_{n \geq 0} V_\alpha^n$	7
$V(\Omega, \Sigma^\alpha)$	$\{u \in H_0^1(\Omega) : u _{\Sigma^\alpha} \in D_0(\Sigma^\alpha)\}$	13
$V(\Omega, \Sigma_n^\alpha)$	$\{u \in H_0^1(\Omega) : u _{\Sigma_n^\alpha} \in H_0^1(\Sigma_n^\alpha)\}$	18

# Appendix A

## Some Relevant Spaces and Definitions

This appendix is a collection of definitions of spaces and other objects that are relevant to the thesis. They are included here, and not in the main text of the thesis, as most of them are already well-known. They are included here for reference.

**Definition A.0.1** (Hausdorff measure). Let  $A \subset \mathbb{R}^n$ ,  $0 \leq s < \infty$ ,  $0 < \delta \leq \infty$ . Define

$$\mathcal{H}_\delta^s(A) := \inf \left\{ \sum_{j=1}^{\infty} \alpha(s) \left( \frac{\text{diam} C_j}{2} \right)^s \mid A \subset \bigcup_{j=1}^{\infty} C_j, \text{diam} C_j \leq \delta \right\},$$

where

$$\alpha(s) := \frac{\pi^{s/2}}{\Gamma(\frac{s}{2} + 1)}$$

and  $\Gamma(s) = \int_0^\infty e^{-x} x^{s-1} dx$ , ( $0 < s < \infty$ ), is the usual gamma function. Then

$$\mathcal{H}^s(A) := \lim_{\delta \rightarrow 0} \mathcal{H}_\delta^s(A) = \sup_{\delta > 0} \mathcal{H}_\delta^s(A).$$

We call  $\mathcal{H}^s$  the  $s$ -**dimensional Hausdorff measure** on  $\mathbb{R}^n$ .

**Definition A.0.2** (Hausdorff dimension). The **Hausdorff dimension** of a set  $A \subset \mathbb{R}^n$  is defined to be  $\inf\{0 \leq s < \infty \mid \mathcal{H}^s(A) = 0\}$ .

**Definition A.0.3** (Hölder continuous). Let  $C^{0,\beta}(K)$  denote the space of **Hölder con-**

**tinuous functions of order  $\beta$**  on  $K$ , defined as

$$\{u : K \rightarrow \mathbb{R} \mid |u(x) - u(y)| \leq M |x - y|^\beta, \forall (x, y) \in K\}.$$

# Appendix B

## Miscellaneous Results

### B.1 Controlling the Aspect Ratio with a Minimum Angle

The following is a simple proof showing that controlling the minimum angle in a mesh puts a limit on the aspect ratio for all triangles appearing in the mesh. The Triangle program ([25], [24]) introduced in Section 3.1 controls the minimum angle in the triangulation, thereby controlling the aspect ratio for the mesh.

**Lemma B.1.1.** *The aspect ratio for any triangle having minimum angle  $\theta_1$  is in the interval*

$$\left[ \frac{1 + \sin(\frac{\theta_1}{2})}{\sin \theta_1}, \frac{1 + \cos \theta_1}{\sin \theta_1} \right]. \quad (\text{B.1})$$

*Proof.* Fix the value of  $\theta_1$  and denote the other angles of the triangle by  $\theta_2$  and  $\theta_3$ , choosing in such a way that  $\theta_1 \leq \theta_2 \leq \theta_3$ . Denote the side of the triangle opposite  $\theta_i$  by  $s_i$ , as shown in Figure B.1. Since similar triangles have the same aspect ratio, without

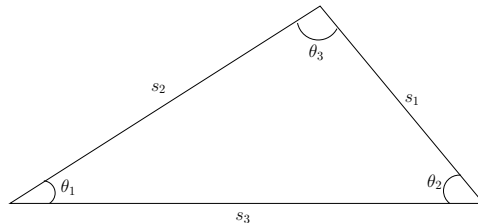


Figure B.1: triangle diagram

loss of generality, we may assume that the length of side  $s_1$  is 1. From the Law of Sines, it follows that

$$s_2 = \frac{\sin \theta_2}{\sin \theta_1} \quad \text{and} \quad s_3 = \frac{\sin \theta_3}{\sin \theta_1}.$$

The area of the triangle, which is denoted by  $A$ , is thus  $\frac{\sin \theta_2 \sin \theta_3}{2 \sin \theta_1}$ . Since the longest side of the triangle is opposite the largest angle, we have  $h = s_3$ . We then calculate the diameter of a circle inscribed in the triangle to be

$$\rho = \frac{4A}{s_1 + s_2 + s_3} = \frac{2 \sin \theta_2 \sin \theta_3}{\sin \theta_1 + \sin \theta_2 + \sin \theta_3}. \quad (\text{B.2})$$

Using the fact that  $\theta_3 = \pi - \theta_1 - \theta_2$ , the aspect ratio of the triangle is

$$\frac{h}{\rho} = \frac{\sin \theta_1 + \sin \theta_2 + \sin(\theta_1 + \theta_2)}{2 \sin \theta_1 \sin \theta_2} \quad (\text{B.3})$$

Since  $\theta_1$  is fixed, we have assumed that  $\theta_1 \leq \theta_2 \leq \theta_3$ , and  $\theta_1 + \theta_2 + \theta_3 = \pi$ ,  $\theta_2$  must be in the interval  $[\theta_1, \frac{1}{2}(\pi - \theta_1)]$ . So, the maximum value of the ratio (B.3) can be determined by finding the value of  $\theta_2$  in the interval that maximizes

$$f(\theta_2) = \frac{\sin \theta_1 + \sin \theta_2 + \sin(\theta_1 + \theta_2)}{2 \sin \theta_2}. \quad (\text{B.4})$$

Taking the derivative of  $f$  and simplifying using trigonometric identities yields

$$f'(\theta_2) = \frac{-\sin \theta_1 (1 + \cos \theta_2)}{2 \sin^2 \theta_2}. \quad (\text{B.5})$$

Since  $\sin \theta_1$ ,  $1 + \cos \theta_2$ , and  $\sin^2 \theta_2$  are positive for all values of  $\theta_1, \theta_2 \in (0, \pi)$ , it follows that  $f$  is decreasing on the interval  $[\theta_1, \frac{1}{2}(\pi - \theta_1)]$ . Thus, the aspect ratio achieves a maximum at  $\theta_2 = \theta_1$  and achieves a minimum at  $\theta_2 = \frac{1}{2}(\pi - \theta_1)$ . The result follows by substituting these values for  $\theta_2$  into (B.3) and simplifying using trigonometric identities.  $\square$

**Remark:** Note that in the case of an equilateral triangle, where  $\theta_1 = \frac{\pi}{3}$ , we have  $\frac{1 + \sin(\frac{\theta_1}{2})}{\sin \theta_1} = \frac{1 + \cos \theta_1}{\sin \theta_1} = \sqrt{3}$ . Since this is the best case for any triangle, we always have  $\sigma \geq \sqrt{3}$ .

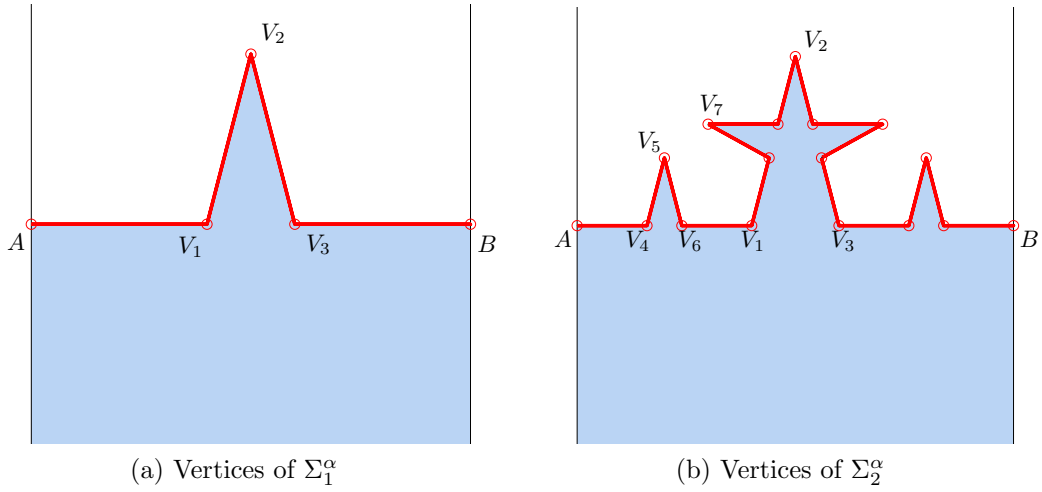


Figure B.2: Vertices of prefractal curves,  $\alpha = 2.5$

## B.2 Distance Between Vertices of Domain

For the weighting function of Definition 3.1.1, the minimum distance between any two vertices of the polygonal domains  $\Omega_{\alpha,n}^1$  and  $\Omega_{\alpha,n}^2$  must be known. Recall that  $\Omega = (0, 1) \times (-1, 1)$  and  $\Omega_{\alpha,n}^1$  and  $\Omega_{\alpha,n}^2$  are the portions of  $\Omega$  above and below the prefractal von Koch curve, respectively.

Regardless of the values of  $\alpha$  and  $n$ , the prefractal curve  $\Sigma_n^\alpha$  is always contained in the triangle with vertices  $(0, 0)$ ,  $(1, 0)$ , and  $(\frac{1}{2}, \frac{1}{2})$ . So, it is clear that the distance between any vertex of the prefractal curve and a vertex of  $\Omega$  is greater than  $\frac{1}{2}$ . So, we will focus on finding the minimum distance between vertices of the prefractal von Koch curve.

Although the number of vertices in  $V_n^\alpha$  is increasing as  $n$  increases, self-similarity makes it relatively easy to find the distance between any two points in the set. In Figures B.2a and B.2b the first two generations of the prefractal von Koch curve with  $\alpha = 2.5$  are shown. The value of  $\alpha$  is insignificant in this context as all of the remarks made here will hold for each value of  $\alpha \in (2, 4)$ . In the figures, each vertex of the curve is represented by an open circle. Several of the vertices in each figure are labeled for easy reference.

Looking only at Figure B.2a initially, it is evident that the distances we should be concerned with are those between consecutive vertices of the curve (like  $A$  and  $V_1$ ), and those between vertices that form the base of a triangle (like  $V_1$  and  $V_3$ ). The distance between the peak of the triangle (vertex  $V_2$ ) and either of the endpoints  $A$  or  $B$  is

necessarily greater than the two previously mentioned distances. As was noted in Section 1.2, any two consecutive points on the  $n^{\text{th}}$ -generation prefractal curve are separated by a distance of  $\alpha^{-n}$ . So, we have  $|A - V_1| = |V_1 - V_2| = |V_2 - V_3| = |V_3 - B| = \alpha^{-1}$ . The length of the base of the triangle,  $|V_1 - V_3|$  is also easily calculated using this information. It is simply  $|A - B| - |A - V_1| - |V_3 - B| = 1 - 2\alpha^{-1} = \alpha^{-1}(\alpha - 2)$ .

Because of similarity, many of the distances between points in Figure B.2b can easily be determined from the distance between points in Figure B.2a. The distance between consecutive vertices along the curve is now  $\alpha^{-2}$  and the length of the base of each of the smaller triangles in the figure, like  $|V_4 - V_6|$ , is  $\alpha^{-2}(\alpha - 2)$ . However, with this second iteration of the maps, triangles appear that neighbor one another and the vertices at the peak of these neighboring triangles seem to be close. So, we must calculate the distance between any two of these such points. We take the distance between  $V_5$  and  $V_7$  as representative.

To calculate the distance between  $V_5$  and  $V_7$ , we use the coordinates of the points given by the maps that generate these vertices. First, using the definitions of the maps in Section 1.2, we see that  $V_5 = \psi_1^\alpha(V_2)$ ,  $V_7 = \psi_2^\alpha(V_2)$  and  $V_2 = \psi_2^\alpha(B) = \psi_3^\alpha(A)$ . This gives us:

$$V_5 = \frac{1}{\alpha} \left( \frac{1}{2}, \sqrt{\frac{1}{\alpha} - \frac{1}{4}} \right) \quad \text{and} \quad V_7 = \frac{\alpha - 1}{\alpha} \left( \frac{1}{2}, \sqrt{\frac{1}{\alpha} - \frac{1}{4}} \right)$$

A simple calculation shows that  $|V_5 - V_7| = \alpha^{-\frac{3}{2}}(\alpha - 2)$ . However, regardless of the choice of  $\alpha \in (2, 4)$ ,  $\alpha^{-\frac{3}{2}}(\alpha - 2) > \alpha^{-2}(\alpha - 2)$ , so the distance between the peaks of neighboring triangles is not the minimum distance between vertices of the curve.

With continued iteration of the maps, these patterns repeat and there are no new distances between vertices that need to be checked. So, using similarity again, the minimum distance between two vertices of the  $n^{\text{th}}$ -generation prefractal curve is  $\min\{\alpha^{-n}, \alpha^{-n}(\alpha - 2)\}$ . This is clearly less than  $\frac{1}{2}$  for any  $\alpha \in (2, 4)$  and  $n \geq 1$ , so the minimum distance between vertices of  $\Omega_{\alpha,n}^i$ , for  $i = 1, 2$ , is

$$\begin{cases} \alpha^{-n}(\alpha - 2) & \text{if } 2 < \alpha < 3 \\ \alpha^{-n} & \text{if } 3 \leq \alpha \leq 4. \end{cases} \quad (\text{B.6})$$

### B.3 Finding the Aspect Ratio after Refinement

When  $K_0$  is refined according to one of the refinements expressed in Section 3.1, the aspect ratio of a triangle produced by refining  $K_0$  may be greater than  $K_0$ . Our goal in this section is to find a limit for the aspect ratio of a triangle created by refining a triangle  $K_0$  known to have aspect ratio less than or equal to  $\sigma$ .

So, let  $K_0$  be a triangle with vertices  $V_1$ ,  $V_2$  and  $V_3$ , and suppose that the aspect ratio for  $K_0$  is less than or equal to  $\sigma$ . Now, suppose  $K_0$  is refined according to one of the refinements detailed in Section 3.1. Figure 3.8 shows all of the possible ways in which  $K_0$  may be refined. Since similar triangles have the same aspect ratio, we only need to find a bound for the aspect ratio for any triangle in a similarity class. In Figure 3.8, shading is used to mark triangles that are similar to  $K_0$ . The numbers in the interior of the other triangles indicate the similarity class of the triangle. Since the shaded triangles are similar to  $K_0$ , they must have an aspect ratio less than or equal to  $\sigma$ . In the remainder of this section, the goal is to calculate a bound for the aspect ratio for the remaining 13 similarity classes in terms of  $\sigma$ .

Since we wish to express the aspect ratio for each subtriangle in terms of that of the triangle  $K_0$ , we must first calculate that ratio. Recall that the aspect ratio of a triangle  $K$  is  $\frac{h_K}{\rho_K}$ , where  $h_K$  is the length of the longest side of  $K$  and  $\rho_K$  is the diameter of the largest circle that can be inscribed in  $K$ . Calculating  $h_{K_0}$  requires simply finding

$\max_{i,j \in \{1,2,3\}} |V_i - V_j|$ . Given any triangle  $K$ ,  $\rho_K$  is given by

$$\rho_K = \frac{|K|}{|\partial K|} \tag{B.7}$$

where  $|K|$  is the area of  $K$  and  $|\partial K|$  is the length of the boundary of  $K$ , i.e. the perimeter of  $K$ . The perimeter of  $K_0$  is easily found to be  $|V_1 - V_2| + |V_2 - V_3| + |V_3 - V_1|$ . Letting  $\theta_i$  represent the angle of  $K_0$  at the vertex  $V_i$  for  $i = 1, 2$ , or  $3$ , the area of  $K_0$  is given by the following expressions

$$\begin{aligned} |K_0| &= \frac{1}{2} |V_3 - V_1| \cdot |V_2 - V_1| \sin \theta_1 \\ &= \frac{1}{2} |V_3 - V_2| \cdot |V_1 - V_2| \sin \theta_2 \\ &= \frac{1}{2} |V_1 - V_3| \cdot |V_2 - V_3| \sin \theta_3. \end{aligned} \tag{B.8}$$

So, the value for  $\rho_{K_0}$  can easily be found by combining these results.

Now, we wish to compare these calculations with similar ones performed for subtriangles of  $K_0$  created by the refinement process. For this, it will be convenient to be able to look at examples of refined triangles, so in Figure B.3 we have reproduced the figures introduced in Section 3.1 to explain the refinement process. The outermost triangle in each subfigure is the triangle  $K_0$  with vertices  $V_1$ ,  $V_2$ , and  $V_3$ . The vertices of the other subtriangles are numbered since we will need to refer to them. We will use the notation  $N_i$  to refer to a node labeled with  $i$  in one of the subfigures.

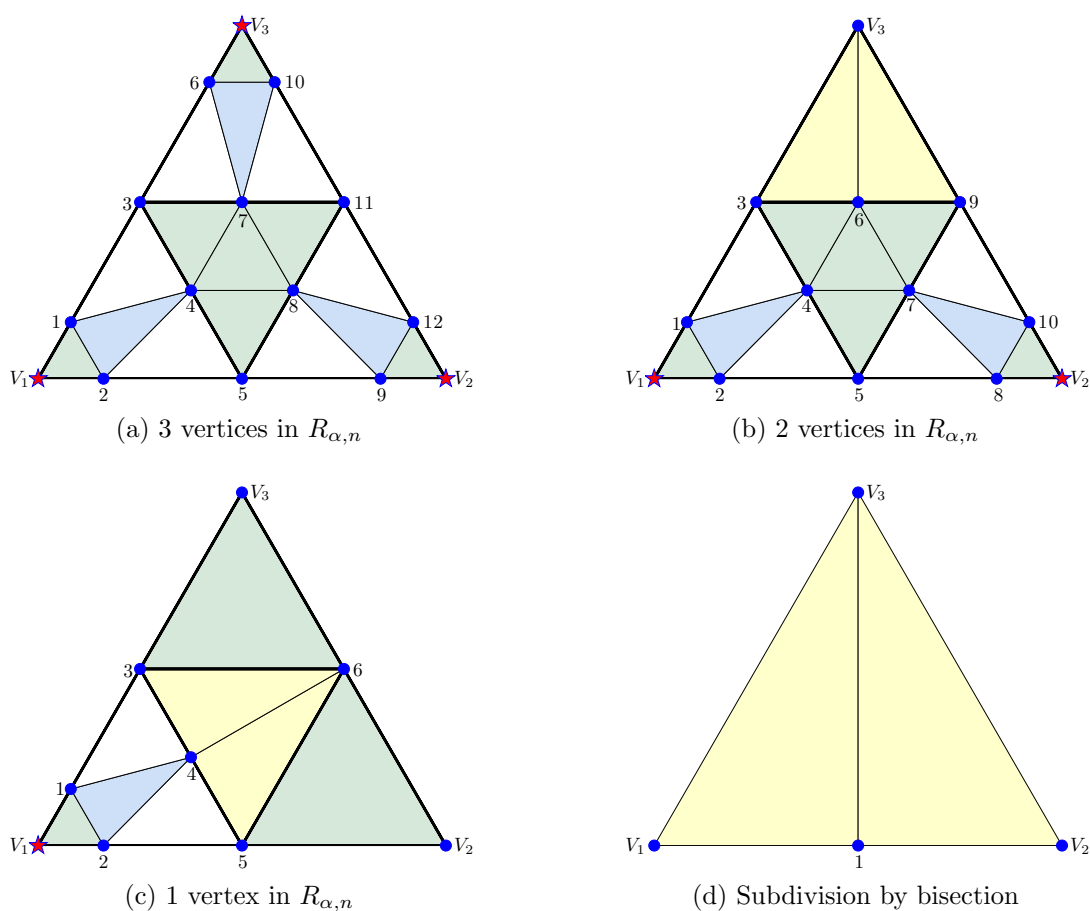


Figure B.3: Refinement labeled according to similarity class

Let us begin by considering the white triangle in Figure B.3a with vertices  $N_2$ ,  $N_5$  and  $N_4$ . For reference, call this triangle  $K_1$ . First, using the barycentric coordinates

that describe the refinement (found in Section 3.1),

$$\begin{aligned} N_2 &= (1 - \lambda)V_1 + \lambda V_2, \\ N_4 &= \frac{1}{2}V_1 + \frac{1}{4}V_2 + \frac{1}{4}V_3, \text{ and} \\ N_5 &= \frac{1}{2}V_1 + \frac{1}{2}V_2, \end{aligned}$$

where  $\lambda = \left(\frac{1}{3}\right)^{1/(1-\mu)} \in (0, \frac{1}{3})$  for some specified  $\mu \in (0, 1)$ . From this information, one may easily verify that

$$|N_5 - N_2| = \left(\frac{1}{2} - \lambda\right) |V_2 - V_1|, \quad \text{and} \quad |N_4 - N_5| = \frac{1}{4}|V_3 - V_2|.$$

Using Figure B.3a, it is clear that  $|N_4 - N_2| < |N_4 - V_1|$ , so using the expression for  $N_4$ ,

$$|N_4 - N_2| < |N_4 - V_1| = \frac{1}{4}|(V_2 - V_1) + (V_3 - V_1)| \leq \frac{1}{4}(|V_2 - V_1| + |V_3 - V_1|).$$

Thus, we have the following estimate of the perimeter of  $K_1$ :

$$|\partial K_1| < \left(\frac{3}{4} - \lambda\right) |V_2 - V_1| + \frac{1}{4}|V_3 - V_2| + \frac{1}{4}|V_3 - V_1|.$$

Using the definition of  $\lambda$ ,  $\lambda \in (0, \frac{1}{3})$  for any  $\mu \in (0, 1)$ , so  $|\partial K_1| < \frac{3}{4}|\partial K_0|$ .

To calculate the area of  $K_1$ , we first determine the measure of the angle in  $K_1$  with vertex  $N_5$ . The barycentric coordinates defining  $N_5$  and  $N_3$  show that the triangle with vertices  $N_5$ ,  $N_3$ , and  $V_1$  is similar to  $K_0$  with sides half the length of those in  $K_0$ . Additionally, the segment from  $N_3$  to  $N_5$  is parallel to the segment from  $V_2$  to  $V_3$ , so the angle at  $N_5$  must be  $\theta_2$ . Using the above lengths of sides of  $K_1$ , the area of  $K_1$  is

$$|K_1| = \frac{1}{2} \left[ \left(\frac{1}{2} - \lambda\right) |V_2 - V_1| \right] \left[ \frac{1}{4}|V_3 - V_2| \right] \sin \theta_2 = \frac{1}{4} \left(\frac{1}{2} - \lambda\right) |K_0| \quad (\text{B.9})$$

Again using the fact that  $\lambda \in (0, \frac{1}{3})$ , we have  $|K_1| \geq \frac{1}{24}|K_0|$ . Thus,

$$\rho_{K_1} \geq \frac{\frac{1}{24} \cdot 4|K_0|}{\frac{3}{4}|\partial K_0|} = \frac{1}{18}\rho_{K_0}.$$

Finally, to calculate the aspect ratio of  $K_1$ , we must know  $h_{K_1}$ . Since  $K_1$  is contained

in the triangle with vertices  $N_5$ ,  $N_3$ , and  $V_1$ , and we have already stated that the latter triangle is similar to  $K_0$  with edges half the length of the corresponding edges of  $K_0$ ,  $h_{K_1} \leq \frac{1}{2}h_{K_0}$ . Combining this with the earlier estimate of  $\rho_{K_1}$ , we have the following bound for the aspect ratio of  $K_1$

$$\frac{h_{K_1}}{\rho_{K_1}} \leq \frac{\frac{1}{2}h_{K_0}}{\frac{1}{18}\rho_{K_0}} \leq 9\sigma.$$

Furthermore, any triangles similar to  $K_1$  also have an aspect ratio that is less than or equal to  $9\sigma$ . Making only slight changes to the above argument, we can show that any of the unshaded triangles in Figure B.3 have an aspect ratio that is less than or equal to  $9\sigma$ .

Now, let us consider the triangle shaded blue in Figure B.3a with vertices  $N_1$ ,  $N_2$ , and  $N_4$ . We will refer to this triangle as  $K_2$ . From the barycentric coordinates that describe the points, we have

$$\begin{aligned} N_1 &= (1 - \lambda)V_1 + \lambda V_3, \\ N_2 &= (1 - \lambda)V_1 + \lambda V_2, \text{ and} \\ N_4 &= \frac{1}{2}V_1 + \frac{1}{4}V_2 + \frac{1}{4}V_3, \end{aligned}$$

so one can easily verify that  $|N_1 - N_2| = \lambda|V_3 - V_2|$ . From above, we have that  $|N_4 - N_2| < \frac{1}{4}(|V_2 - V_1| + |V_3 - V_1|)$ , and by a virtually identical argument,  $|N_4 - N_1| < \frac{1}{4}(|V_2 - V_1| + |V_3 - V_1|)$ . Thus,

$$|\partial K_2| < \frac{1}{2}|V_2 - V_1| + \frac{1}{2}|V_3 - V_1| + \lambda|V_3 - V_2|.$$

Since  $\lambda \in (0, \frac{1}{3})$  and using the value of  $|\partial K_0|$ , it follows that  $|\partial K_2| < \frac{1}{2}|\partial K_0|$ .

To calculate the value of  $\rho_{K_2}$ , we also need  $|K_2|$ . Recalling from an earlier argument that the triangle with vertices  $V_1$ ,  $N_5$  and  $N_3$  is similar to  $K_0$  with a proportionality constant of  $\frac{1}{2}$ , this triangle containing  $K_3$  must have area  $\frac{1}{4}|K_0|$ . If the areas of all of the other triangles contained in this large triangle are known, the area of  $K_2$  can be found by subtracting the other areas from  $\frac{1}{4}|K_0|$ .  $|K_1|$  is given by (B.9) and a similar argument shows that the triangle with vertices  $N_1$ ,  $N_3$  and  $N_4$  has the same area. It can also easily be shown that the triangle with vertices  $V_1$ ,  $N_2$  and  $N_1$  is similar to  $K_0$  with a proportionality constant of  $\lambda$ , so the area of this triangle is  $\lambda^2|K_0|$ . Therefore, using

again that  $\lambda \in (0, \frac{1}{3})$ ,

$$|K_2| = \frac{1}{4}|K_0| - \lambda^2|K_0| - \frac{1}{2}\left(\frac{1}{2} - \lambda\right)|K_0| = \lambda\left(\frac{1}{2} - \lambda\right)|K_0| \geq \frac{\lambda}{6}|K_0|. \quad (\text{B.10})$$

So, using the expressions for  $|K_2|$  and  $|\partial K_2|$ , we have  $\rho_{K_2} \geq \frac{\lambda}{3}\rho_{K_0}$ . Finally, to calculate a bound for the aspect ratio, we need an estimate of  $h_{K_2}$ . Using the same logic as for  $K_1$ ,  $h_{K_2} \leq \frac{1}{2}h_{K_0}$ , and thus

$$\frac{h_{K_2}}{\rho_{K_2}} \leq \frac{\frac{1}{2}h_{K_0}}{\frac{\lambda}{3}\rho_{K_0}} \leq \frac{3}{2\lambda}\sigma \quad (\text{B.11})$$

Although all of the triangles shaded blue in Figure B.3 are not of the same similarity class, they are created in a similar fashion. So with only minor changes to the argument made for calculating the aspect ratio of  $K_2$ , it can be shown that all of these triangles have an aspect ratio that is no greater than  $\frac{3}{2\lambda}\sigma = \frac{\sigma}{2}3^{1+1/(1-\mu)}$ .

Finally, let us consider the triangles shaded yellow in Figure B.3. These triangles are all created by bisecting an edge of  $K_0$  or a triangle similar to  $K_0$ . For a typical example, let us consider the triangle in Figure B.3d with vertices  $V_1$ ,  $N_1$ , and  $V_3$ , which we will refer to as  $K_3$ . Since  $N_1 = \frac{1}{2}(V_1 + V_2)$ , this triangle has sides of length  $|V_3 - V_1|$ ,  $\frac{1}{2}|V_2 - V_1|$ , and  $|V_3 - N_1| \leq \frac{1}{2}(|V_3 - V_1| + \frac{1}{2}|V_3 - V_2|)$ . Thus,  $|\partial K_3| \leq \frac{3}{2}|\partial K_0|$ . Since  $N_1$  is at the midpoint of the edge between  $V_1$  and  $V_2$ , it is clear that  $|K_3| = \frac{1}{2}|K_0|$ . Therefore,  $\rho_{K_2} \geq \frac{1}{3}\rho_{K_0}$ . Since  $K_2$  contains an edge of  $K_0$ ,  $h_{K_2} \leq h_{K_0}$ , and therefore the aspect ratio of  $K_2$  is less than or equal to  $3\sigma$ . This same bound can be found for all of the other triangles shaded yellow in Figure B.3 by an analogous argument.

So, if  $K_0$  is a triangle with aspect ratio less than or equal to  $\sigma$ , and  $K$  is a triangle produced by the refinement of  $K_0$  according to the refinement scheme in Section 3.1, then the aspect ratio of  $K$  satisfies

$$\frac{h_K}{\rho_K} \leq \frac{3}{2}\sigma \min(6, 3^{1/(1-\mu)}), \quad (\text{B.12})$$

where  $\mu \in (0, 1)$  is specified prior to refinement.



# Bibliography

- [1] David R. Adams and Lars Inge Hedberg. *Function spaces and potential theory*, volume 314 of *Grundlehren der Mathematischen Wissenschaften [Fundamental Principles of Mathematical Sciences]*. Springer-Verlag, Berlin, 1996.
- [2] Jochen Albrety, Carsten Carstensen, and Stefan A. Funken. Remarks around 50 lines of Matlab: short finite element implementation. *Numer. Algorithms*, 20(2-3):117–137, 1999.
- [3] I. Babuška, R. B. Kellogg, and J. Pitkäranta. Direct and inverse error estimates for finite elements with mesh refinements. *Numer. Math.*, 33(4):447–471, 1979.
- [4] Patrizia Bagnerini, Annalisa Buffa, and Elisa Vacca. Finite elements for a prefractal transmission problem. *C. R. Math. Acad. Sci. Paris*, 342(3):211–214, 2006.
- [5] Randolph E. Bank, Andrew H. Sherman, and Alan Weiser. Refinement algorithms and data structures for regular local mesh refinement. In *Scientific computing (Montreal, Que., 1982)*, IMACS Trans. Sci. Comput., I, pages 3–17. IMACS, New Brunswick, NJ, 1983.
- [6] Dietrich Braess. *Finite elements*. Cambridge University Press, Cambridge, second edition, 2001. Theory, fast solvers, and applications in solid mechanics, Translated from the 1992 German edition by Larry L. Schumaker.
- [7] Franco Brezzi and Gianni Gilardi. *Finite element handbook*, pages 3–121. McGraw-Hill Book Co., New York, 1987.
- [8] Philippe G. Ciarlet. *The finite element method for elliptic problems*. North-Holland Publishing Co., Amsterdam, 1978. Studies in Mathematics and its Applications, Vol. 4.

- [9] Kenneth Falconer. *Fractal geometry*. John Wiley & Sons Inc., Hoboken, NJ, second edition, 2003. Mathematical foundations and applications.
- [10] David Gilbarg and Neil S. Trudinger. *Elliptic partial differential equations of second order*. Classics in Mathematics. Springer-Verlag, Berlin, 2001. Reprint of the 1998 edition.
- [11] Mark S. Gockenbach. *Understanding and implementing the finite element method*. Society for Industrial and Applied Mathematics (SIAM), Philadelphia, PA, 2006.
- [12] Pierre Grisvard. *Elliptic problems in nonsmooth domains*, volume 24 of *Monographs and Studies in Mathematics*. Pitman (Advanced Publishing Program), Boston, MA, 1985.
- [13] Wolfgang Hackbusch. *Elliptic differential equations*, volume 18 of *Springer Series in Computational Mathematics*. Springer-Verlag, Berlin, 1992. Theory and numerical treatment, Translated from the author's revision of the 1986 German original by Regine Fadiman and Patrick D. F. Ion.
- [14] Pham Huy Hung and Enrique Sánchez-Palencia. Phénomènes de transmission à travers des couches minces de conductivité élevée. *J. Math. Anal. Appl.*, 47:284–309, 1974.
- [15] John E. Hutchinson. Fractals and self-similarity. *Indiana Univ. Math. J.*, 30(5):713–747, 1981.
- [16] Alf Jonsson and Hans Wallin. Function spaces on subsets of  $\mathbf{R}^n$ . *Math. Rep.*, 2(1):xiv+221, 1984.
- [17] Alois Kufner. *Weighted Sobolev spaces*. A Wiley-Interscience Publication. John Wiley & Sons Inc., New York, 1985. Translated from the Czech.
- [18] Maria R. Lancia. A transmission problem with a fractal interface. *Z. Anal. Anwendungen*, 21(1):113–133, 2002.
- [19] Maria R. Lancia, Umberto Mosco, and Maria A. Vivaldi. Homogenization for thin layers of pre-fractal type. Preprint, 2007.
- [20] Maria R. Lancia and Maria A. Vivaldi. On the regularity of the solutions for transmission problems. *Adv. Math. Sci. Appl.*, 12(1):455–466, 2002.

- [21] Maria R. Lancia and Maria A. Vivaldi. Asymptotic convergence of transmission energy forms. *Adv. Math. Sci. Appl.*, 13(1):315–341, 2003.
- [22] Tom Lindstrøm. Brownian motion on nested fractals. *Mem. Amer. Math. Soc.*, 83(420):iv+128, 1990.
- [23] Umberto Mosco. An elementary introduction to fractal analysis. In *Nonlinear analysis and applications to physical sciences*, pages 51–90. Springer Italia, Milan, 2004.
- [24] Jonathan Richard Shewchuk. Triangle: Engineering a 2D Quality Mesh Generator and Delaunay Triangulator. In Ming C. Lin and Dinesh Manocha, editors, *Applied Computational Geometry: Towards Geometric Engineering*, volume 1148 of *Lecture Notes in Computer Science*, pages 203–222. Springer-Verlag, May 1996. From the First ACM Workshop on Applied Computational Geometry.
- [25] Jonathan Richard Shewchuk. Delaunay refinement algorithms for triangular mesh generation. *Comput. Geom.*, 22(1-3):21–74, 2002. 16th ACM Symposium on Computational Geometry (Hong Kong, 2000).
- [26] Gilbert Strang and George Fix. *An Analysis of the Finite Element Method*. Wellesley-Cambridge Press, Wellesley, MA, 1988.
- [27] Elisa Vacca. *Galerkin Approximation for Highly Conductive Layers*. PhD thesis, Università degli Studi di Roma “LaSapienza”, 2005.